UNIVERSIDAD COMPLUTENSE DE MADRID
FACULTAD DE MEDICINA

TESIS DOCTORAL

Papel de *X-binding protein-1* (Xbp1) en hepatocitos en un modelo preclínico de toxicidad por fármacos

Role of hepatocytic *Xbp1* in a preclinical model of toxic liver injury

MEMORIA PARA OPTAR AL GRADO DE DOCTOR

PRESENTADA POR

Hui Ye

DIRECTOR

Francisco Javier Cubero Palero

Madrid

UNIVERSIDAD COMPLUTENSE DE MADRID

FACULTAD DE MEDICINA

TESIS DOCTORAL

Papel de *X-binding protein-1* (Xbp1) en hepatocitos en un modelo precl ínico de toxicidad por f ármacos

Role of hepatocytic *Xbp1* in a preclinical model of toxic liver injury

MEMORIA PARA OPTAR AL GRADO DE DOCTOR

PRESENTADA POR

Hui Ye

DIRECTOR

Francisco Javier Cubero Palero

Madrid, 2020

UNIVERSIDAD COMPLUTENSE DE MADRID

FACULTAD DE MEDICINA

TESIS DOCTORAL

Papel de *X-binding protein-1* (Xbp1) en hepatocitos en un modelo precl ínico de toxicidad por f ármacos

MEMORIA PARA OPTAR AL GRADO DE DOCTOR

PRESENTADA POR

Hui Ye

DIRECTOR

Francisco Javier Cubero Palero

Madrid, 2020

COMPLUTENSE UNIVERSITY OF MADRID

SCHOOL OF MEDICINE

DOCTORAL THESIS

Role of hepatocytic *Xbp1* in a preclinical model of toxic liver injury

MEMORY TO OPT FOR THE DEGREE OF DOCTOR

PRESENTED BY

Hui Ye

Director

Francisco Javier Cubero Palero

Madrid, 2020

UNIVERSIDAD COMPLUTENSE DE MADRID

FACULTAD DE MEDICINA

Departamento de Inmunología, Oftalmología y ORL

TESIS DOCTORAL

Papel *de X-binding protein-1* (Xbp1) en hepatocitos en un modelo preclínico de toxicidad por fármacos

MEMORIA PARA OPTAR AL GRADO DE DOCTOR

PRESENTADA POR

Hui Ye

Director

Francisco Javier Cubero Palero

Madrid

COMPLUTENSE UNIVERSITY OF MADRID

SCHOOL OF MEDICINE

Department of Immunology, Ophthalmology and ENT

DOCTORAL THESIS

Role of hepatocytic *Xbp1* in a preclinical model of toxic liver injury

MEMORY TO OPT FOR THE DEGREE OF DOCTOR

PRESENTED BY

Hui Ye

Director

Francisco Javier Cubero Palero

Madrid

UNIVERSIDAD COMPLUTENSE DE MADRID

FACULTAD DE MEDICINA

TESIS DOCTORAL

Papel de *X-binding protein-1* (Xbp1) en hepatocitos en un modelo precl ínico de toxicidad por f ármacos

Hui Ye

Madrid, 2020

Director: Francisco Javier Cubero Palero

COMPLUTENSE UNIVERSITY OF MADRID

SCHOOL OF MEDICINE

DOCTORAL THESIS

Role of hepatocytic *Xbp1* in a preclinical model of toxic liver injury

Hui Ye

Madrid, 2020

Director: Francisco Javier Cubero Palero

Acknowledgements

The four years of studying in Madrid have been an important life experience for me. On the occasion of this paper, I would like to express my sincere gratitude to my teachers, colleagues and family members who have been teaching, supporting and helping me over the past few years!

First of all, I would like to express my heartfelt gratitude to Prof. Francisco Javier Cubero Palero who gave me the opportunity to study in the Department of Immunology at the Complutense University School of Medicine in Madrid, Spain. My director has devoted a lot of hard work to my project, and this thesis was completed under his careful guidance. From the topic selection, the determination of the research project, the design of the experiment plan to the final thesis framework and detailed revision, he gave patient guidance and help, and put forward many valuable opinions and suggestions. Every time I met problems during my experiments, he always encouraged me and patiently helped me analyze the cause. Over the past years, Prof. Francisco Javier Cubero provided me with a good and relaxed learning and working environment. His profound knowledge, meticulous attitude, unique insights into scientific research have benefited me a lot and led me into the gate of medical science.

I would like to thank the dean of the Immunology Department, Prof. Jose Ramon Regueiro Gonzalez-Barros, for supporting me to study in the Department of Immunology. The successful completion of this thesis is also inseparable from his great help and support.

Furthermore, I would like to thank Prof. Yulia Alexandrowna Nevzorova, the leader of our cute liver lab. She is always willing to answer my questions many times without hesitation and giving a lot of technical support. Her rigorous attitude towards scientific research leaves a profound impact on me, and will always guide me during my research work.

Thanks to Chaobo Chen, Kang Zheng, Fengjie Hao, and Feifei Guo for their selfless help during my experiments. They taught me how to manage mice in the animal facility, and gave me suggestions when my experiment was not going well. Thanks to Chaobo Chen for his help and encouragement during the quarantine

period of the coronavirus-19 epidemic. We have had a deep friendship in the long years of getting along together, and this precious love will last a lifetime.

Thanks to Arantza Lamas Paz for her warm help at the beginning I came here and taking me into the big family of the laboratory. Because of knowing little about Spanish, I encountered some troubles during the renewal of residence and registration. She was always kind to translate for me and patiently helped me solve the problems. Thanks to Laura Moran Blanco, Raquel Bened éUbieto, Olga Est évez V ázquez, Nuria L ópez Alc ántara, Carlos Sanz Garc á and Marina Mazariegos Le ón. Thanks for all the help in my study and living. Because of all of you, our laboratory is full of warmth and joy. It is a great honor for me to be able to study and live in such an atmosphere for four years.

My appreciation would also go to Prof. Eduardo Martinez Naves, Prof. Manuel G ómez del Moral, Beatriz Mart ín-Adrados, Beatriz Amor ós P érez, Sergio Alegre G ómez, and many others in the Department of Immunology. Beside lots of help in the work, you endow me with precious love and friendship in this country that far from my homeland.

My warmest thanks further go to all those who have helped me with my work in this University, including the staff members of the animal facility and the Faculty of Biology.

In particular, I want to thank my motherland, the People's Republic of China. Without the financial support of China Scholarship Council, I would not have been able to come here and study a PhD degree in Biomedical Research. Thanks for giving me this precious opportunity and providing the strong support all the times.

Thanks to Zhongda hospital and Southeast University for supporting and sending me to study abroad. When the epidemic was at its worst, the leaders of the hospital and university enthusiastically asked about my condition and sent masks and drugs for me.

Last but not least, I have to thank my dear family, my parents and my grandmother. My parents always understand and support me. For me you are the best parents in the world. Without your love, I would not have been able to resist

and continue my study during the tough time. Hope what I did can also make you happy and feel proud for me.

Index

1. Abstract

1.1 Resumen

Introducción

La lesión hepática inducida por fármacos (DILI) es una de las principales causas de lesión hepática aguda, incluida la sobredosis de acetaminofén (APAP). El estrés del retículo endoplásmico (ER) es un mecanismo sin explorar, pero muy probablemente, desencadenante de la lesión hepática inducida por APAP. En condiciones de estrés, ER puede iniciar la respuesta de proteína desplegada. Sin embargo, los mecanismos del estrés ER y UPR siguen siendo poco conocidos. En este estudio, nuestro objetivo general fue develar la relevancia del brazo IRE1α-XBP1, el brazo más conservado de UPR, durante la insuficiencia hepática aguda inducida por APAP y proporcionar la base para la intervención terapéutica.

Métodos

Los HepaRG se desafiaron con diferentes concentraciones de APAP (0, 5, 10 y 20 mM). En paralelo, ratones macho C57BL/6 en ayunas durante la noche se expusieron a una inyección intraperitoneal de APAP [0, 75, 150 y 300 (mg/kg)]. Se utilizaron ratones con deleción específica de hepatocitos de Xbp1 (*Xbp1*$^{\Delta hepa}$) usando la recombinasa Alb-CRE. Se usaron Xbp1-floxed (*Xbp1*$^{f/f}$) como ratones de control. Todos los ratones se mantuvieron en ayunas durante la noche y se les administró una dosis subletal de APAP (>300 mg/kg) o vehículo. Veinticuatro horas más tarde, se sacrificaron los ratones y se recogieron tejidos y células. Se realizaron exámenes histopatológicos de hígados y células, inmunofluorescencia (IF) e inmunohistoquímica (IHC), Western Blot y estudios de qPCR en tiempo real y microscopía electrónica de transmisión (TEM).

Resultados

Los experimentos in vitro mostraron que una dosis superior a 10 mM o 300 mg/kg in vivo provocaba daño en las células del parénquima hepático (LPC), pérdida de la polaridad de los hepatocitos y activación de la respuesta de la UPR. La activación de UPR y JNK1/2 fue característica de la hepatotoxicidad mediada por APAP humana y murina. La ablación de *Xbp1* en hepatocitos redujo el daño hepático inducido por APAP.

Los ratones con deleción de *Xbp1* en las células parenquimatosas hepáticas mostraron una mortalidad significativamente menor a APAP que los compañeros de camada de flox. Los marcadores séricos de lesión hepática, focos necróticos, muerte celular, acumulación de lípidos, estrés oxidativo (por ejemplo: CYP2E1, 4HNE) e infiltración inmunitaria, inflamación y activación del inflamasoma se redujeron drásticamente en hígados de $Xbp1^{\Delta hepa}$ en comparación con ratones $Xbp1^{f/f}$. Además, se encontró un aumento de la expresión de mRNA y proteínas de pIRE1α y la presencia de autofagosomas en animales $Xbp1^{\Delta hepa}$, un fenómeno relacionado con la sobreexpresión de *atg5* y pAMPK y la regulación negativa de P62.

Conclusiones

Nuestro estudio sugiere fuertemente que una dosis subletal de APAP indujo la activación del brazo IRE1α-XBP1, el aumento de especies reactivas de oxígeno (ROS) y la infiltración de citocinas inflamatorias, lo que finalmente condujo a la muerte de los hepatocitos y daño hepático. La ablación de *Xbp1* en hepatocitos mejora el DILI derivado de APAP, evidenciado por una disminución de la expresión de JNK1/2, menos estrés oxidativo y activación del inflamasoma. Como resultado de la pérdida de *Xbp1*, la hiperactivación de IRE1α en los hepatocitos da como resultado la activación de la desintegración dependiente de IRE1 regulada (RIDD) y la supresión de la actividad del citocromo P450. Y la activación de la autofagia también se asocia con la protección contra la lesión hepática mediada por APAP. Nuestro estudio muestra una nueva perspectiva sobre la lesión hepática inducida por APAP y también proporciona la base para terapias clínicas dirigidas a la restauración de la función hepática después de una lesión hepática aguda.

1.2 Abstract

Introduction

Drug-induced liver injury (DILI) is a leading cause of acute liver injury, including acetaminophen (APAP) overdose. Endoplasmic reticulum (ER) stress is an unexplored but very likely a triggering mechanism of APAP-induced liver injury. Under stress conditions, ER can initiate the unfolded protein response (UPR). However, the mechanisms of ER stress and UPR remain poorly understood. In this study, we overall aimed to unveil the relevance of the IRE1α-XBP1 arm, the most highly conserved arm of UPR, during APAP-induced acute liver failure (ALF) and provide the basis for therapeutic intervention.

Methods

HepaRGs were challenged with different concentrations of APAP (0, 5, 10&20 mM). In parallel, overnight fasted C57BL/6 male mice were challenged with an intraperitoneal injection of APAP [0, 75, 150&300 (mg/kg)]. Mice with hepatocyte-specific deletion of *Xbp1* (*Xbp1*$^{\Delta hepa}$) using the Alb-CRE recombinase were used. Xbp1-floxed (*Xbp1*$^{f/f}$) were used as control mice. All mice were fasted overnight and given a sublethal dose of APAP (>300 mg/kg) or vehicle. Twenty-four h later, mice were sacrificed, tissues and cells collected. Histopathological examination of livers and cells, immunofluorescence (IF) and immunohistochemistry (IHC), Western Blot and Real time-qPCR studies and transmission electron microscopy (TEM) were performed.

Results

In vitro experiments showed that a dose greater than 10 mM or 300 mg/kg in vivo elicited liver parenchymal cells (LPC) damage, loss of hepatocyte polarity and activation of the UPR response. Activation of the UPR and JNK1/2 was characteristic of human and murine APAP-mediated hepatotoxicity. Ablation of *Xbp1* in hepatocytes reduced APAP-induced hepatic damage. Mice with deletion of *Xbp1* in liver parenchymal cells (LPC) showed significantly less mortality to APAP than flox littermates. Serum markers of liver injury, necrotic foci, cell death, lipid accumulation,

oxidative stress (eg: CYP2E1, 4HNE) and immune infiltration, inflammation and inflammasome activation were dramatically reduced in livers of *Xbp1*$^{\Delta hepa}$ compared with *Xbp1*$^{f/f}$ mice. Furthermore, increased mRNA and protein expression of pIRE1α and presence of autophagosomes was found in *Xbp1*$^{\Delta hepa}$ animals, a phenomenon linked with *atg5* upregulation and pAMPK overexpression and downregulation of *p62*.

Conclusions

Our study strongly suggests that a sublethal dose of APAP induced the activation of the IRE1α-XBP1 arm, the increase of reactive oxygen species (ROS) and the infiltration of inflammatory cytokines, ultimately leading to hepatocyte death and liver injury. The ablation of *Xbp1* in hepatocytes ameliorates APAP-derived DILI, evidenced by decreased JNK1/2 expression, less oxidative stress and inflammasome activation. As a result of loss of *Xbp1*, hyperactivation of IRE1α in hepatocytes results in activation of regulated IRE1-dependent decay (RIDD) and suppression of cytochrome P450 activity. And the activation of autophagy is also associated with protection against APAP-mediated liver injury. Our study shows a new perspective on APAP-induced liver injury, and also provides the basis for clinical therapies targeting the restoration of liver function after acute liver injury.

2. Abbreviations

Abbreviations

Abbreviations	Full Name
ADRs	Adverse drug reactions
AIF	Apoptosis-inducing factor
ALF	Acute liver failure
ALT	Alanine aminotransferase
AMPK	AMP-activated protein kinase
ANGPTL3	Angiopoietin-like 3
APC	Antigen presenting cells
APS	Ammonium Persulfate
APAP	Acetaminophen
APAP-AD	APAP-Adducts
ASK1	Apoptotic signal-regulated kinase-1
AST	Aspartate aminotransferase
ATP	Adenosine triphosphate
ATF	Activating transcription factor
ATG	Autophagy related gene
BCRP	Breast cancer resistance protein
BIP	Binding immunoglobulin protein
BSA	Bovine serum albumin
BSEP	Bile salt export protein
Caspase	Cysteine-dependent aspartate-directed protease
CCK-8	Cell counting kit-8
CC3	Cleaved caspase-3
CCl_4	Carbon tetrachloride
cDNA	Complementary DNA
CHOP	CCAAT-enhancer-binding protein homologous protein
CSE1	Carboxylesterase 1
CYP450	Cytochrome P450

DAMP	Damage-related molecular patterns
DAB	3,3'-diaminobenzidine
DAPI	4,6-diamino-2-phenylindole
DHE	Dihydroethidium
DILI	Drug-induced liver injury
DMSO	Dimethyl sulfoxide
Δhepa	Deleted in hepatocytes
DNA	Deoxyribonucleic acid
dNTP	Deoxyribonucleoside triphosphate
DTT	Dithiothreitol
eIF2α	Eukaryotic initiation factor-2α
ECL	Enhanced chemiluminescence
EDTA	Ethylenediaminetetraacetic acid
ER	Endoplasmic reticulum
ERAD	ER-associated protein degradation
EtOH	Ethanol
FBS	Fetal bovine serum
GAPDH	Glyceraldehyde 3-phosphate dehydrogenase
GLDH	Glutamate dehydrogenase
GRP78	Glucose-regulated protein, 78 kDa
GSK-3β	Glycogen synthase kinase-3β
GSH	Glutathione
H&E	Hematoxylin and eosin
HMGB1	High mobility group-1
HRP	Horseradish peroxidase
H_2O_2	Hydrogen peroxide
HO-1	Heme oxygenese-1
HSCs	Hepatic stellate cells
iDILI	Idiosyncratic DILI

IF	Immunofluorescence
IHC	Immunohistochemistry
IL-1α	Interleukin-1α
IL-1β	Interleukin-1β
IL-18	Interleukin-18
IP	Intraperitoneal injection
iNOS	Inducible nitric oxide synthase
IRE1α	Inositol-requiring enzyme 1-α
JNK	c-Jun NH2-terminal kinase
KCs	Kupffer cells
LC3	Light chain-3
LDH	Lactate dehydrogenase
LIR	LC3-interaction region
LPC	Liver parenchymal cells
LSECs	Liver sinusoidal endothelial cells
MAPK	Mitogen-activated protein kinase
MAP2K	Mitogen-activated protein kinase kinase
MAP3K	Mitogen-activated protein kinase kinase kinase
$MgCl_2$	Magnesium chloride
MKK4	MAP kinase kinase-4
MLK3	Mixed lineage kinase-3
MMP	Mitochondrial membrane potential
MPT	Mitochondrial permeability transition
mRNA	Messenger RNA
mTOR	Mammalian target of rapamycin
NADPI	N-acetyl-p-benzoquinone imine
NAC	N-Acetylcysteine
NAFLD	Non-alcoholic fatty liver disease
Nrf_2	Nuclear erythroid-2-related factor 2

NTCP	The sodium-taurocholate co-transporting polypeptide
NF-κB	Nuclear factor kappa-B
NO	Nitric oxide
OATP	The organic anion transporting polypeptide
OAT	The organic anion transporter
OCTNs	Organic cation transporters
OD	Optical density
ORO	Oil Red O
PBS	Phosphate buffered saline
PBST	Phosphate buffered saline supplemented with Tween 20
PCR	Polymerase chain reaction
PDI	Protein disulfide isomerase-A1
PE	Phosphatidylethanolamine
PERK	The protein kinase RNA -like ER kinase
PFA	Paraformaldehyde
P-gp	P-glycoprotein
PKC	Protein kinase C
RER	Rough endoplasmic reticulum
RIDD	Regulated IRE1-dependent decay
RNA	Ribonucleic acid
ROS	Reactive oxygen species
RT	Reverse transcription
$O2^{\bullet-}$	Superoxide anion
SDS	Sodium dodecyl sulphate
SER	Smooth surface endoplasmic reticulum
SMA	Smooth muscle actin
SULTs	Sulfotransferases
TAE	Tris Acetate EDTA Buffer
TAA	Thioacetamide

TBS	Tris buffered saline
TBST	Tris buffered saline supplement with Tween 20
TEMED	N ´,N,N ´,N ´-Tetramethyl diamine
TEM	Transmission electron microscopy
TG	Hepatic triglyceride
TJs	Tight junctions
TLR	Toll-like receptors
TMRM	Tetramethylrhodamine, methyl ester
TNF-α	Tumor necrosis factor-α
TRAF2	TNF receptor associated factor-2
Tris	2-Amino-2 (hydroxymethyl)-1,3-propandiol
TUNEL	Terminal deoxynucleotidyl transferase dUTP nick end labeling
Tween 20	Polyoxyethylene (20) Sorbitan Monolaureat
UBA	Uubiquitin-associated domain
UCM	Complutense University
UGTs	UDP-glucuronosyltransferases
ULK1	Unc-51 like autophagy activating kinase-1
UPR	Unfolded protein response
XBP1	X-box binding protein-1
ZO-1	Zonula occludens-1
4-HNE	4-Hydroxynonenal

3. Introduction

3.1 Anatomy, physiology and function of the liver

The liver is a dynamic and heterogeneous organ, and controls numerous physiological processes, including the production of bile, regulation of plasma proteins and glucose, and biotransformation of drugs and toxins. The liver is involved in the maintenance of the whole homeostasis as an active, bidirectional biofilter (1). It filters the portal blood that transports nutritional and toxic compounds from the environment through the gastrointestinal tract and it also filters the systemic blood, thus providing the only way to remove non-water-soluble substances. It also rapidly metabolizes most nutritional compounds, and neutralizes and removes toxic exogenous and endogenous materials (2).

The liver is also a unique organ in that it is supplied by both arterial and venous blood. The hepatic artery carries oxygen-rich blood from the aorta via the celiac trunk, whereas the portal vein carries blood rich in digested nutrients from the entire gastrointestinal tract and from the spleen and pancreas. All the blood in the liver ends up in the sinusoids, and is collected by the hepatic veins, then reaches the systemic circulation via the inferior vena cava (3).

The liver is composed of several cell types of different origin including hepatocytes, biliary epithelial cells (cholangiocytes), hepatic stellate cells (HSCs), Kupffer cells (KCs) and liver sinusoidal endothelial cells (LSECs) (4). All of these cells in the liver function cooperatively and regulate hepatic function at multiple levels. The basic functional unit of the liver is the hepatic lobule, consisted of chords of hepatocytes, the hepatic artery, portal vein and bile ducts (5). The terminal branch of the hepatic vein is in the center of the hepatic lobule, and hepatocytes are arranged radially around the central vein to form hepatic cords. The sinusoids are among the hepatic cords. The corners of the lobule are occupied by the portal triads. The portal triads of the normal liver are distributed regularly in the histological structure, and separated by liver parenchyma containing hepatocytes and sinusoids (6) (**Fig. 1**).

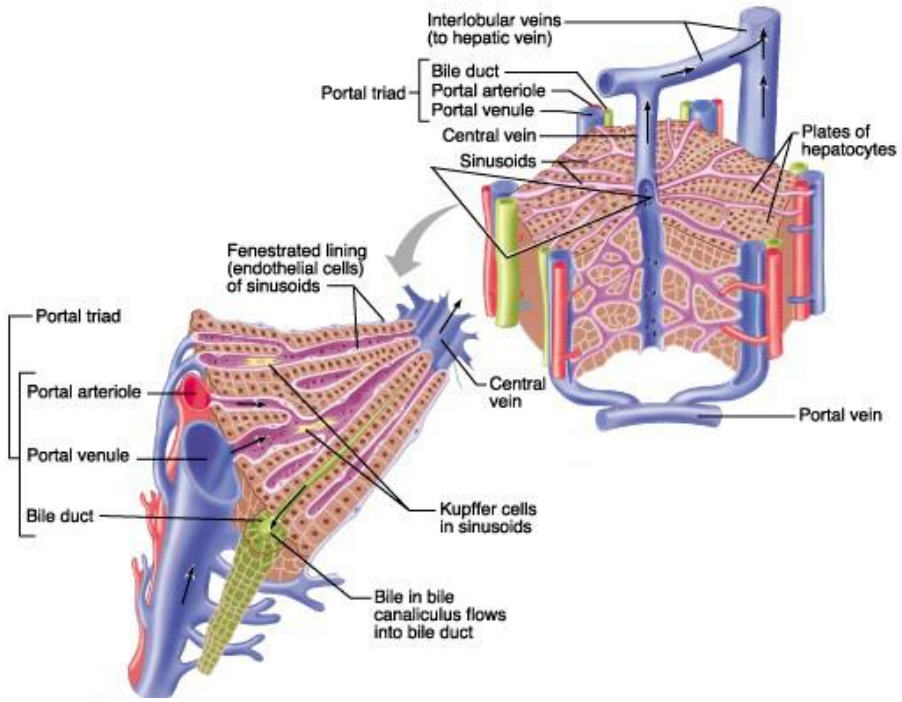

Figure 1. Diagrammatic representation of a liver lobule and its vascular network. On the edge of the lobule, portal triads containing three vessels (bile duct, portal vein and hepatic artery) are arranged, and a central vein is placed on the center of the lobule. Branches of the hepatic artery and portal vein are located on the periphery of the lobule, and the blood from hepatic artery and portal vein both perfuse the sinusoids. Bile ducts located peripherally drain the bile canaliculi that run between the hepatocytes (6).

3.1.1 The classification and function of liver cells

3.1.1.1 Parenchymal cells

The hepatocytes are the most crucial parenchymal cells of the hepatic tissue and the primary epithelial cell population of the liver, representing about 60% of all cells in the parenchymal matrix and making up the majority of the liver volume (around 80%) (7). Hepatocytes are shaped as complex rhomboids with several distinct surfaces and the nuclear is in the middle of the cells (8). The hepatocyte is the main site that manufactures serum albumin, lipid protein, fibrinogen and the prothrombin group of clotting factors. It also forms fatty acids from carbohydrates and synthesizes triglycerides from fatty acid and glycerol (9). According to molecular specialization of their various surface membranes in the forms of receptors, pumps, transport channels and carrier proteins, there are three functionally distinct domains. Hepatocytes have the ability to metabolize, detoxify and inactivate exogenous

compounds such as drugs and endogenous compounds such as steroids through the developed smooth endoplasmic reticulum (SER) (10).

3.1.1.2 Non-parenchymal cells

LSECs are the highest proportion of non-parenchymal cells in the liver, and its fenestration structure and high capacity of clearance plays an indispensable role in the physiological and pathological processes of the liver. LSECs mainly regulate the occurrence and development of liver disease through anti-inflammatory, endocytosis clearance, hepatic sinusoidal capillarity, secretion of pro-angiogenic signal factors and maintenance of HSCs (11). LSECs adjust the material exchange and information exchange inside and outside the liver sinusoids by changing the diameter and the number of holes in the LSECs (12). LSECs also play an important role in plasma ultrafiltration and liver microcirculation. There are three endocytosis receptors in LSECs: hyaluronan/scavenger receptor, collagen-α-chain/mannose receptor and Fc γ-receptor Iib2. Hyaluronic acid/scavenger receptors include SR-A, SR-B (SR-B1 and CD36) and SR-H (stabilin-1 and stabilin-2), among which SR-H is the main scavenger receptor for LSECs. LSECs can swallow a large amount of exogenous and endogenous substances, and remove soluble macromolecules and some particles with a diameter of less than 0.5 μm from the blood (13).

HSCs are located in the Disse space and account for 30% of nonparenchymal cells, which is a key factor in the development of liver fibrosis (14). It is close to sinusoidal endothelial cells and hepatocytes, and distributes numerous roots around the hepatic sinusoids. Under normal circumstances, HSCs participate in the metabolism and storage of Vit A and the synthesis and degradation of extracellular matrix, and express cytokines and receptors. Once liver damage, HSCs are activated as a result of the collaboration of paracrine and autocrine effects of many cytokines. Stellate cells become activated myofibroblast-like cells and keep on proliferation. The cells become bigger, vitamin A lipid droplets disappear, and the secretion of collagen fibers and other extracellular matrix increases. The expression of α-Smooth muscle actin (SMA) is a sign of HSC activation. Studies have shown that the activated HSCs not only promote proliferation and secretion of extracellular matrix, but also increase

sinusoidal pressure through cell contraction, which ultimately laid the pathological basis for liver fibrosis and portal hypertension (15).

The cholangiocytes, also named biliary epithelial cells, comprising less than 1% of the total number of cells in the liver parenchyma, form the channels of the biliary system, produce bile and modify the composition of the bile (16). Besides, the cholangiocytes also play an important role in immunoregulation. The cholangiocytes not only tackle the microorganism, xenobiotics and foreign antigens in the biliary tract, but also produce antibacterial products, like defensins, lysozyme and transport IgA, and express MHC class I and II molecules and antigen presenting cells (APC) (17).

Due to the exposure to a variety of viruses, bacteria, parasites and tumor cells, the liver contains a large amount of lymphocytes of different phenotypes and the macrophages (18). Hepatic macrophages can be divided into two classes based on their origin, bone marrow-derived macrophages and resident macrophages (19). The Kupffer cells are the resident macrophages in the liver, and perform the immunoregulatory function, which makes the liver as the largest organ in the immune system with the presence of almost all subtypes of lymphocytes and dendritic cells.

3.1.2 The metabolism of drugs in the liver

The liver is one of the main organs of drug metabolism and elimination in the body. Drugs enter the liver and undergo a series of processes under the action of multiple drug-metabolizing enzymes, which is called biotransformation or drug metabolism (20). There are two results after biotransformation of the drugs in the body: one is inactivation, becoming a drug without pharmacological activity; the other one is activation, from pharmacological inactivity to pharmacologically active metabolites or toxic metabolites, or remaining the original pharmacological effects after metabolism (21, 22).

3.1.2.1 Drug transporters in the liver

It is thought that drugs are taken into the hepatocytes via passive diffusion across the basolateral hepatocyte membrane for a long time, but then this concept was challenged because it was found that bile salts enter the hepatocytes in a carrier-

mediated, sodium-dependent process (23). Fat-soluble compounds can pass through the lateral membrane of the bile duct by passive diffusion, while organic compounds in polar or ionic form, such as cyclosporine and statins (24), need to be transferred into hepatocytes with the assistance of transporters. Drug transporters are functional proteins located on the cell membranes, and the loss or inhibition of its functions is the main cause of drug interaction and certain diseases (25). The uptake transporters, including the sodium-taurocholate co-transporting polypeptide (NTCP) (26), the organic anion transporting polypeptide (OATP) (27), the organic anion transporter (OAT) (28) and carnitine/organic cation transporters (OCTNs) (29), are located on the sinusoid membranes, and affect the concentration and metabolism of the drugs in the liver. After the drug enters the liver, it is metabolized by abundant drug-metabolizing enzymes, then excreted from the liver with the help of efflux transporters, such as P-glycoprotein (P-gp), breast cancer resistance protein (BCRP) and bile salt export protein (BSEP), in the form of prototype or its metabolites (30-32). Otherwise, the drugs or its metabolites can also pass through the efflux transporters in the lateral membrane of hepatocytes, and return to the systemic circulation.

Although transporters do not have the ability to metabolize drugs, transmembrane transport mediated by them is the rate-limiting step. Only the drug entering the hepatocytes can be catalyzed by phase I or II metabolic enzymes and generate the metabolites (33, 34).

3.1.2.2 Biotransformation of drugs

The concentration of a drug, especially when administered orally, is greatly reduced before it reaches the systemic circulation, which called the first pass effect (35). It is due to the process of absorption happened in the liver and gut wall. Once drugs enter the blood, they enter the liver through the portal vein, and most drugs undergo varying degrees of structural change in the liver, including oxidation, reduction, decomposition and combination. After metabolism, its pharmacological effects are weakened or diminished. Only a few drugs are metabolized and have a therapeutic effect, like cyclophosphamide (36).

The liver is rich in various enzymes required for phase I and phase II metabolism (20). Phase I metabolism are mainly oxidation, reduction and decomposition reactions. After phase I metabolism, the drugs may have some polar groups such as cholesterol and oxides, but can exhibit very different pharmacological actions. Oxidation reactions are the most common phase I reactions. Monooxygenase is one of the most important enzymes for oxidizing heterologous substances, and mainly located in the microsomes of the smooth endoplasmic reticulum, including cytochrome P450 (CYP450), $NADP^+$ and NADPH reductase (37). CYP450 enzymes can be divided into different categories according to the similarity of amino acid sequence. The most important enzymes in the human are CYP1A2, CYP2A6, CYP2B6, CYP2C8, CYP2C9, CYP2C19, CYP2D6, CYP2E1, CYP3A4 and CYP3A5 (38). CYP450 enzymes have obvious differences among species, and the metabolic pathways and metabolites of drugs in animals and humans may be also different. Polymorphism is an important feature of CYP450 enzymes, and an important reason for individual differences in drug reactions (39). The so-called polymorphism refers to the large difference in the number of certain P450 enzymes between different individuals of the same genus. The individual having a large number of enzymes have a faster metabolic rate, which is called a broad metabolizer (40).

The activated CYP450 contains a heme-iron center. The iron binds to proteins through cysteine thiolate ligands. These cysteine ligands and several flanking residues are highly conserved in known CYPs, and have a common pattern (**Fig. 2**).

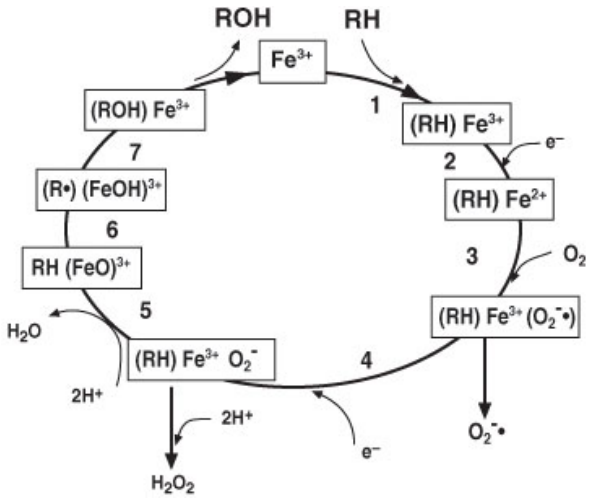

Figure 2. Mechanism of action of cytochrome P450. This scheme is a simplification of the mechanism of action of cytochrome P450 (CYP450). In it, Fe^{3+} represents iron from the heme group of oxidized CYP, RH and ROH substrates and products respectively. In this oxide-reduction cycle superoxide anion ($O2^{\bullet-}$) and hydrogen peroxide (H_2O_2) are released (41).

A large number of drugs are metabolized by CYP enzymes, which inevitably leading to the competitive binding of the drug to the active site. This can be illustrated by the interaction between the central muscle relaxant tizanidine and the selective serotonin reuptake inhibitor fluvoxamine (42). Besides, many drugs can affect the activity of CYP enzymes through inducing isoenzymes biosynthesis or directly inhibiting the activity of CYP enzymes. A typical example is phenytoin, which could induce CYP1A2，CYP2C9，CYP2C19 and CYP3A4 (43). When applying two or more drugs at the same time, one drug could change the metabolism of other drugs, leading to the change of plasma concentration. These drug-drug interactions at the level of the metabolizing enzyme are potentially dangerous, and the main source of adverse drug reactions (ADRs) (44). Therefore, considering these drug interactions, dose adjustment or selection of drugs that do not interact with CYP enzymes need to be required, especially using drugs that are vital to the patients.

3.2 Drug-induced liver injury (DILI)

DILI is defined as a chemical insult resulting in injury to the liver (45). Nowadays, DILI is one of the most common and serious ARDs (46), and is a leading reason for drug withdrawal and the high attrition rates in drug development (**Table 1**). It can be triggered by the parent drug and/or its metabolites, or as a reaction of

hypersensitivity to the compound. A wide variety of drugs can cause DILI, including anti-tumor chemotherapy drugs, anti-tuberculosis drugs, antipyretic analgesics, immunosuppressive agents, hypoglycaemic therapies, or anti-bacterial, anti-fungal and antiviral drugs. DILI leads to multiple presentations in the clinic, including elevated liver enzymes, hepatitis, hepatocellular necrosis, cholestasis, fatty liver and liver cirrhosis. In some patients, liver injury is easily detected by blood tests. However, in some patients, the clinical symptoms are not specific and hard to distinguishable from other hepatic diseases.

Table 1. The incidence of drug-induced liver injury (47)

Country	France	Iceland	Korea	Spain	United Kingdom	United States	Sweden
Crude DILI incidence rate,‰	0.139	0.191	0.12	0.03	0.007-0.013	0.10-1.50	0.023

DILI can be divided into two subtypes according to the drug hepatotoxicity: “intrinsic” and “idiosyncratic”. The former refers to dose-dependent hepatotoxicity that is predictable in humans or animal models, while idiosyncratic DILI (iDILI) is an unpredictable injury that cannot be explained by the known pharmacological properties (48). Most DILI cases are idiosyncratic and become a major problem in the development of new medications (49, 50).

Acetaminophen, also known as paracetamol, has already became the most commonly used antipyretic and analgesic drug since 1955 (51). Up to now, acetaminophen still takes up an important position in clinical medicine. The use of APAP is normally believed to be safe at therapeutic doses. The main indications are fever caused by cold, as well as migraine, neuralgia, arthralgia and postoperative pain. In the more than half a century using APAP to fight against diseases, people also suffer from the adverse reactions caused by it. It has been found that APAP has varying degrees of influence on the digestive system, respiratory system and blood system, immune system. The most serious adverse reaction of APAP is liver toxicity.

Long-term or overdose will cause liver damage, even acute liver failure (ALF) (52). In the United Kingdom, APAP-induced liver injury accounts for 57% of ALF cases (53), and the number is 39% in the United States (54). Every year, around 30,000 patients are admitted to the hospital in the United States due to APAP hepatotoxicity. Although some symptoms are mild, such as hepatitis, cholestasis and asymptomatic transaminase elevation, up to 48% of patients are still diagnosed with ALF (55, 56).

According to papers published, the research on liver injury caused by APAP began in 1966. However, despite half a century of research, the specific mechanism of APAP hepatotoxicity is still not fully explained, and clinical treatment is limited. It is generally believed that APAP toxicity is caused mainly by the excess formation of the reactive intermediate, N-acetyl-p-benzoquinone imine (NAPQI), which is generated by oxidation of APAP by CYP450-dependent metabolism (57, 58).

When APAP enters into the body, only a small part is excreted in urine in the form of a prototype, and almost 90% is metabolized to non-toxic conjugates through UDP-glucuronosyltransferases (UGTs) or sulfotransferases (SULTs), then excreted from the urine (59, 60) (**Fig. 3**). At therapeutic doses, NAPQI can be quickly detoxified by combining with cysteine and thiol uric acid or regenerating non-toxic APAP. At a toxic dose, a large amount of NAPQI is produced, which results in its robust reaction with hepatic glutathione stores and subsequently saturates the detoxification pathway and leads to the depletion of glutathione (GSH). The excessive amounts of NAPQI is available for reaction with protein sulfydryl groups to form APAP protein adducts, thereby resulting in increased oxidative stress and hepatocyte damage (61). Moreover, the accumulated NAPQI further combine with biological macromolecules inside and outside the cell membrane and cause the necrosis of the liver lobule, eventually leading to liver dysfunction (62).

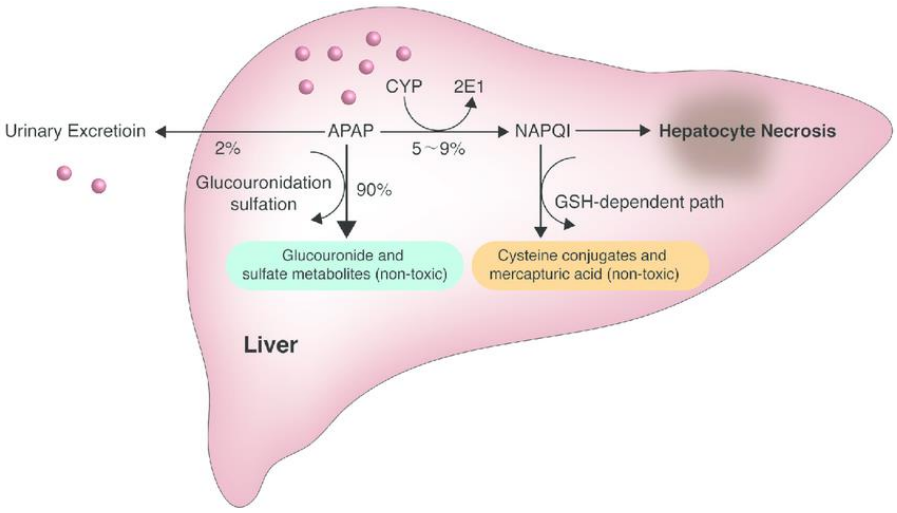

Figure 3. Acetaminophen (APAP) metabolic pathways. When consumed at therapeutic doses, the majority (80%–90%) of APAP is conjugated with glucuronic acid or sulfate and excreted through the kidneys. A minor component is acted upon by cytochrome P450 (CYP450) enzymes such as CYP2E1 and CYP1A2 to form a reactive metabolite, *N*-acetyl-*p*-benzoquinone imine (NAPQI). Though highly reactive, NAPQI is rarely harmful after consumption of therapeutic doses because it is rapidly conjugated with abundant glutathione stores in the liver and excreted through the bile (63).

Metabolism of APAP can be influenced by genotype differences. Due to the polymorphism of the UGT enzyme, variations in glucuronidation have been observed in different populations. Recently, it has been demonstrated that the concentration of APAP protein adduct is higher in UGT2B15*2/*2 genotype subjects than UGT2B15*1/*2 and UGT2B15*1/*1 individuals (64). In fact, protein adducts can be detected in the vast majority of people taking therapeutic doses of APAP (65), and protein adducts are formed before significant GSH depletion (60, 66, 67). Rather than assessing the formation of protein adducts in cells, which were initially considered to be critical for cell death (68), it is better to assess that the effect of protein adducts formation on mitochondrial proteins, which is most correlated with toxicity (69, 70).

At present, the traditional serum biomarker cannot meet the requirements for early detecting DILI. Several new biomarkers have been reported, including apoptosis-related caspase cleaved keratin 18 (cCK18), necrosis-related HMGB1and microRNA (especially microRNA-122), specific mitochondrial injury biomarker glutamate dehydrogenase (GLDH), biomarkers reflecting cholestasis (*e.g*. BAs) as

well as genetic biomarkers reflecting the susceptibility to DILI, such as the genetic polymorphisms of HLA, drug metabolizing enzymes and drug transport proteins (47). Some of these biomarkers are already being used in early clinical trials. Though current biomarkers are not specific to DILI and their value for clinical use still needs to be widely verified, their addition to conventional measurements could soon transform DILI prediction and detection, thereby promoting earlier treatment.

The therapy for acetaminophen-induced liver injury is mainly supportive treatment, and the common recognized specific antidote is N-acetylcysteine (NAC). On the one hand, NAC supplements and maintains the liver GSH by providing cysteine, on the other hand, it can also provide raw materials for the synthesis of sulfonic acid group to enhance the sulfonated metabolic pathway. Besides, NAC can also prevent the oxidization of thiol group on the molecule by NAPQI (71). However, the incidence of allergic reactions is high in intravenous injection, and NAC is contraindicated in patients with coma, pancreatitis, intestinal obstruction and gastrointestinal insufficiency (72). Additionally, it is recommended to use NAC within 12 h after acute APAP poisoning. The longer the injury time, the worse the detoxification effect is (73). Therefore, more effective treatments of APAP-induced injury are urgently needed.

3.3 The mechanism of acetaminophen (APAP)-induced liver injury

The mechanisms of APAP-induced liver injury are complicated, and nowadays the release of inflammatory cytokines, mitochondrial dysfunction and endoplasmic reticulum (ER) stress are recognized as main causes of APAP-induced liver injury (74, 75).

3.3.1 Reactive oxygen species (ROS) and oxidative stress

Oxidative stress is the result of the generation of ROS, which are a by-product of normal metabolism and have roles in cell signaling and homeostasis. Oxidative stress in acetaminophen toxicity is triggered by the formation of cellular superoxide or its dismutation, resulting in the formation of increased hydrogen peroxide through a variety of mechanisms, including the uncoupling of CYP450 or other enzymes from mitochondria (76, 77), or activation of NADPH oxidase (78). Glutathione depletion

results in increased intracellular peroxide levels and increased oxidative stress through the Fenton mechanism. This mechanism involves the reduction of peroxides by ferrous ions to the formation of highly reactive hydroxyl radicals, which can in turn lead to lipid peroxidation and the oxidation of proteins and nucleic acids (79).

The discovery of nitric oxide (NO) as an important signaling molecule has given people a deeper understanding of the mechanism of oxidative stress. Oxidative stress includes not only the classic Fenton mediated mechanism, but also nitric oxide. Enhanced production of superoxide radicals ($O_2^{\bullet}$) reacts with nitric oxide (NO), produced by inducible nitric oxide synthase (iNOS), forming peroxynitrite ($ONOO^-$) (80). The effects of iNOS on the liver have been studied in rats and mice. Gardner and colleagues (81) reported that a toxic dose of acetaminophen to rats can induce iNOS in centrilobular hepatocytes. The development of toxicity is related to the expression of iNOS. In addition, treatment of rats with iNOS inhibitor can reduce liver toxicity. The highly reactive and potent oxidant $ONOO^-$ causes nitration of protein tyrosine residues (82) which induces damage to mitochondrial DNA and the opening of the mitochondrial membrane pore.

The mechanism of the increase of reactive oxygen/nitrogen species in the toxicity of APAP has been extensively studied. Three different mechanisms have been proposed to explain the increase of reactive oxygen levels: uncoupled CYP2E1 or other enzymes (83), activated NADPH oxidase (78) and mitochondrial uncoupling (76). Through each mechanism, it can be foreseen that increased superoxide ($O_{2^{\cdot}}^{-}$) production is a key event. The increased level of superoxide can lead to an increase in the formation of hydrogen peroxide and peroxynitrite ($ONOO^-$) in cells.

However, mitochondrial oxidative stress alone is not sufficient to ultimately trigger cell death. A number of molecules have been found to participates in the regulation of APAP-induced oxidative stress, such as c-Jun N-terminal kinases (JNK) and the nuclear erythroid-2-related factor 2 (Nrf2), which may serve as potential therapeutic targets (84). JNK is a family of serine/threonine kinase belonging to the mitogen-activated protein kinases (MAPKs) family, and plays a conclusive role in DILI (85). Liver cell-specific *jnk1/2* deletion caused severe hepatic damage (86),

unraveling not only synergistic and protective actions of JNK1 and JNK2 in hepatocytes, but also that specific signaling cascades might be activated in other cell types (e.g. immune cells), and aggravate the course of DILI. Phosphorylation of JNK occurs early after APAP overdose and is mediated by MAP kinase kinases (MAP2Ks), which in turn are activated by MAP kinase kinase kinases (MAP3Ks) (29). The best characterized MAP3Ks are apoptosis signal-regulating kinase-1 (ASK1) and mixed-linage kinase 3 (MLK3). The oxidation of thioredoxin due to oxidative stress causes ASK1 to dissociate from its binding partner and then be activated. MLK3, a member of the Ser/Thr protein kinases family, mediates the initial phase of JNK activation (87). Glycogen synthase kinase 3β (GSK-3β) is also involved in the early-phase of JNK activation. Inhibition of GSK-3β in mice prevents JNK activation and ameliorates APAP-derived toxicity (88). The MAP2Ks, including mitogen-activated protein kinase kinase (MKK) 4 and MKK7, are capable of phosphorylating JNKs at Thr/Tyr residues (89). Furthermore, MKK4 activates both JNK and p38 and MKK7 activates only JNK (90). A feedforward self-sustaining signaling pathway referred as the JNK amplification loop (91, 92) would maintain sustained JNK activation, directly leading to liver damage and dysfunction. Activated JNK (p-JNK) translocates to mitochondria and binds to the Sab protein on the outer mitochondrial membrane (93, 94), impairing mitochondrial respiration and enhancing the release of ROS (95). ROS release, in turn, activates ASK1 and MKK4, which sustains JNK activity and amplifies the toxic effect (**Fig. 4**).

3.3.2 Mitochondrial dysfunction

Electron microscope examination of APAP-treated liver by the Racz laboratory indicated the changes of the mitochondrial morphology (96). Jollow *et al.* reported that the mitochondria is the target of acetaminophen reactive metabolites (68), and many arylated proteins have been found in mitochondria (97). Functional changes in the ability to chelate calcium have been reported (98). In isolated rat liver cells and *in vivo*, mitochondrial respiration is inhibited in complex I and II, but not in complex III (99-101). In addition, adenosine triphosphate (ATP) levels in the body and treated liver cells were reduced (101). Adding NAPQI to hepatocytes also showed similar

changes (102). The laboratories of Moldeus and Orenius reported that adding NAPQI to isolated rat liver mitochondria caused the release of chelated Ca^{2+} (103).

Given a toxic dose of APAP, superoxide anions are produced which increase ROS accumulation through a variety of mechanisms (104, 105). Free radical metabolites participate in the redox process and are capable of inducing cell damage and abnormal protein expression. The amplification of mitochondrial oxidative stress can reduce the synthesis of mitochondrial proteins and increase mitochondrial permeability transition (MPT), which increase mitochondrial membrane permeability (106) and lead to the collapse of the mitochondrial membrane potential (MMP). The mitochondria then swell, rupture and release proteins from the intermembrane space (107), a sequence implicated in cell death pathways such as apoptosis (108). Excessive APAP causes a series of toxic events such as mitochondrial respiratory depression, ATP depletion and mitochondrial oxidative stress (109).

According to reports, MPT inhibitors can block the toxicity of APAP *in vitro* and *in vivo*. Kon and colleagues (110) showed that cyclosporine A and the non-immunosuppressive Cyclosporine A analog NM811 inhibited the toxicity of APAP in cultured mouse liver cells. Cyclosporine A does not change the glutathione depletion caused by APAP, which indicated that inhibiting the metabolism of APAP to NAPQI could not prevent toxicity. Reid and his colleagues (111) studied the effects of MPT inhibitors in freshly isolated mouse liver cells (112, 113). In these studies, hepatocytes were incubated with APAP for 2 h, then washed out the APAP and incubated with medium alone. This method clearly separated direct metabolism from those occurring downstream of APAP metabolism. Toxicity occurred during the reincubation phase (3-5 hours). Adding MPT inhibitor or NAC during the reincubation stage could completely suppress toxicity. Through tetramethylrhodamine methyl ester (TMRM) and fluorescence analysis, it was shown that the loss of mitochondrial membrane potential caused by APAP can be prevented by adding MPT inhibitor and NAC during the reincubation period.

Necrosis is mediated by the opening of MPT pores in the inner mitochondrial membrane leading to the loss of ATP production capacity, and apoptosis may also be

caused by the opening of holes or channels in the outer mitochondrial membrane. It is believed that the pore releases pro-apoptotic factors, including cytochrome C, endonuclease G, Smac/Diablo, and apoptosis-inducing factor (AIF) from the cell membrane space into the cytosol (114, 115) (**Fig. 4**).

The phosphorylated JNK as a result of oxidative stress translocates to the mitochondria and binds to Sab on the outer mitochondrial membrane, thereby further inhibiting the transport of mitochondrial electrons through the Src-mediated pathway (116). The development of mitochondrial apoptosis-induced pathways seems to be sensitively regulated by Bcl-2 family proteins and is composed of pro-apoptotic proteins (eg: Bax) and anti-apoptotic proteins (eg: Bcl-2). In particular, the pro-apoptotic protein Bax is usually in the cytosol. Activation causes Bax to translocate to the mitochondria, insert into the outer membrane, and oligomerize to form channels (117-119). Apoptotic proteins were released from these channels (120). Whether hepatocytes die due to necrosis or apoptosis, the relative content of ATP seems to be an important factor. Low ATP levels are associated with necrosis, while adequate ATP levels contribute to cell apoptosis. It's showed that cultured mouse hepatocytes died mainly due to necrosis after APAP challenge. However, adding fructose (a glycolytic substrate for ATP production) and glycine (a membrane stabilizer) into the medium can reduce necrosis and promote cell apoptosis (121).

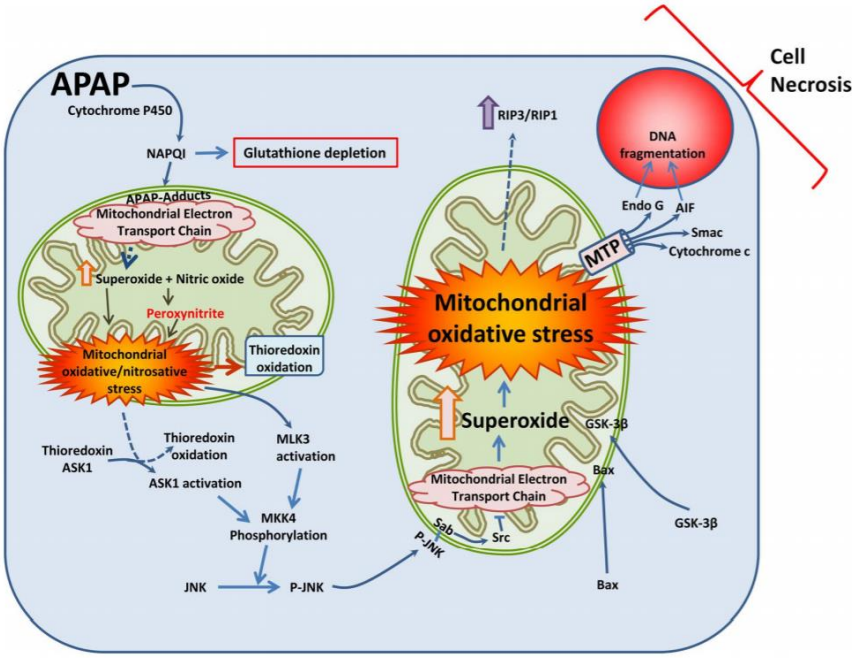

Figure 4. The mechanism of hepatocyte death induced by acetaminophen (APAP). At high concentrations of acetaminophen, components of the electron transport chain (such as ATP synthase) are affected, which disrupts the function of the respiratory chain and enhances the production of free radicals (such as superoxide). It reacts with nitric oxide (NO) in the mitochondria to form highly reactive nitrite, which weakens the mitochondria's antioxidant defense capabilities, leading to mitochondrial oxidative stress and the oxidation of proteins, such as mitochondrial thioredoxin. In the cytosol, the phosphorylated JNK translocates to the mitochondria and binds to Sab on the outer mitochondrial membrane, thereby further inhibiting the transport of mitochondrial electrons through the Src-mediated pathway. These events activate mitochondrial permeability transition and release mitochondrial inner membrane proteins, such as endonuclease G and apoptosis inducing factor (AIF), as well as cytochrome c and Smac, eventually leading to cell death (116).

3.3.3 Unfolded protein response (UPR) and endoplasmic reticulum (ER) stress

ER is the major cellular site of protein folding and modification, and made up of two subunits - rough ER (RER) and smooth ER (SER). The two types of ER share many of the same proteins and engage in certain common activities such as the synthesis of certain lipids and cholesterol. ER stress occurs when the amount of protein entering the ER exceeds its folding capacity. ER stress and the activation of UPR are associated with multiple liver diseases, including DILI. ER stress is induced late after APAP intoxication (a sublethal dose of over 300 mg/kg) in murine models, and becomes significant 12 h following APAP administration (122). There are some hypotheses on the mechanism how APAP induces ER stress. The first one is the

occurrence of microsomal alterations secondary to NAPQI generation. APAP induced GSH depletion, lipid peroxidation and an oxidative shift of the ER oxidoreductases Erp72 and protein disulfide isomerase (PDI) in liver microsomes (123). Moreover, NAPQI could bind with several microsomal proteins such as PDI and calreticulin, which play a major role in protein folding and calcium concentration within the ER (124). The other hypothesis is that ER stress might be the secondary consequence of mitochondrial dysfunction (125).

Under stress conditions, the ER initiates UPR to restore the balance. The UPR contains three signaling arms: inositol-requiring enzyme 1 (IRE1α), the protein kinase RNA-like ER kinase (PERK) and activating transcription factor 6 (ATF6) (126). These signaling pathways increase ER capacity, degrade misfolded proteins, reduce the synthesis of new protein entering the ER, and ultimately restore ER homeostasis. IRE1α is an ER transmembrane protein and maintained in an inactive state through binding to the glucose-regulated protein 78 kDa (GRP78), also known as binding immunoglobulin protein (BIP), in non-stressed cells. Upon APAP-mediated ER stress, IRE1α initiates splicing of the message RNA (mRNA) encoding X-box binding protein 1 (XBP1) and translocates to the nucleus, triggering an inflammatory response and promoting apoptosis mediated via ASK1 and JNK (127). Among the JNK apoptosis-inducing substrates, Bcl-2 and Bim are inhibited and activated by JNK phosphorylation, respectively (128, 129). If the stress is not relieved, a downstream transcription repressor of UPR, CCAAT-enhancer-binding protein homologous protein (CHOP), is activated (130). P38, one member of MAPK, phosphorylates and activates the transcription factor CHOP, thereby causing changes in gene expression that are conducive to apoptosis, including increasing the expression of Bim and DR5, while reducing the expression of Bcl-2 (131, 132). CHOP expression has been shown to sensitize cells to apoptosis (133). Dot and Uzi showed in their research that CHOP KO mice were protected from APAP induced damage and exhibited decreased liver necrosis and increased survival (122). All these data implicate that the arm of IRE1α- XBP1 plays a critical role in the APAP toxicity.

Moreover, IRE1α can also regulates the degradation of messenger RNA

encoding membrane proteins and secreted proteins through a process termed regulated IRE1-dependent decay (RIDD), which may have effects on the adaptive survival under ER stress. The RIDD process selectively targets and degrades mRNA encoding proteins involved in protein folding. Hur reported that in genetically deleted XBP1 mice, constitutive IRE1α hyperactivation in hepatocytes resulted in reduced JNK activation and protection from APAP through activation of RIDD and suppression of cytochrome P450 activity (134). However, the detailed mechanism of RIDD that mediated by IRE1α activation is still unknown and needs further study (**Fig. 5**).

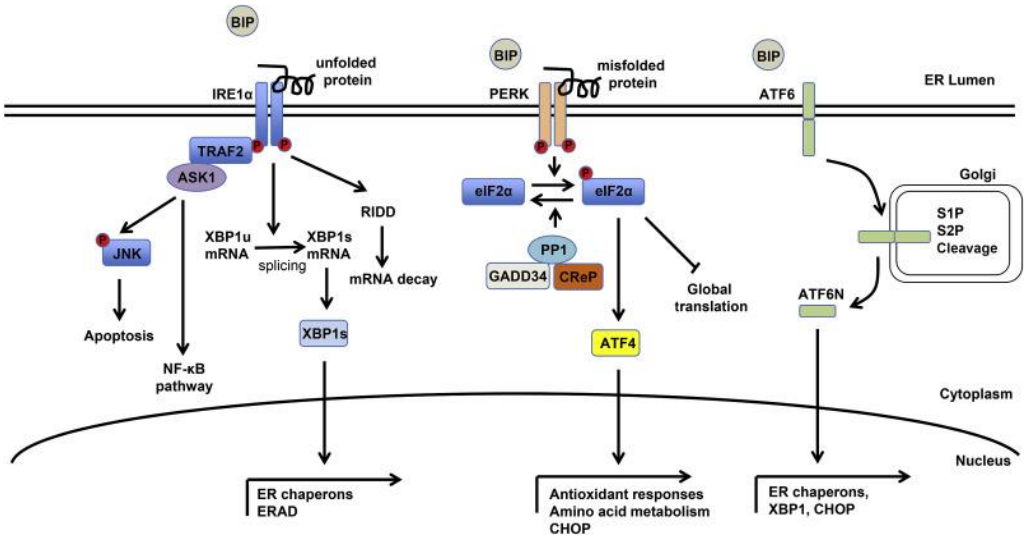

Figure 5. Unfolded protein response (UPR) pathways in the endoplasmic reticulum (ER) stress. The increase of misfolded or unfolded proteins in the ER lumen triggers ER stress-mediated UPR, which has three different effectors: the protein kinase RNA-like ER kinase (PERK), the activating transcription factor 6 (ATF6) and the inositol-requiring enzyme 1 (IRE1). Under ER Stress, IRE1α initiates splicing of the mRNA encoding X-box binding protein 1 (XBP1), PERK phosphorylates eukaryotic initiation factor 2α (eIF2α) and ATF6 is cleaved (clv. ATF6) and translocates to the nucleus, triggering apoptosis. IRE1α also recruits tumor necrosis factor (TNF) receptor associated factor 2 (TRAF2) and apoptosis signal-regulating kinase 1 (ASK1) to mediate the activation of c-jun N-terminal kinase (JNK) and nuclear factor kappa B (NF-κB) pathways, and regulates gene expression through regulated IRE1α-dependent decay of mRNA (RIDD)-mediated mRNA decay (135).

3.3.4 Sterile inflammation

Extensive cell necrosis after APAP overdose can lead to the release of damage-related molecular patterns (DAMP), including mitochondrial DNA, nuclear DNA

fragments and high mobility group-1 (HMGB1) protein (75, 136, 137). DAMP binds to pattern recognition receptors on inflammatory cells, such as toll-like receptors (TLR), and transcriptionally activates cytokines (138, 139). Some of these inflammatory mediators have constitutive activity, such as tumor necrosis factor α (TNFα) and interleukin-1α (IL-1α), while others are produced as precursors that require proteolytic cleavage, such as interleukin-1β (IL-1β) and interleukin-18 (IL-18) (138). The pro-inflammatory cytokines and chemokines can activate neutrophils and monocytes, and recruit these cells into the liver, which may aggravate existing liver injury (139). Although it is generally believed in the literature that APAP-induced cell necrosis will lead to the release of DAMPs, the formation of pro-inflammatory mediators and the recruitment of inflammatory cells to the liver, the effect of sterile inflammation is controversial. The first controversy is whether neutrophils, the first responder to the initial cell death, cause the damage. The main support for this hypothesis comes from research that shows that neutropenia has a protective effect on APAP hepatoxicity (140). However, long-term neutropenia can lead to a preadaptation effect, which is protective independent of the actual neutrophil (141). In addition, inactivating neutrophils by inhibitor or the use of knockout mice cannot resist APAP-induced liver damage (142, 143). In human patients, no neutrophil activation or neutrophil-mediated oxidative stress was observed (144). In short, these findings strongly oppose the direct involvement of neutrophils in the injury. The second controversy is the role of certain proinflammatory mediators, especially IL-1β. It is reported that DNA fragments can promote the formation of pro-IL-1β. The Nalp3 inflammasome is activated, leading to the activation of caspase 1, and processing pro-IL-1β into active cytokine (145). However, caspase inhibitors can prevent the formation of IL-1β but cannot protect against APAP toxicity, and adding high doses of exogenous IL-1β can enhance the recruitment of neutrophils, but will not affect APAP-induced liver damage (146). Recently, another study showed that mice deficient in IL-1β, caspase 1 or Nalp3 have no protection against APAP hepatotoxicity (147), indicating that inflammasome activation and IL-1β formation are of limited importance for APAP-induced liver damage. However, Zhang and

colleagues suggested that IL-1α plays a role in pathophysiology. IL-1α is produced by KCs through toll-like receptor (TLR) 4 stimulation, not by TLR9 or TLR3-dependent mechanisms (147). Subsequent studies have shown that the administration of recombinant human IL-1R antagonists may also ameliorate APAP-induced liver injury (148). The mice lacking TLR9, Nalp3, Caspase-1 or ASC and the pharmacological antagonism of TLR9 alleviated APAP-induced liver injury and increased survival 72 h after administration (145).

In view of all above information, it is obvious that a large amount of DAMP is released after APAP-induced necrosis, and excessive DAMPs lead to characteristic neutrophil and monocyte recruitment (142, 149-151) and affect signaling mechanisms in the cells (152) after APAP overdose. In addition, the expression of precursor of IL-1β gene increases, which indicates that the release of DAMP after APAP challenge can activate the inflammasome and change plasma IL-1β which can be routinely detected when APAP overdose (146). In this way, the idea that the sterile inflammatory response involving the activation of inflammasomes potentially contributes to liver damage caused by APAP in mice, which is clearly supported by many convincing evidences.

4. Objectives

In this study, we aimed to:

1) Correlate APAP hepatotoxicity with activation of UPR and markers of ER stress *in vitro*;
2) Correlate APAP hepatotoxicity with activation of UPR and markers of ER stress *in vivo*;
3) To understand the role of hepatocytic *Xbp1* in APAP-mediated hepatotoxicity;
4) To analyze the molecular mechanisms in $Xbp1^{\Delta hepa}$ mice with APAP challenge, in order to evaluate its potential pathophysiological relevance and provide the basis for therapies after DILI.

5. Materials and Methods

5.1 Materials

5.1.1 Chemicals

Reagent	Manufacturer	Catalog
4X Laemmli buffer	Bio-Rad, Hercules, USA	16107474
Acetaminophen	Sigma-Aldrich, Steinheim, Germany	A7085
Acetic acid reagent plus I,>=99%	Sigma-Aldrich, Steinheim, Germany	A6283
Acetone	AppliChem, Darmstadt, Germany	131007
30% Acrylamide/Bis Solution	Bio-Rad, China	1610156
AEBSF hydrochloride	Thermo Fisher Scientific, Karlsruhe, Germany	10563165
Agarose electrophoresis grade	Sigma-Aldrich, Steinheim, Germany	A9539
Ammonium persulfate (APS)	Bio-Rad, Shinagawa, Japan	1610700
Bovine Serum Albumin (BSA, lyophilized powder, ≥96%)	Sigma-Aldrich, Steinheim, Germany	A2153
Calcium chloride	Sigma-Aldrich, Steinheim, Germany	C5670
Cell counting Kit – 8	Sigma-Aldrich, Steinheim, Germany	96992
Cell incubator clean reagent	AppliChem, Barcelona, Spain	A5230,1000
Chloroform	AppliChem, Barcelona, Spain	A3691.1000
Complete mini	Roche, Mannheim, Germany	11836153001
Vectasheld mounting medium with DAPI	Vector Laboratories, Burlingame, USA	H-1200
ImmPACT DAB HRP Substrate	Vector Laboratories, Burlingame, USA	SK-4105

D (+)-Sucrose	AppliChem, Barcelona, Spain	131621.1211
DEPC water (Water for molecular biology)	AppliChem, Barcelona, Spain	A7398.0500
DMEM with high glucose, without L-glutamine, with sodium pyruvate	GE Healthcare, Logan, USA	SH30285.01
Dimethyl sulfoxide (DMSO)	Sigma-Aldrich, Saint-Quentin-Fallavier, France	D4540
Dithiothreitol (DTT)	Thermo Fisher Scientific, Rockford, USA	20291
DNA Ladder (50 bp)	Invitrogen, Vilnius, Lithuania	10416014
di-Sodium hydrogen phosphate 7-hydrate for analysis	AppliChem, Barcelona, Spain	132656.1211
ECL prime western blotting detection reagents	GE Healthcare, Amersham, UK	RPN2232
Eosin Y	Sigma-Aldrich, Steinheim, Germany	E4009
Ethanol absolute for analysis	AppliChem, Barcelona, Spain	131086.1214
Ethylenediamine-tetraacetic acid disodium salt dihydrate (EDTA)	Sigma-Aldrich, Steinheim, Germany	E5134
Fetal bovine serum (FBS)	Thermo Fisher Scientific, Boston, USA	10270106
Formaldehyde stabilized with methanol for clinical diagnosis	AppliChem, Barcelona, Spain	252931.1214
Gelatin from bovine skin, Type B	Sigma-Aldrich, Steinheim, Germany	G6650-500G
Glutaraldehyde	Electron Microscopy Sciences, Hatfield, USA	16400
Glycine for molecular biology	AppliChem, Barcelona, Spain	A1067,5000

Glycerol, for molecular biology, ≥99%	Sigma-Aldrich, Steinheim, Germany	G5516-500ML
Gibco™ Goat Serum	Gibco, Paisley, UK	11530526
HepaRG differenctiation medium	Biopredic international, Saint-Grégoire, France	ADD720
HepaRG growth medium	Biopredic international, Saint-Grégoire, France	ADD710
HepaRG thawing/plating/general purpose medium suplement with antibiotics	Biopredic international, Saint-Grégoire, France	ADD670
HepaRG maintenance and metabolism medium supplement with antibiotics	Biopredic international, Saint-Grégoire, France	ADD620
HyClone L glutamine	GE healthcare life sciences, Logan, USA	SH30034.01
Trypsin EDTA	Lonza, Verviers, Belgium	BE17-161E
Mayer's hematoxylin	AppliChem, Barcelona, Spain	254766.1611
37 % Hydrochloric acid technical grade	AppliChem, Barcelona, Spain	211020.1611
30 % Hydrogen peroxide	AppliChem, Barcelona, Spain	121076.1211
Isopropanol	AppliChem, Barcelona, Spain	131090.1612
Isoflutek	Karizoo, Barcelona, Spain	586259.0
Magnesium chloride hexahydrate	Sigma-Aldrich, Steinheim, Germany	M2670
Midori green advance	Nippon genetics, Düren, Germany	MG04
Methanol BioChemica	AppliChem, Barcelona, Spain	A3493.5000
Nonfat dried milk powder	AppliChem, Barcelona, Spain	A0830,0500
Nonidet P-40	AppliChem, Barcelona, Spain	A1694,0250

Oil Red O	Sigma-Aldrich, Steinheim, Germany	O0625-25G
Osmium tetroxide	Electron Microscopy Sciences, Hatfield, USA	19172
PhosSTOP	Roche, Mannheim, Germany	4906837001
Ponceau S solution	Sigma-Aldrich, Steinheim, Germany	P7170
Potassium chloride> 99.0% KCl	Sigma-Aldrich, Steinheim, Germany	P9541-500G
Protein assay dye reagent concentrate	Bio-Rad, Hercules, USA	5000006
Roti-histokit	Carl Roth, Karlsruhe, Germany	6638.2
Restore western blot stripping buffer 500ml	Thermo Fisher Scientific, Rockford, USA	21059
Sodium chloride for molecular biology	AppliChem, Barcelona, Spain	A2942,5000
Sodium dhydrogen phosphate momohydrate	AppliChem, Barcelona, Spain	106346,1000
Sodium fluoride	Sigma-Aldrich, Steinheim, Germany	215309
Sodium dodecyl sulfate (SDS)	AppliChem, Barcelona, Spain	A2572,0500
Sodium hydroxide	AppliChem, Barcelona, Spain	131687
STF-083010	Medchemexpress, New Jersey, USA	307543-71-1
TEMED	Bio-Rad, Hercules, USA	1610801
Tissue-Tek® O.C.T.™ Compound	Sakura, Warsaw, Poland	4583
Trizol reagent	Thermo Fisher Scientific, Austin, USA	5596018

Tris	AppliChem, Barcelona, Spain	A1379,1000
tri-Sodium citrate 2-hydrate	AppliChem, Barcelona, Spain	1316551210
Triton X-100	AppliChem, Barcelona, Spain	A4975,0100
Tween 20	Sigma-Aldrich, Saint-Quentin-Fallavier, France	P1379-500ML
William's E medium, GlutaMAX™ Supplement	Gibco, Paisley, UK	3255108
Xylene	Carl Roth, Karlsruhe, Germany	9713.5

5.1.2 Standard buffer and media

10x SDS-Running Buffer	**Volume/Quality**
Tris	30.3 g
Glycine	144.13 g
SDS	10 g
dH_2O add to	1 L

10x Transfer Buffer	**Volume/Quality**
Tris	30.3 g
Glycine	144.13 g
dH_2O add to	1 L
1x Transfer Buffer	**Volume/Quality**
10x Transfer Buffer	100 ml
Methanol	200 ml
dH_2O add to	1 L

10x TBS	**Volume/Quality**	**PH value**
Tris	24.2 g	PH=7.6
NaCl	80 g	
dH_2O add to	1 L	

1x TBST	**Volume/Quality**	
10x TBS	100 ml	
Tween-20	0.5 ml	
dH_2O add to	1 L	

10x PBS	**Volume/Quality**
NaCl	78.8 g
KCl	3.5 g
Na_2HPO_4	26.8 g
NaH_2PO_4	2.76 g
dH_2O add to	1 L

NP40 Buffer	**Volume**	**Final concentration**
Tris/HCl 7.5 pH (1 M)	25 ml	50 mM
NaCl (5 M)	15 ml	150 mM
Nonidet P-40	2.5 ml	0.5 %
Sodium Fluoride	1.05 g	50 mM
dH_2O added to	500 ml	

NID buffer	**Volume/Quality**	**Final Concentration**	**PH value**
KCl	3.73 g	0.05 M	PH=8.3
Tris	10 ml	0.01 M	
$MgCl_2$	0.41 g	2 mM	
Gelatine Type B	0.1 g	0.1 mg/ml	
NP-40	4.5 ml	0.45 %	
Tween-20	4.5 ml	0.45 %	

5.1.3 Standard kits and enzymes

Kit / Assay	**Manufacturer**

In Situ Cell Death Detection Kit, Fluorescein	Roche, Mannheim, Germany
High Capacity cDNA Reverse Transcription Kit	Thermo Fisher Scientific, Vilnius, Lithuania
Cell Counting Kit - 8	Sigma-Aldrich, Darmstadt, Germany
Triglycerides liquicolor mono kit	RAL, Barcelona, Spain
ImmPACTI DAB HRP Substrate	Vector Laboratories, Burlingame, USA

Enzyme	**Manufacturer**
Proteinase K-Solution	AppliChem, Darmstadt, Germany
ReadyMixTM redtaq^{TM} PCR reaction mix with MgCl2	Sigma-Aldrich, Steinheim, Germany
RNAse	Sigma-Aldrich, Steinheim, Germany
SYBR® GreenER^{TM} qPCR Super Mix	Invitrogen, Karlsruhe, Germany

5.1.4 Antibodies used for immunostaining and/or western blot

5.1.4.1 Primer antibodies

Product	**Manufacturer**	**Catalog**	**Concentration**
pAKT	Cell Signaling Technology	9271S	1:1000 (WB)
AKT	Cell Signaling Technology	9272S	1:1000 (WB)
p-AMPKα (T172)	Cell Signaling Technology	2535S	1:1000 (WB)
AMPKα	Cell Signaling Technology	2532S	1:1000 (WB)
BIP	Cell Signaling Technology	3177S	1:1000 (WB)
Cytochrome P450	Abcam	ab28146	1:1000 (WB)

2E1 (CYP2E1)			
CD11b	BD Bioscience	550282 (M1/70)	1:100 (IF)
CD45	BD Bioscience	550539 (30-F11)	1:100 (IF)
CHOP	Cell Signaling Technology	2895S	1:1000 (WB)
Cleaved Caspase3	Cell Signaling Technology	9661S	1:1000 (WB)
F4/80	BIO-RAD	MCA497	1:100 (IF)
GAPDH	BIO-RAD	MCA4739	1:5000 (WB)
4HNE	Abcam	ab46545	1:100 (IHC)
p-IRE1α	NOVUS BIOLOGICALS	NB100-2323	1:1000 (WB)
IRE1α	Cell Signaling Technology	3294S	1:1000 (WB)
IL-1β	Abcam	ab9722	1:1000 (WB)
Ki67	Abcam	ab16667	1:100 (IHC/IF)
pJNK	Cell Signaling Technology	9251S	1:1000 (WB)
JNK	Cell Signaling Technology	9252S	1:1000 (WB)
pJNK1	BIONOVA (Novus Biologicals)	NB100-82009	1:1000 (WB)
JNK1	Cell Signaling Technology	3708S	1:1000 (WB)
pJNK2	BIONOVA (Novus Biologicals)	NBP1-45787	1:1000 (WB)
JNK2	Cell Signaling	4572S	1:1000 (WB)

	Technology		
LC3A/B (D3U4C)	Cell Signaling Technology	12741	1:1000 (WB)
NLRP3	Abcam	ab214185	1:1000 (IHC)
P62	Cell Signaling Technology	39749	1:1000 (WB)
XBP1s (D2C1F)	Cell Signaling Technology	12782S	1:1000 (WB)
XBP1	Abcam	ab37152	1:1000 (WB)
ZO-1	Invitrogen	61-7300	1:1000 (WB)
XBP1	Abcam	ab220783	1:1000 (WB)

5.1.4.2 Secondary antibodies

Product	**Manufacturer**	**Catalog**	**Concentration**
Anti-rabbit-HRP	Cell Signaling Technology	7074S	1:3000 (WB)
Anti-Mouse-HRP	BIO-RAD	STAR207P	1:5000 (WB)
Anti-Rabbit-HRP IgG	Vector Laboratories	MP-7401	ready-to-use (IHC)
Anti-Mouse-HRP IgG	Vector Laboratories	MP-7402	ready-to-use (IHC)
Goat-Anti-Rat (IF, 488)	Invitrogen	A-11006	1:400 (IF)
Goat-Anti-Mouse (IF, 488)	Invitrogen	A-11001	1:400 (IF)
Donkey-Anti-Rabbit (IF, 488)	Invitrogen	A-21206	1:500 (IF)

5.1.5 Primer sequences used for RT-qPCR

5.1.5.1 Primer for Human:

Gene	Forward	Reverse
Ire1α	TGCTTAAGGACATGGCTACCATCA	CTGGAACTGCTGGTGCTGGA
Bip	GCTCGACTCGAATTCCAAAG	TTTGTCAGGGGTCTTTCACC
sXbp1	CGCTTGGGGATGGATGCCCTG	CCTGCACCTGCTGCGGACT
uXbp1	TGGCCGGGTCTGCTGAGTCCG	ATCCATGGGGAGATGTTCTGG
Chop	TTCTCTGGCTTGGCTGACTG	CTGCGTATGTGGGATTGAGG
Gapdh	CAAGGTCATCCATGACAACTTTG	GTCCACCACCCTGTTGCTGTAG

5.1.5.2 Primer for Mouse:

Gene	Forward	Reverse
Atg5	ACAGCTTCTGGATGAAAGGC	TGGGACTGCAGAATGACAGA
Beclin1	TGA TCC AGG AGC TGG AAG AT	CAA GCG ACC CAG TCT GAA AT
Bip	TTC AGC CAA TTA TCA GCA AAC TC	TTT TCT GAT GTA TCC TCT TCA CC
Casp1	TCC CAG TCA GTC CTG GAA ATG	ACA AGG CAC GGG ACC TAT G
Chop	CCA CCA CAC CTG AAA GCA GAA	AGG TGA AAG GCA GGG ACT CA
Cye2e1	CGCTTCGATTACGATGACAA	TGTGCTGGTGGTCTCTGTTC
eIF2α	GGA CCA CCA CAC TTC ACA GA	TCC CTT GTT AGC GAC ATT GA

Gapdh	TGTTGAAGTCACAGGAGACAA CCT	AACCTGCCAAGTATGATGA CATCA
HO-1	GAATCGAGCAGAACCAGCCT	GCCTTCTCTGGACACCTGA C
IL-1β	TGT GTG ACG TTC CCA TT	CAG CAC GAG GCT TTT TTG TTG
Ire1α	TGC TCA AGG ACA TGG CTA CCA TTA	CTG GAA CTG TTG GTG CTG GA
Lc3b	CCG AGA AGA CCT TCA AGC AG	ACA CTT CGG AGA TGG GAG TG
Nlrp3	TGT GAG AAG CAG GTT CTA CTC T	TGT AGC GAC TGT TGA GGT CCA
p62	AGA ATG TGG GGG AGA GTG TG	TCG TCT CCT CCT GAG CAG TT
Tnfα	CCTCTTCTCATTCCTGCTTGTGG	GAGAAGATGATCTGAGTGT GAGG
sXbp1	CTGAGTCCGAATCAGGTGCAG	GTCCATGGGAAGATGTTCT GG
uXbp1	TGGCCGGGTCTGCTGAGTCCG	GTCCATGGGAAGATGTTCT GG

5.1.6 Primer sequences used for genotyping PCR

Reagent	**Forward**	**Reverse**
Xbp1	CAAGGTGGTTCACTGCCTGTA AT	ACTTGCACCAACACTTGCC ATTT
AlbCre-01	TGC AAA CAT CAC ATG CAC AC	
AlbCre-02	TTG GCC CCT TAC CAT AAC TG	
AlbCre-03	GAA GCA GAA GCT TAG GAA GATGG	

5.1.7 Instruments and equipment

Product	**Manufacturer**
Adobe Photoshop CS6 13.0*32	Adobe Systems, San Jose, USA
AxioVision SE64. Rel.4.9	Carl Zeiss Microscopy GmbH, München, Germany
Centrifuge 5415 D	Eppendorf AG, Hamburg, Germany
Centrifuge 5804/5804R	Eppendorf AG, Hamburg, Germany
Centrifuge 5920 R	Eppendorf AG, Hamburg, Germany
Centrifuge 4K15 10740	DJB Labcare Ltd, Buckinghamshire, UK
Centrifuge Z233M-2 and Refrigerated Z233MK-2	Hermle Labor Technik GmbH, Wehingen Germany
Class II Bio II Advance Plus Microbiological Safety Cabinet	Azbil Telstar Technologies Slu, Barcelona, Spain
Cryostat CM1950	Leica Biosystems Nussloch GmbH, Wetzlar, Germany
Digital microscope camera Moticam 2500	Ryf AG, Bettlachstrasse, Switzerland
Gel Doc 2000 System	BioRad, Neuberg, Germany
ImageJ Version 1.52u	LOCI, University of Wisconsin, USA
Leica EG1160 Embedding Center, Dispenser + hot Plate	Leica Biosystems Nussloch GmbH, Wetzlar, Germany
Leica MZ16 Stereomicroscope with Leica DFC480 Digital Camera	Leica Microsystems, Milton Keynes, United Kingdom
Leica HI1210 Water bath for paraffin sections	Leica Biosysetems, Heidelberger, Germany
Leica RM2125 RTS - The Essential Microtome	Leica Biosysetems, Heidelberger, Germany
Microcentrifuge	National Labnet, Madrid, Spain

7300 Real Time PCR System AND Sequence Detection Software Version 1.3.1	Applied Biosystems, Darmstadt, Germany
2100-Retriever	Aptum Biologics, Hants, United Kingdom
Odyssey Fc Imaging system	LI-COR, Madrid, Spain
Transmission electron microscope (TEM) Jeol 1010	Jeol, Peabody, USA
Thermo Scientific Forma Steri-Cycle i250 C02 incubator	Thermo Fisher Scientific, Boston, USA
Thermomixer	Eppendorf, Hamburg, Germany
Vertical laminar flow workbench, Mini-V/PCR	Azbil Telstar Technologies Slu, Barcelona, Spain
Vortex Reax 200	Heildophin, Nürnberg, Germany
Video Copy Processor P90E	Mitsubishi, Kyoto, Japan
Water bath (STANDARD of 12877)	DILABO, Torralba de Calatrava, Spain
ZEISS Axio Lab.A1	Carl Zeiss Microscopy GmbH, Jena, Germany

5.1.8 Other equipment

Plastic and Glassware	**Manufacturer**	**Catalog**
Big flacon 50ml	Labbox, Barcelona, Spain	PTGP-E050-500
Blue tips 1ml	Greiner Bio-One, Frickenhausen, Germany	740290
Cell culture plate sterile, 96 Well, F-bottom with lid	Greiner Bio-One, Frickenhausen, Germany	655180
CellStar® Cell Culture Multiwell Plates, Wells=6	Greiner Bio-One, Frickenhausen, Germany	657160
CELLSTAR® Cell Culture	Greiner Bio-One,	665180

Multiwell Plates, Wells=12	Frickenhausen, Germany	
Centrifuge tube 50ml (falcon)	Labbox, Barcelona, Spain	PTGP-E50-025
Coverslips	Hirschmann, Neckartenzlingen, Germany	8000120
Cryogenic tubes	Thermo Fisher Scientific, Suzhou, China	375353PK
Easypet 3 electronic pipetting	Eppendorf, Hamburg, Germany	4430000018
Eppendorf® Reference® 2 G single-channel, fixed, volume (10 µl)	Eppendorf, Hamburg, Germany	EP4925000049
Eppendorf® Reference® 2 G single-channel, fixed, volume (100 µl)	Eppendorf, Hamburg, Germany	EP4925000103
Eppendorf® Reference® 2 G single-channel, fixed, volume (1000 µl)	Eppendorf, Hamburg, Germany	EP4925000154
Eppendorf™ Tubes (1.5ml)	Thermo Fisher Scientific, Hamburg, Germany	10398031
Falcon Tissue Culture Treated Flasks (50ml)	Thermo Fisher Scientific, Hamburg, Germany	10634501
Falcon Tissue Culture Treated Flasks (250ml)	Thermo Fisher Scientific, Hamburg, Germany	10537161
Graduated Filter Tip (Sterile) 10 µl	STARLAB, Hamburge, Germany	S1120-3810
MicroAmp Fast Optical 96 Well Reaction Plate, 0.1ml	Thermo Fisher Scientific, Suzhou, China	43-469-06
MicroAmp Optical Adhesive Film	Thermo Fisher Scientific,	43-119-71

	Carlsbad, USA	
MicroAmp Optical 8-Tube Strip with attached optical caps	Thermo Fisher Scientific, Cramlington, UK	A30588
Mini Trans-Blot® Electrophoretic Transfer Cell	Bio-Rad, Portland, USA	170-3930
Nitrocellulose blotting membrane, 0.2 μm	Amersham, Dornstadt, Germany	A19478273
Nitrocellulose blotting membrane, 0.45 μm	Amersham, Dornstadt, Germany	A10021531
Pipettes 5 ml	Greiner Bio-One, Frickenhausen, Germany	606107
Pipettes 10ml	Greiner Bio-One, Frickenhausen, Germany	607180
Polyvinylidene difluoride (PVDF) membrane	Bio-Rad, Hercules, USA	1620264
Sarstedt Inc PC MTUBE 1.1ML SER-GEL/PK100	Thermo Fisher Scientific Suzhou, China	NC9436363
Slides	Klinipath, Lutterworth, UK	PR-S-100
Syringes 1 mL Luer	BD Plastipak, Madrid, Spain	303172
Small falcon 15ml	Labbox, Barcelona, Spain	PTGP-E15-500
Syringe 1 ml with 27 × 13 needle	BD Plastipak, Madrid, Spain	300635
Whatman® paper (Thick Blot Filter Paper, For WB)	BIO-RAD, Hercules, USA	1704085
Yellow tips 200μl	Greiner Bio-One, Frickenhausen, Germany	739290

5.2 Methods

5.2.1 Housing and breeding of mice

All mice strains were housed in filter-top cages and bred in a pathogen-free, temperature and humidity-controlled facility at the Institute for Medicine faculty, Complutense University (UCM). The animal facility was standardized with 12 h light-dark cycles and the mice had free access to standard food and water. All animal experiments were approved by the authorities and all animal received humane care according to laws on protection of animals and University requirements and guidelines (PROEX- 218/17).

5.2.2 Mice strain

For our study we used WT male mice with C57BL/6 background (ENVIGO, Valencia, Spain), and mice of male gender with specific hepatic-knockout of *Xbp1* (*Xbp1*$^{\Delta hepa}$) and *Xbp1* floxed (*Xbp1*$^{f/f}$) littermates from same breeding couples with C57BL/6 background. C57BL/6-*Xbp1*$^{f/f}$ mice with loxP sites flanking exon 2 of the *Xbp1* gene were kindly provided by prof. Eduardo Martinez Naves (153), and C57BL/6-Albumin-Cre mice were purchased from The Jackson Laboratory (B6.Cg-Tg(Alb-cre)21Mgn/J, Maine, USA). Alb Cre mice were crossed to *Xbp1*$^{f/f}$ mice to generate *Xbp1*$^{\Delta hepa}$ mice. These mice allowed to analyze XBP1 function selectively in hepatocytes *in vivo*.

5.2.3 Genotyping of genetically modified mice

The correct genotypes were verified by PCR analysis. DNA was prepared from fresh mouse tail biopsies using NID buffer. Each tail was digested with 200 µl of NID buffer and 1 µl of proteinase K (AppliChem, Darmstadt, Germany) at 56 ℃ overnight. Enzyme activity was stopped by heating at 95 ℃ for 10 min. Then the tails were centrifuged at 12000 *rpm* for 10 min, and 2 µl of the supernatant was used for PCR reaction.

NID buffer was prepared as follows:

Reagent	**Volume/Quality**	**Final Concentration**	**PH value**
KCl	3.73 g	0.05 M	PH=8.3
Tris	10 ml	0.01 M	
$MgCl_2$	0.41 g	2 mM	

Gelatine Type B	0.1 g	0.1 mg/ml	
NP-40	4.5 ml	0.45 %	
Tween-20	4.5 ml	0.45 %	

PCR reaction reagents were as follows:

a. Mixture for genotyping for *Xbp1*:

Reagent	**Volume**
DNA	2 µl
Primer 01	1 µl
Primer 02	1 µl
RedTaq	12.5 µl
DEPC H_2O	8.5 µl
TOTAL	25 µl

b. Mixture for genotyping for *AlbCre*:

Reagent	**Volume**
DNA	2 µl
Primer 01	1 µl
Primer 02	1 µl
Primer 03	1 µl
RedTaq	12.5 µl
DEPC H_2O	7.5 µl
TOTAL	25 µl

PCR was carried out according to the following cycling programs:

a. Program for genotyping for *Xbp1*:

PCR program	**temperature**	**time (h:min:sec)**	**Cycles**
initial denaturing	94 ℃	00:03:00	
denaturing	94 ℃	00:00:30	X 30
annealing	56 ℃	00:00:45	
elongation	72 ℃	00:00:45	
final elongation	72 ℃	00:10:00	

conservation	4 ℃	00:00:00	

b. Program for genotyping for *Albcre*:

PCR program	**temperature**	**time (h:min:sec)**	**Cycles**
initial denaturing	94 ℃	00:02:00	
denaturing annealing elongation	94 ℃ 65 ℃ 72 ℃	00:00:20 00:00:15 -0.5 ℃ per cycle 00:00:10	X 10
denaturing annealing elongation	94 ℃ 60 ℃ 72 ℃	00:00:15 00:00:15 00:00:10	X 28
final elongation conservation	72 ℃ 10 ℃	00:02:00 00:00:00	

PCR products were separated by 2% (w/v) agarose gels. The agarose was boiled in 1x TAE buffer until the solution is completely clear and no small floating particles are visible, cooled at room temperature for 5-10 min, and 6 µl of MIDORI Green Advance (Nippon genetics, Düren, Germany) was added and mixed gently. Gel were run in 1x TAE buffer at 120 V. DNA ladders (Invitrogen, Vilnius, Lithuania) were used to determine the specific size of fragments. After the electrophoretic run, view the results on a UV-transilluminator and print out with Video copy processor.

5.2.4 Blood and tissue sampling procedures

5.2.4.1 Taking of blood samples

8-12 weeks old mice were sacrificed under overdose by isoflurane, following the abdominal cavity was cut open along the linea alba. Intestine was moved aside to expose the inferior vena cava. Blood samples were extracted out by penetrating the inferior vena cava with a 1 ml syringe and then were collected in a serum tube and centrifuged at 12000 *rpm* for 10 min. Serum transaminases are specific markers for liver damage. For this study, serum was diluted 1:5 for measuring serologic markers such as alanine aminotransferase (ALT), aspartate aminotransferase (AST) and lactate dehydrogenase (LDH) in the clinical laboratories of hospital Gregorio Maranon,

Madrid. The left serum was stored at -80 ℃.

5.2.4.2 Extraction and sectioning of liver

At the mice were sacrificed, their body weight was recorded. The liver was carefully taken out and the liver weight was recorded. Then the liver was cut into small pieces in the same way for RNA isolation and protein isolation stored in liquid nitrogen and then transferred to -80 ℃. And two pieces from different livers were fixed in 4% formaldehyde for 48 h and then embedded in paraffin. Using paraffin blocks, serial 5 μm sections were performed and subsequently stained with H&E or immunohistochemical staining following routine protocols. The same part of each liver was taken and put the fresh liver tissue in Tissue-Tek® O.C.T.™ Compound (Sakura, Warsaw, Poland) and kept in -80 ℃ for the frozen section.

5.2.5 Intraperitoneal injection of APAP and STF-083010

10-12 weeks old WT mice got an intraperitoneal (IP) injection of acetaminophen (0-300 mg/kg). Before injection, mice were fasted overnight. Mice were gently restrained by grasping the mice by the loose skin of the neck and back to immobilize the head. Identify anatomical landmarks in order to inject into the appropriate area of the abdomen, usually the lower right quadrant of the mice abdomen. Disinfect the skin, insert needle with bevel facing "up" towards the head at 30-40^{o} angle to horizontal, and then inject acetaminophen (Sigma-Aldrich, Steinheim, Germany). *Xbp1*$^{\Delta hepa}$ and *Xbp1*$^{f/f}$ littermates were challenged with an intraperitoneal (IP) injection of acetaminophen (500 mg/kg) or vehicle. Because the dose is high and acetaminophen is insoluble in water, acetaminophen should be dissolved in DMSO first, then dilute to 50 mg/ml acetaminophen solution in warm PBS. Control mice received an equivalent volume of PBS with DMSO. The concentration of DMSO should be less than 1%. Then the mice were kept fasted for another 2 h, and allowed food *ad libitum*.

We also applied STF-083010 (MedchemExpress, New Jersey, USA) in WT mice to further explore the role of *Xbp1* in APAP-induced liver injury. STF-083010 is a small molecule inhibitor of *Xbp1* splicing by directly inhibiting IRE1α RNase activity, as the potent treatment modality for ER stress-induced impairments. Similar to APAP, STF-083010 was first dissolved in 10% DMSO then diluted in room temperature PBS. 75

mg/kg STF-083010 or equal volume of PBS with 10% DMSO were intraperitoneally injected 1 h before APAP model induction based on the study of Chen Shen *et al* (154).

5.2.6 Cell culture

5.2.6.1 Cell culture procedures

HepaRG™ cells (Biopredic international, Saint-Grégoire, France) is a unique and well-established hepatic cell system, which can produce not only early hepatic progenitor cells but also mature human hepatocytes. HepaRG cells provide an *in vitro* tool to do research in a fully metabolic and scalable system. HepaRG cells were purchased from Biopredic (Saint Gregoire, France).

HepaRG cells is cultured using specialized media at 37 ℃, 5% CO_2 and saturating humidified atmosphere following the supplier's protocols. Each medium was made up using William's Medium E with 1% GlutaMAX (Gibco, Paisley, UK) as the basal medium with appropriate additives. Number was determined using counting chamber and trypan blue staining. Viability of cells was measured by cell counting kit-8 (CCK-8) (Sigma-Aldrich, Darmstadt, Germany). Cells were first maintained in growth medium for 2 weeks, then changed to differentiation medium for another 2 weeks. At this stage, HepaRG cells reach a differentiated hepatocyte-like morphology and express liver-specific functions. Then differentiated cells were plated on 6-well tissue culture plate (protein and RNA extraction), 96-well cell culture plate (quantitation of cell viability) or 12-well tissue culture plate with coverslips (immunofluorescence) with thaw, plate & general purpose working medium, 2 days later changed to maintenance/metabolism medium. 7 days after plating, the cells are ready for experiments. Differentiated HepaRG cells were fasted 4 h and challenged with different concentrations of acetaminophen (0-20 mM). 24 h after APAP challenge, HepaRG cells and supernatant were collected. The coverslips were fixed with 4% PFA for 14 min, then stored in PBS at 4 ℃ for TUNEL, ORO and ZO-1 staining.

5.2.7 Isolation and analysis of RNA

5.2.7.1 RNA isolation and determination of RNA concentration

RNA was extracted from frozen mouse liver using TRIZOL (Thermo Fisher Scientific, Austin, USA) according to the manufacturer's recommendations. A little

piece of liver tissue was minced in TRIZOL with an electric homogenizer. After adding 200 µl chloroform, the lysates were incubated at room temperature for at least 20 min followed by centrifugation at 12000 *rpm* at 4℃. The upper supernatant was incubated 15 min with isopropanol and RNA was pelleted by centrifugation at 12000 *rpm* at 4℃. The supernatant was discarded and the pellets were washed twice with 1 ml 70% ethanol, then dried at room temperature. According to the size of the pellets, appropriate volume of DEPC water was added and the pellets were resuspended. RNA concentration of each sample was measured using spectrophotometry at an optical density (OD) of 260 nm. dH_2O was used as blank. Purity of the sample was determined by the ratio of E260/ E280. RNA was stored at -80 ℃.

5.2.7.2 Reverse transcription (RT)

Reverse transcription is a process to transcribe single-stranded RNA to complementary DNA (cDNA). According to the results of concentration measurement, each RNA sample was standardized into a dilution with a concentration of 1 µg/µl. Reverse transcription was performed with Applied Biosystems™ High-Capacity cDNA Reverse Transcription Kit (Thermo Fisher Scientific, Vilnius, Lithuania) following the manufacturer's instructions. The reaction system is prepared in 20 µl volume. The components and the ratio are as follows:

Reagents	**Volume**
RNA sample	Total 10 µl
DEPC WATER	
DEPC WATER	4.2 µl
10x buffer RT	2 µl
25x dNTPs	0.8 µl
10X random PRIMER	2 µl
Enzyme Reversetranscriptase	1 µl
Total volume	20 µl

Reactions were incubated in a PCR thermocycler at 25 ℃ for 10 min, followed by at 37 ℃ for 120 min, at 85 ℃ for 5 min and then cooled to 4 ℃. After reverse

transcriptase, the cDNA was diluted 1:5 with purified water and stored at -20 ℃.

5.2.7.3 Real-time PCR

Quantitative real-time PCR is a method that uses fluorescent chemicals to measure the total amount of products after each polymerase chain reaction (PCR) cycle in a DNA amplification reaction. qPCR was performed in 20 µl reaction volume using SYBR Green Master Mix (Invitrogen, Karlsruhe, Germany) and a 7300 real time PCR system. At the end of the PCR, baselines and threshold values were established using AB 7300 System SDS software, and the CT values were exported to Microsoft Excel to calculate relative mRNA expressions according to the ΔΔCT method (155). The CT value of each sample was compared with the control group and normalized against *Gapdh* gene expression as an internal reference. The compositions of real-time PCR in this study were as followed:

Reagents	**Volume**
cDNA	5 µl
Forward primer	1 µl
Reverse primer	1 µl
SYBR green master mix	10 µl
DEPC water	3 µl
Total reaction volume	20 µl

5.2.8 Protein extraction and analysis

5.2.8.1 Isolation of whole cell protein from the liver

Appropriate size of the frozen liver tissue (approximately 1 mg) was homogenized on ice with 500 µl NP40 lysis buffer. The composition of NP40 buffer was as follow:

NP40-Buffer	**Volume**	**Final concentration**
Tris/HCl 7.5 pH (1 M)	25 ml	50 mM
NaCl (5 M)	15 ml	150 mM
Nonidet P-40	2.5 ml	0.5 %
Sodium Fluoride	1.05 g	50 mM
dH_2O added to	500 ml	

Reagents shown as follow need to be added fresh before use:

Freshly added components	**Volume**
PhosSTOP	1 tablet
Complete Mini (protease inhibitors)	1 tablet
DTT (1 M)	20 µl
AEBSF Hydrochloride (100 mM)	100 µl
NP40 buffer added to	10 ml

The homogenate was incubated on ice for at least 1 h, then centrifuged for 10 min at 12000 *rpm* and 4 ℃. The supernatant was transferred into a fresh tube.

5.2.8.2 Protein quantification

Protein concentrations from liver tissue were measured according to Bradford method using BIO-RAD Protein Assay reagent (156). BSA was diluted to 0.5 mg/ml, 1 mg/ml, 2 mg/ml, 4 mg/ml, 6 mg/ml, 8 mg/ml, 10 mg/ml in NP40 buffer for generating the standard curve. NP40 buffer was used as blank control. 2 µl of each protein sample or BSA standard was mixed with 998 µl Bio-Rad protein reagent (Bio-Rad, Hercules, USA), which had been diluted in MilliQ water with the final concentration of 20%. 200 µl mixed solution was added into 96-well plate and measured using a spectrophotometer at OD_{630}. Protein concentrations were calculated according to the standard curve drawn from the OD_{630} values of BSA standard proteins. The final concentration of proteins was diluted to 4 µg/µl with NP40 lysis buffer and stored at -80 ℃.

5.2.8.3 Western blot

Handmade gels and buffers were prepared ahead. The concentrations of separating gel depend on the molecular weight of target proteins. The compositions of gels and buffers were as follows:

Separating Gel	**8 %**	**10 %**	**12 %**	**15 %**
dH_2O (ml)	9.3	7.9	6.6	4.6
30% Acrylamide/Bis Solution (ml)	5.3	6.7	8.0	10.0

Tris/HCl PH=8.8 (ml)	5.0	5.0	5.0	5.0
SDS 10% (ml)	0.2	0.2	0.2	0.2
APS 10 % (ml)	0.2	0.2	0.2	0.2
TEMED (ml)	0.012	0.008	0.008	0.008
Total volume (ml)	20	20	20	20

Stacking Gel	**Volume**
dH_2O	4.5 ml
30% Acrylamide/Bis Solution	1.3 ml
Tris/HCL PH=6.8	2 ml
SDS 10%	0.08 ml
APS 10 %	0.08 ml
TEMED	0.008 ml
Total volume	8 ml

The molecular weights of proteins separated by different concentrations of separation gel are as follows (4):

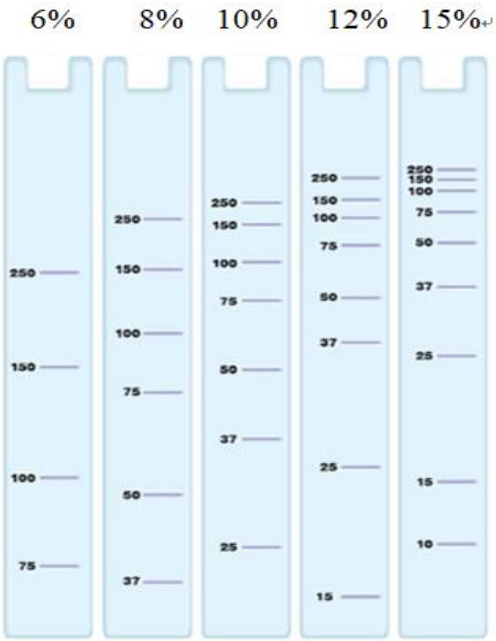

The buffers used in WB are as follow:

10x SDS-Running Buffer	**Volume/Quality**
Tris	30.3 g
Glycine	144.13 g
SDS	10 g
dH_2O add to	1 L

10x Transfer Buffer	**Volume/Quality**
Tris	30.3 g
Glycine	144.13 g
dH_2O add to	1 L
1x Transfer Buffer	**Volume/Quality**
10x Transfer Buffer	100 ml
Methanol	200 ml
dH_2O add to	1 L

10x TBS	**Volume/Quality**	**PH value**
Tris	24.2 g	PH=7.6
NaCl	80 g	
dH_2O add to	1 L	
1x TBST	**Volume/Quality**	
10x TBS	100 ml	
Tween-20	0.5 ml	
dH_2O add to	1 L	

1/4 volume of loading buffer was added into protein samples and the mixtures were denatured for 5 min 300 *rpm* at 95 ℃ in the thermomixer. 80-100 µg proteins were loaded on a handmade gel and separated at 80-120 V for approximately 2 h in 1x SDS-Running buffer. After electrophoresis, the separated proteins were transferred from the gel onto a PVDF membrane or a Nitrocellulose membrane in the wet blotting chamber for 2 h at 300 mA on ice. Whatman® paper, membrane and gel were made like the

sandwich then immersed in 1x transfer buffer. The transfer was carried out in accordance with standard procedures (157) and the transfer sequence is critical and need to be placed correctly. The successful transfer was confirmed by Ponceau S Red staining. The membrane was cutting according to the molecular weight of target proteins, and incubated in 5% BSA/0.5% TBS-Tween 20 (TBST) or 5% non-fat milk/0.5% TBST for 1 h at room temperature to block non-specific binding sites. After blocking, the membranes were incubated with primary antibody diluted in 2.5% BSA/0.5% TBST or 2.5% non-fat milk/0.5% TBST overnight at 4℃ on a shaker. On the second day, the membranes were washed three times in TBST for 10 min, then incubated with the horseradish peroxidase (HRP)-conjugated secondary antibody in 5% BSA/0.5% TBST or 5% non-fat milk/0.5% TBST at room temperature. One hour later, secondary antibody was taken away and the membranes were washed three times in TBST for 10 min again. Target bands were visualized using Amersham enhanced chemiluminescence (ECL) Prime (GE Healthcare, Amersham, UK). After incubation for 2 min, the membrane was exposed to an odyssey Fc Imaging system (LI-COR, Madrid, Spain) until specific signals were detectable.

5.2.9 Histological analysis

5.2.9.1 Immunofluorescence (IF) staining

Five μM cryosections from mouse liver were air dried for 20 min, then fixed in 4% formaldehyde at room temperature, followed by washing with PBS three times for 5 min. A humid box was made to prevent the slides from dying and fading. PBS containing 5% goat serum and 0.3% Triton was used for blocking followed by incubation with primary antibody in blocking solution at optimized dilutions at 4℃ overnight. On the second day, slides were washed with PBS three times for 10 min and incubated with secondary antibody labeled with Alexa fluorescent dye in blocking solution for 1 h at room temperature. Then slides were washed three times for 10 min in PBS. Nuclei were counterstained with Vectashield mounting medium containing DAPI (Vector Laboratories, Burlingame, USA). Microscopy and image acquisition were performed using an Axio Imager A1 microscope and AxioVision software. ImageJ software was used for image analysis and quantification.

5.2.9.1.1 Terminal deoxynucleotidyl transferase dUTP nick end labeling (TUNEL) staining

The coverslips were put in 6-well plate and incubated in 3% Hydrogen peroxide diluted in Methanol (30% Hydrogen peroxide : Methanol = 1:9) for 10 min in the dark, followed by incubated in PBS for another 10 min. 150 mM Na-Citrate solutions were prepared and dropped on the coverslips. 2 min later, the Na-Citrate solution was removed and the coverslips were washed with PBS solution for 5 min three times, followed by incubating with labeling mixture solution overnight at 4 ℃. On the second day, the coverslips were washed in PBS solution three times for 10 min, then mounted with DAPI for nuclear counterstaining.

Five μM cryosections from mouse liver were dried in air for 30 min, then fixed in 4% formaldehyde at room temperature for 20 min, followed by washing with PBS three times for 10 min. Then slides were incubated in 3% Hydrogen peroxide diluted in Methanol (20 ml 30% Hydrogen peroxide + 180 ml Methanol) for 10 min in the dark, followed by incubated in PBS for another 10 min. To have access to the DNA, the nuclei were permeabilized in 150 mM Na-Citrate solution. 150 mM Na-Citrate solutions were prepared as follows and cooled with glass tank at advance:

Reagent	**Volume/Quality**	**PH value**
150 mM Na-Citrate	8.8 g	PH=6.0
PBS solution	200 ml	
10X Triton-100	0.2 ml	

The permeabilization solution was removed by washing twice in PBS solution for 10 min. Then slides were incubated with labeling mixture solution overnight at 4 ℃. The labeling mixture solution was composed as below:

Reagent	**Volume for 1 section (2 samples)**
Enzyme Solution	1 μl
10X TUNEL Diluent Buffer	10 μl
TUNEL Labeling Solution	89 μl
Total	100 μl

On the second day, the slides were washed with PBS solution four times for 10 min, then mounted with DAPI for nuclear counterstaining.

5.2.9.1.2 Zonula occludens-1 (ZO-1) staining

The coverslips were put on the slides and blocked with PBS containing 10% goat serum, followed by incubation with ZO-1 antibody in PBS containing 1% goat serum at dilution of 1:100 at room temperature for 1 h. After washed with PBS three times for 10 min, the coverslips were incubated with secondary antibody labeled with Alexa fluorescent dye in PBS containing 1% goat serum for 45 min at room temperature, then washed three times for 10 min in PBS and mounted with DAPI for nuclear counterstaining.

Five μM cryosections from mouse liver were dried in air for 25 min, then fixed in 4% formaldehyde at room temperature for 10 min, followed by washing with PBS three times for 10 min. PBS containing 10% goat serum was used for blocking followed by incubation with primary antibody in PBS containing 1% goat serum at dilution of 1:100 at room temperature for 1 h. After washed with PBS three times for 10 min, the slides were incubated with secondary antibody labeled with Alexa fluorescent dye in PBS containing 1% goat serum for 45 min at room temperature. Then slides were washed three times for 10 min in PBS, then mounted with DAPI for nuclear counterstaining.

5.2.9.2 Dihydroethidium (DHE) staining

Fresh five μM cryosections from mouse liver were dried in air for 30 min, followed by washing with PBS for 5 min. Then the slides were incubated 10 μmol DHE at 37 ℃ for 15 min, then washed with PBS for 5 min. After fixed in 4% formaldehyde at room temperature for 5 min, the slides were mounted with DAPI for nuclear counterstaining.

5.2.9.3 Immunohistochemistry (IHC) staining

Five μM Paraffin embedded sections were baked in the oven at 60℃ for 0.5 h, then deparaffinized and rehydrated with xylene and serial ethanol solutions from 100% to 70%. Antigen unmasking was performed by boiling sections in 10 mM sodium citrate buffer using Antigen 2100-Retriever (Aptum Biologics, Hants, UK) for one complete cycle (approximately 2 h). After cooling, sections were rinsed in dH_2O three times for

5 min and treated with 3% H_2O_2 for 10 min to quench endogenous peroxidases. Slides were washed again in dH_2O twice, then washed in PBS for 5 min. Sections were blocked with 2.5% horse serum (Vector Laboratories, Burlingame, USA) for 20 min at room temperature. Removed away blocking solution, the slides were incubated with primary antibody diluted in PBS with 1% BSA and 0.3% Triton overnight at 4℃ in a humid chamber. The next day, the slides were washed with PBS three times for 5 min, then incubated with secondary antibody (Vector Laboratories, Burlingame, USA) at room temperature for 1 h in the humid chamber. After washed three times in PBS, signals were developed with DAB (Vector Laboratories, Burlingame, USA) and counterstained with hematoxylin. Dehydrating was performed in increasing percentages of ethanol and xylene, mounted with Roti-histokit (Carl Roth, Karlsruhe, Germany) and analyzed using microscope system.

5.2.9.4 Hematoxylin and eosin (H&E) staining

Paraffin embedded liver samples were cut 5 μm thick and made into slides, and deparaffinized and rehydrated following protocol as below: 2 x 10 min xylene, 2 x 5 min 100% ethanol, 1 x 3 min 95% ethanol, 1 x 3 min 90% ethanol, 1 x 3 min 85% ethanol, 1 x 2 min tap water. Then the slides were immersed in hematoxylin for 20 min, rinsed under warm tap water for 10 min, then waxed in 1% hydrochloric acid alcohol for 2 sec and rinsed under warm tap water again for 15 min. The slides were incubated in 70% ethanol for 3 min, 85% ethanol for 3 min and 90% ethanol for 2 min respectively, following with eosin staining and dehydration: 1 x 2 min eosin, 1 x 3 sec 95% ethanol, 2 x 3 min 100% ethanol, 2 x 10 min xylene. Coverslip slides using Roti-histokit. Place a drop of Roti-histokit on the slide using a glass rod to allow it to spread beneath the coverslip, covering all the tissue.

5.2.9.5 Oil Red O (ORO) staining

Oil Red O staining is an effective way to detect neutral triglycerides and lipids. Stock solution of ORO needs to be prepared ahead: 0.5 g Oil Red powder was dissolved completely in 100 ml isopropanol, and kept in dark. The working solution needs to be prepared freshly: 48 ml stock solution diluted to 80 ml with dH_2O, and filtered with Whatmann paper for three times.

The coverslips were washed three times in dH_2O and stained in Oil Red O working solution for 40 min at room temperature, then immersed in Hematoxylin for 30 sec. The coverslips were rinsed with tap water until the water runs clear. Mount the coverslips with Roti-histokit and take pictures with a microscope.

Eight μM frozen sections of the liver were cut and air-dried for 40 min, fixed with 4% paraformaldehyde for 25 min, and then washed three times in dH_2O. The slides were then stained in Oil Red O working solution for 40 min at room temperature and rinsed again in dH_2O shortly. Hematoxylin is used for counterstaining. Take pictures with a microscope immediately after staining.

Oil red O stock solution	**Volume**
Oil red O powder	0.5 g
Isopropanol	100 ml
Oil Red O working solution	**Volume**
Oil Red O stock solution	48 ml
dH_2O	32 ml

5.2.10 Hepatic Triglyceride (TG) content

Homogenization buffer for hepatic triglyceride was prepared one day before the experiments and kept in 4℃. The composition of homogenization buffer was as follow:

Homogenization buffer	**Volume/Quality**	**PH value**
Tris	390 mg	PH=7.5
EDTA	110 mg	
Sucrose	21.35 g	
dH_2O	250 ml	

Approximately 20 g liver tissue was cut on dry ice, and homogenized completely with 1 ml homogenization buffer in tissue homogenizer. The homogenate solution was centrifuged for 5 min at 12000 *rpm* and 4 ℃. The upper two layers were mixed gently and transferred into a fresh tube. Hepatic triglyceride concentrations from liver tissue were measured following the manual guide of Triglycerides liquicolor mono kit (RAL,

Barcelona, Spain). Standard solution was diluted to 50 mg/dl, 75 mg/dl, 100 mg/dl, 125 mg/dl, 150 mg/dl, 175 mg/dl, 200 mg/dl in dH_2O for generating the standard curve. dH_2O was used as blank control. 2 µl of each sample was mixed with 200 µl kit reagent and added into 96-well plate. After incubated in room temperature for 45 min, the plate was measured using a spectrophotometer at OD_{450}. Hepatic triglyceride concentrations were calculated according to the standard curve drawn from the OD_{450} values of standard solutions.

5.2.11 Transmission electron microscopy (TEM)

Two mm thickness of liver tissues were fixed in fix solution (4% formaldehyde and 2.5% glutaraldehyde in phosphate solution) for 5 h at 4℃ and incubated in phosphate solution overnight at 4℃. The next day, samples were post-fixed with 1% osmium tetroxide diluted in double-distilled water for 1 h at room temperature, dehydrated through graded acetone (30%-50%-70%-80%-90%-95%-100%-100%), infiltration in resin-acetone, and embedded in resin. Ultrathin sections were cut with a diamond knife on an ultramicrotome. The thin sections were stained and observed using a transmission electron microscope Jeol 1010 (Jeol, Peabody, USA).

Phosphate solution	**Volume**	**PH value**
2.26% $NaHPO_4.H_2O$	41.5 ml	PH=7.2-7.4
2.52% NaOH	8.5 ml	

Fix solution	**Volume**
16% PFA	2.5 ml
25% Glutaraldehyde	1 ml
Phosphate solution	6.5 ml

5.3 Statistical analysis

Statistical analysis was performed using the software Prism v8.0 (GraphPad Software). Statistical significance among groups was determined by one-way analysis of variance between APAP-challenged groups and control group in HepaRG cells or

WT mice, and by two-way ANOVA adjusted for multiple comparisons between *Xbp1*$^{\Delta hepa}$ mice and *Xbp1*$^{f/f}$ mice. Data are expressed as means ± Standard Error of the Mean (SEM). A *p* value equal or less than 0.05 was considered to be statistically significant.

6. Results

6.1 APAP induces cytotoxicity and cell death in HepaRG cells

HepaRGs, a bipotent human hepatic cell line, provide an excellent *in vitro* model system for exploring mechanisms of APAP hepatotoxicity (158). Differentiated HepaRG cells maintain drug-metabolizing enzymes and are more useful human hepatic cellular models for toxicity studies (159). Differentiated HepaRG cells were treated with different concentrations of APAP range from 0 mM to 20 mM for 24 h. HepaRG cells exposed to APAP showed a dose-response reduction in cell viability at 24 h. Cytotoxicity assessments were done by CCK8 assay and morphological assessments by confocal fluorescence microscopy. CCK8 solution is stable and low in cytotoxicity, and can be added directly to the cells. An orange formazan product bioreduced by cellular dehydrogenases was proportional to the number of living cells. Cell viability decreased around 50% with 10 mM and only 30% HepaRGs treated with 20 mM APAP survived at 24 h according to CCK8 measurement (**Fig. 6A**). HepaRG cells contained quite low levels of ALT and AST activity in control group that significantly increased in culture medium of HepaRG cells exposed to APAP reaching its peak with 20 mM (**Fig. 6B-C**). As an indicator of cell death (160), TUNEL staining was tested. TUNEL staining detects several types of cell death, including necrosis, apoptosis and necroptosis. Cell death significantly increased after exposure of APAP, however, the number of TUNEL-positive cells was similar between 10 and 20 mM APAP (**Fig. 6D-E**). This observation associated with the increase of apoptotic DNA fragmentation was also validated by cleaved caspase 3 (CC3) immunoblot (**Fig. 6F**).

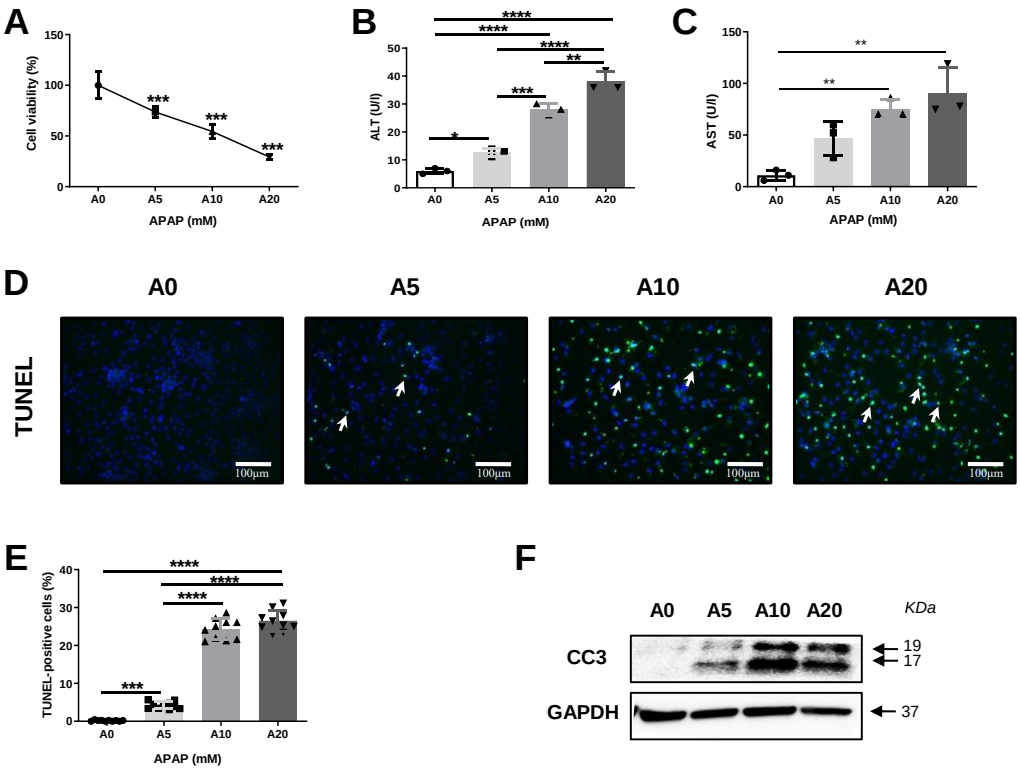

Figure 6. Cytotoxicity of different concentrations of acetaminophen (APAP) in HepaRG cells. (A) Cell viability was determined by CCK8 assay. **(B)** Supernatant ALT levels. **(C)** Supernatant AST levels. **(D)** Representative TUNEL staining performed on coverslips. **(E)** Quantification of TUNEL positive cells per view field was shown. **(F)** Protein levels of cleaved caspase 3 were determined by Western Blot. GAPDH was used as a loading control. Data are expressed as mean ± SEM (*p<0.05, **p<0.01, ***p<0.001, ****p<0.0001). Arrows denote positive cells.

6.2 APAP leads to loss of tight junctions (TJs) and lipid accumulation in HepaRG cells

Elevations of hepatic triglycerides have been reported in APAP toxicity and likely reflect a switch in energy metabolism that occurs during cytotoxicity (161). HepaRGs displayed increasing concentrations of ORO staining after APAP exposure, more evident at an APAP dose of 5 mM and 10 mM (**Fig. 7A**). Tight junctions (TJs) maintain differentiated functional polarity and xenobiotic metabolic competence of hepatocytes. APAP exposure to HepaRGs caused TJ destabilization which was directly proportional to APAP concentration, and confirmed via disruption of the TJ-specific protein zonula occludens-1 (ZO-1) by immunofluorescence and immunoblot (**Fig. 7B-D**). ZO-1 is located in the intracellular membrane and works as a scaffold protein cross-linking and

anchoring TJ strand proteins to the actin cytoskeleton (162). Confocal microscopy demonstrated continuous, membranous staining of ZO-1 in normal HepaRGs and reduced intensity with increasing APAP. In consistent, western blot data showed that ZO-1 protein expression was down-regulated with increasing concentration of APAP.

Altogether, our results using human HepaRGs show that a concentration of 10 mM APAP suffices to induce a cytotoxicity, apoptotic cell death, disruption of TJs and lipid accumulation in human hepatocytes.

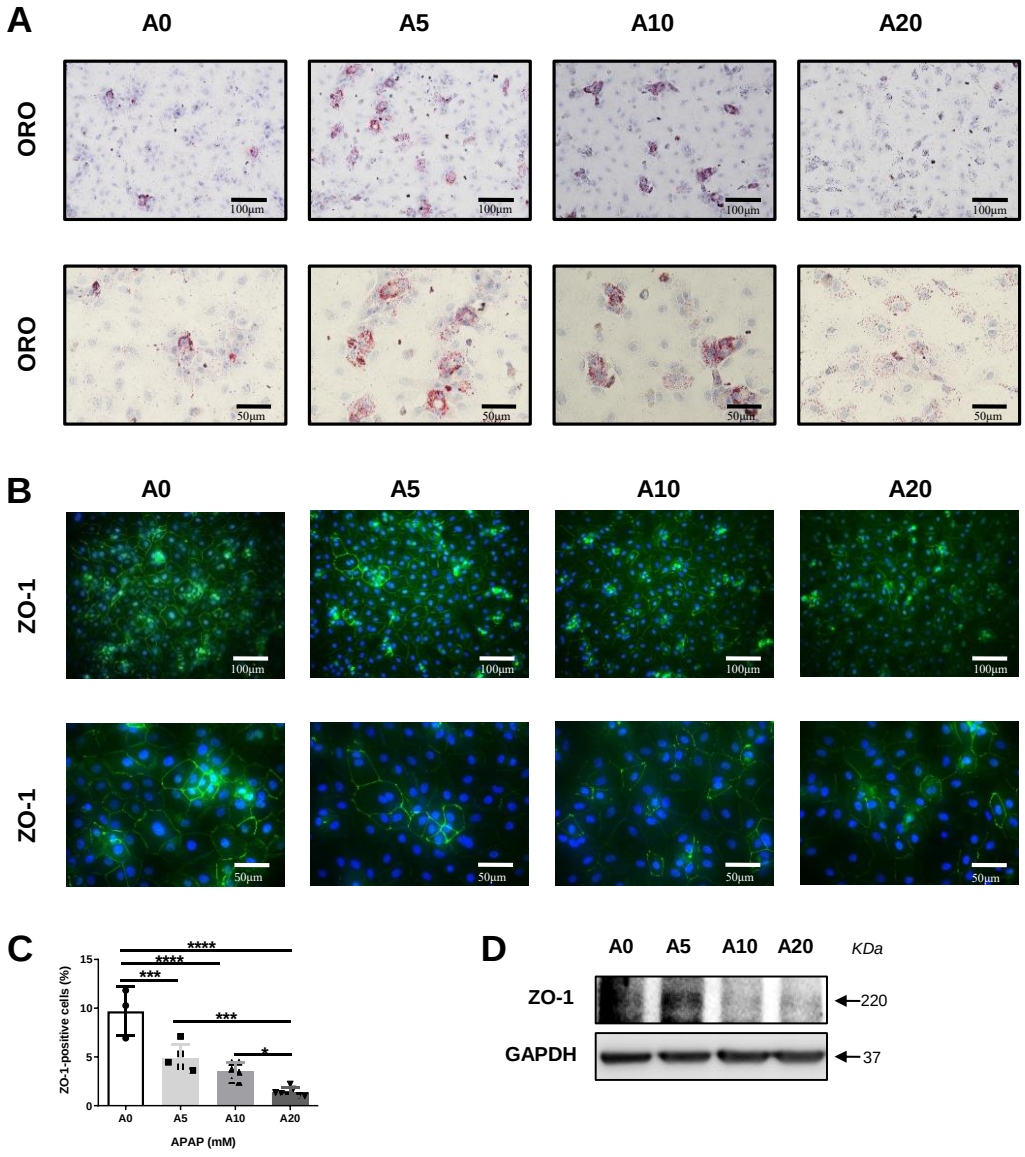

Figure 7. Cytotoxicity of high concentrations of acetaminophen (APAP) lead to lipid accumulation and loss of tight junctions (TJs) in HepaRG cells. (A) Representative ORO staining performed on coverslips. **(B)** Representative ZO-1 staining performed on coverslips. **(C)** Quantification of ZO-1 positive cells per view field was shown. **(D)** Protein levels of ZO-1 were determined by Western Blot. GAPDH was used as a loading control. Data are expressed

as mean ± SEM (*p<0.05, ***p<0.001, ****p<0.0001).

6.3 A sublethal dose of APAP (300 mg/kg) induces liver damage, hepatocyte necrosis, loss of TJs in WT mice

C57BL/6J WT mice were fasted overnight and treated with low to high doses of APAP (0-300 mg/kg) by intraperitoneal injection. Twenty-four hours after intraperitoneal injection, mice were sacrificed and liver damage was assessed. Diagnostic liver function tests were performed to analyzed serum markers of liver damage and cytosolic enzyme leakage. ALT, AST and LDH were markedly increased in treated mice compared to the controls in a dose-dependent fashion, indicating the expected APAP-mediated liver damage (**Fig. 8A-C**). Centrilobular hepatocellular necrosis is the hallmark lesion of acetaminophen injury. As we expected, centrilobular necrosis was more histologically evident after exposure to 300 mg/kg APAP for 24 h (**Fig. 8D**). TUNEL IF staining proved significant hepatocyte death in necrotic areas as a result of APAP toxicity, specifically 24 h after 300 mg/kg APAP (**Fig. 8E-F**). Caspase 3 is a typical caspase protein in caspase-independent apoptotic signaling pathway, where it is responsible for chromatin condensation and DNA fragmentation. Cleaved caspase 3 immunoblot further confirmed the results of TUNEL staining (**Fig. 8G**). In addition, ZO-1 IF was progressively lost with increasing APAP dose and more remarkably after exposure to 300 mg/kg APAP for 24 h (**Fig. 8H-J**).

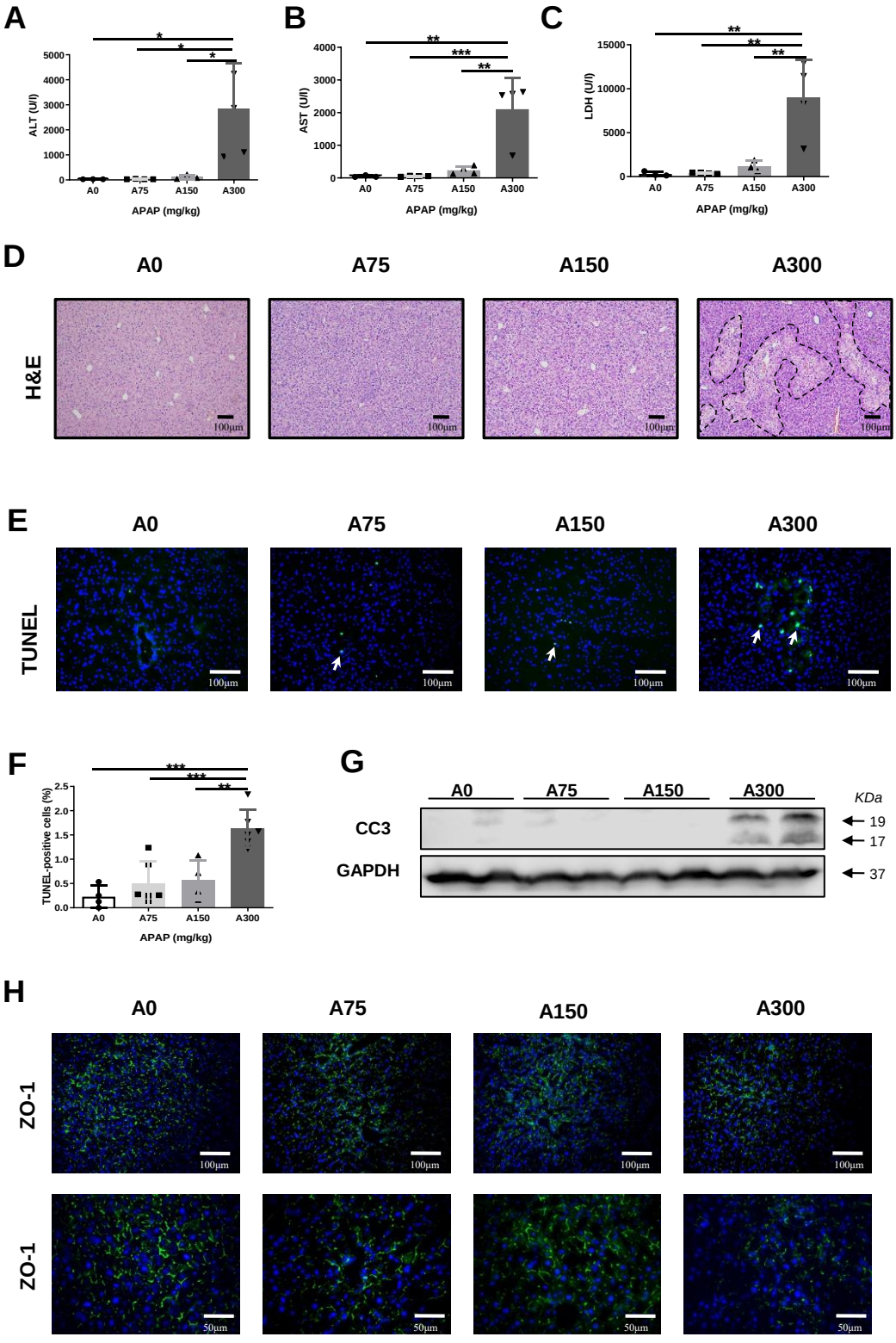
A
ALT (U/l)
APAP (mg/kg)
A0
A75
A150
A300
B
AST (U/l)
C
LDH (U/l)
D
H&E
E
TUNEL
F
TUNEL-positive cells (%)
G
CC3
GAPDH
KDa
19
17
37
H
ZO-1
100μm
50μm

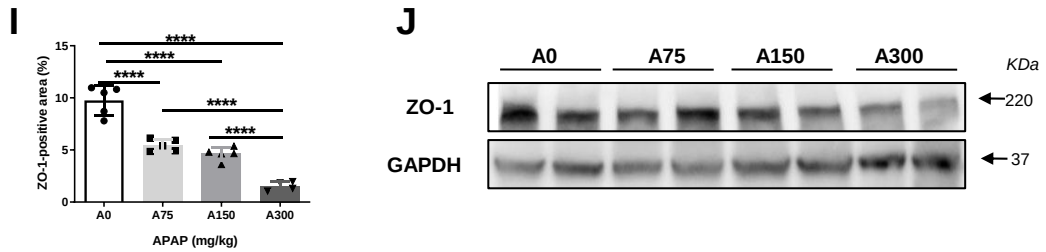

Figure 8. A sublethal dose of APAP (300 mg/kg) triggers strong hepatic damage in WT mice. **(A)** Serum ALT level represented as U/L. **(B)** Serum AST level represented as U/L. **(C)** Serum LDH level represented as U/L. **(D)** Representative H&E staining performed on paraffin liver sections. **(E)** Representative TUNEL staining performed on frozen liver sections. **(F)** Quantification of TUNEL positive cells per view field was shown. **(G)** Protein levels of cleaved caspase 3 were determined by Western Blot. **(H)** Representative ZO-1 staining performed on frozen liver sections. **(I)** Quantification of ZO-1 positive cells per view field was shown. **(J)** Protein levels of ZO-1 were determined by Western Blot. GAPDH was used as a loading control. Data are expressed as mean ± SEM (*p<0.05, **p<0.01, ***p<0.001, ****p<0.0001). Arrows denote positive cells.

6.4 A sublethal dose of APAP induces oxidative stress in WT mice

APAP overdose depletes cellular GSH and induces mitochondrial oxidative stress. A considerable amount of research has shown that together with lipotoxicity, the generation of free radicals such as superoxide, are pivotal for APAP-induced hepatocyte necrosis (163). During the past decade, several fluorescent dyes have been widely used to quantify cellular $O_2^{\bullet-}$ and H_2O_2, for example by DHE. DHE can freely permeate cell membrane and be oxidized by cellular $O_2^{\bullet-}$ to produce two red fluorescent products, namely ethidium (E^+), which is typically formed by a non-specific redox reaction, and 2-hydroxyethidium (2-OH-E^+), a specific adduct of cellular $O_2^{\bullet-}$. Recently, many investigators use fluorescent microscopy to measure DHE-derived fluorescence in the artery from diabetes (164), hypertension (165) and atherosclerosis (166). 4-hydroxynonenal (4-HNE) is one major product of lipid peroxidation. 4-HNE-protein adducts are contained in hepatocytes displaying intact morphology, and reliable biomarkers of hepatic lipid peroxidation associated with liver injury. In our study, DHE IF and 4-HNE IHC staining were significantly elevated 24 h after 300 mg/kg APAP in C57BL/6J WT mice while no observed in control group (**Fig. 9A-B; Fig. 9C**).

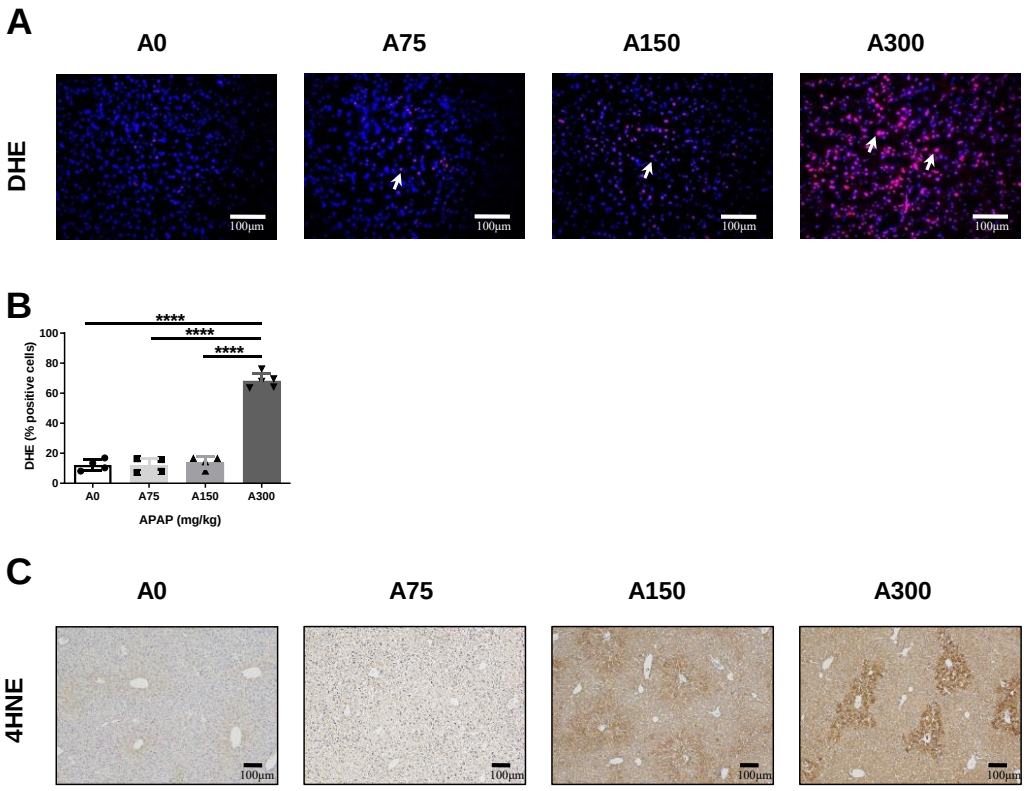

Figure 9. A sublethal dose of APAP (300mg/kg) triggers oxidative stress in WT mice. (A) Representative DHE staining performed on frozen liver sections. **(B)** Quantification of DHE positive cells per view field was shown. **(C)** Representative 4HNE staining performed on paraffin liver sections. Data are expressed as mean ± SEM (****p<0.0001). Arrows denote positive cells.

6.5 A sublethal dose of APAP induces accumulation of triglyceride and hepatic steatosis in WT mice

Some drugs can induce microvesicular steatosis. Liver pathology shows the presence of numerous lipid droplets, which can be stained with Oil Red O (167). ORO is a fat-soluble diazo dye used for staining of triglycerides and lipids on frozen sections and lipoproteins on paraffin sections. It has the appearance of a red powder. In our study, minimal staining for ORO was detected in the liver sections of the mice treated with PBS in ORO immunohistochemical images of mouse liver. In contrast, ORO staining was localized to the regions surrounding the hepatic vein in WT mice challenged with 300 mg/kg APAP. The pattern of ORO staining with the localization of ORO to the centrilobular regions suggested that lipid deposition occurred at 24 h after APAP toxicity. In consistent with the result of ORO staining, liver triglyceride content had a

significant increase in WT mice challenged with 300 mg/kg APAP, reflecting moderate steatosis and lipid accumulation due to APAP hepatotoxicity in murine (**Fig. 10A-C**).

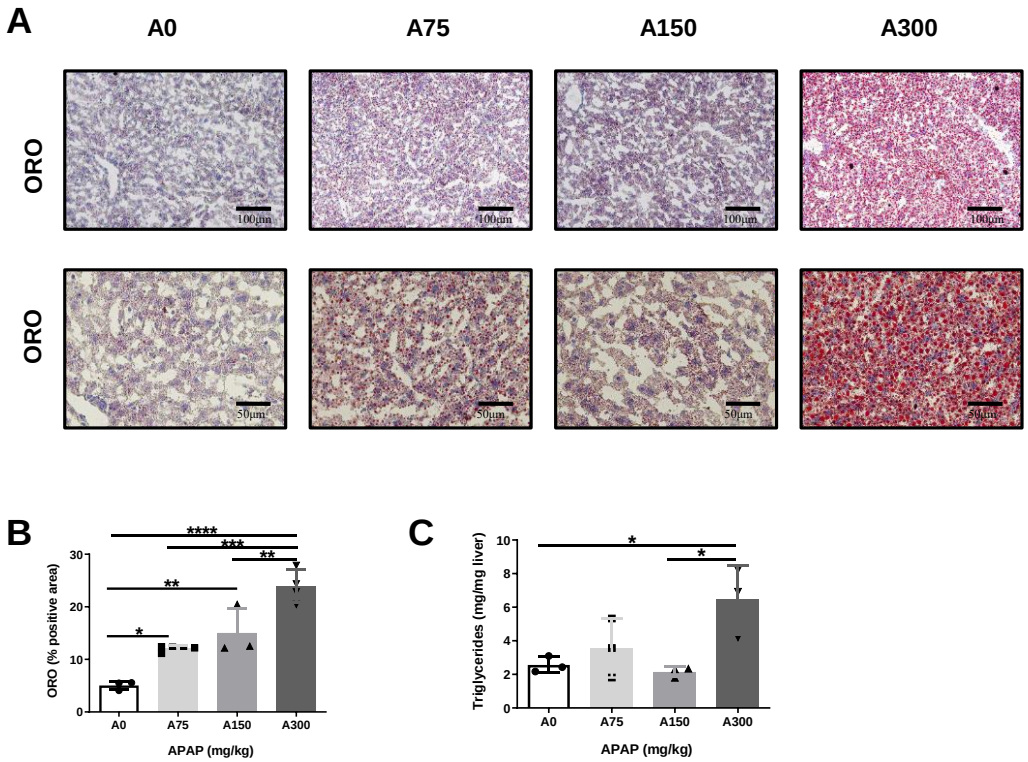

Figure 10. APAP (300mg/kg) induces hepatic steatosis and lipogenesis in wildtype mice. (A) Representative ORO staining performed on frozen liver sections. **(B)** Quantification of ORO positive cells per view field was shown. **(C)** Liver triglycerides content was tested by enzymatic colorimetric tests. Data are expressed as mean ± SEM (*p<0.05, **p<0.01, ***p<0.001， ****p<0.0001).

6.6 A sublethal dose of APAP induces immune infiltration and inflammation in WT mice

A potential source of oxidative stress is inflammatory cells recruited into the liver and liver resident KCs. The development of APAP hepatotoxicity is closely associated with the activation of the innate immune response involving the upregulation of proinflammatory cytokines, including IL-6, TNFα and IL-1β. Therefore, we investigated the characterization of hepatic inflammation in the WT mice. Some isoforms are often used as markers to identify and distinguish between different types of immune cells. For example, CD45 is a receptor-linked protein tyrosine phosphatase that is expressed on all leucocytes. CD11b is expressed on the surface of many leukocytes like monocytes, neutrophils, natural killer cells and so on. And F4/80 has

been established as one of the most specific cell-surface markers for macrophages. Interestingly, the number of CD45, CD11b and F4/80 positive cells increased in a dose-dependent fashion (**Fig. 11A-F**). The mRNA expression levels of proinflammatory cytokines in mouse liver were determined by RT-qPCR. As shown in **Fig. 11G-H**, the mRNA levels of *Tnfα* and *IL-1β* were elevated in WT mice after 300 mg/kg injection (**Fig. 11G-H**). Altogether, our data suggest inflammation was initiated in liver of WT mice, with a characteristic recruitment of inflammatory cells.

In general, our data show that a sublethal dose of APAP (300 mg/kg) induces liver damage, cell death, disruption of TJs, lipid accumulation, and immune cell infiltration and inflammation in mice.

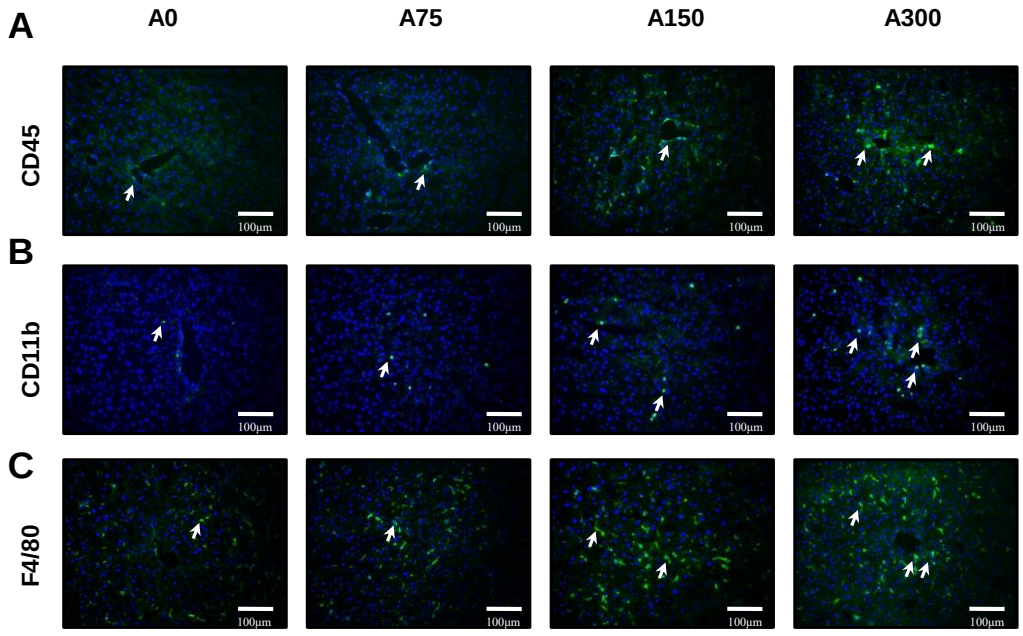

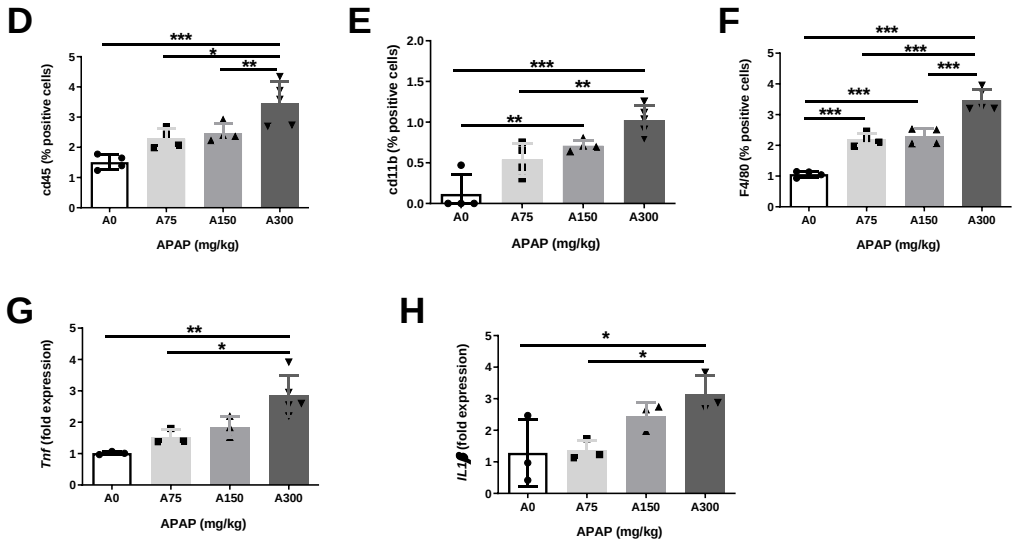

Figure 11. APAP (300mg/kg) induces inflammation and activation of inflammasome in WT mice. (A) Representative CD45 staining performed on frozen liver sections. **(B)** Representative CD11b staining performed on frozen liver sections. **(C)** Representative F4/80 staining performed on frozen liver sections. **(D)** Quantification of CD45 positive cells per view field was shown. **(E)** Quantification of CD11b positive cells per view field was shown. **(F)** Quantification of F4/80 positive cells per view field was shown. **(G)** mRNA level of *Tnfα* was determined by RT-qPCR. **(H)** mRNA level of *IL-1β* was determined by RT-qPCR. Data are expressed as mean ± SEM (*p<0.05, **p<0.01, ***p<0.001, ****p<0.0001). Arrows denote positive cells.

6.7 Activation of the UPR and JNK1/2 is characteristic of human and murine APAP-mediated hepatotoxicity

Since we speculated that APAP-induced ER stress might lead to the deleterious effects observed both in HepaRGs and *in vivo*, we subsequently investigated activation of the UPR response after exposure to APAP in these conditions. The UPR is activated in response to an accumulation of unfolded or misfolded proteins in the lumen of ER. As we expected, we found that the UPR was transcriptionally active in both human HepaRGs and in mice after exposure to a sublethal dose of APAP, including the splicing of *Xbp1* (**Fig. 12A-B**). These results were supported by immunoblotting analyses of various UPR components in HepaRGs (0-20 mM) and WT mice (0-300 mg/kg). Phosphorylation of IRE1α, accumulation of CHOP in the nucleus, loss of BiP/GRP78 and splicing of XBP1 were observed 24 h after exposure to 10 mM APAP in culture HepaRG cells and 24 h after injection of 300 mg/kg APAP in mice (**Fig. 12C**).

Extensive experimental evidences show that JNK activation and its translocation to mitochondria attributes to APAP hepatotoxicity (86). Moreover, JNK activation is sustained in severe ER stress-induced cell death (91). Therefore, we evaluated the activation of the JNK1/2 signaling pathway in HepaRGs (0-20 mM) and WT mice (0-300 mg/kg). Interestingly, phosphorylation of JNK1 and JNK2 were evident 24 h after exposure to 10 mM APAP in culture HepaRG cells and 24 h after injection of 300 mg/kg APAP in mice (**Fig. 12D**). The expression of activated JNK were significantly increased, which indicated the JNK signaling pathway was activated in APAP-induced hepatotoxicity.

In summary, our data indicates that transcriptional and transductional activation of the UPR and phosphorylation of JNK1/2 are major events in the hepatotoxic response to APAP both in human cells and in murine liver.

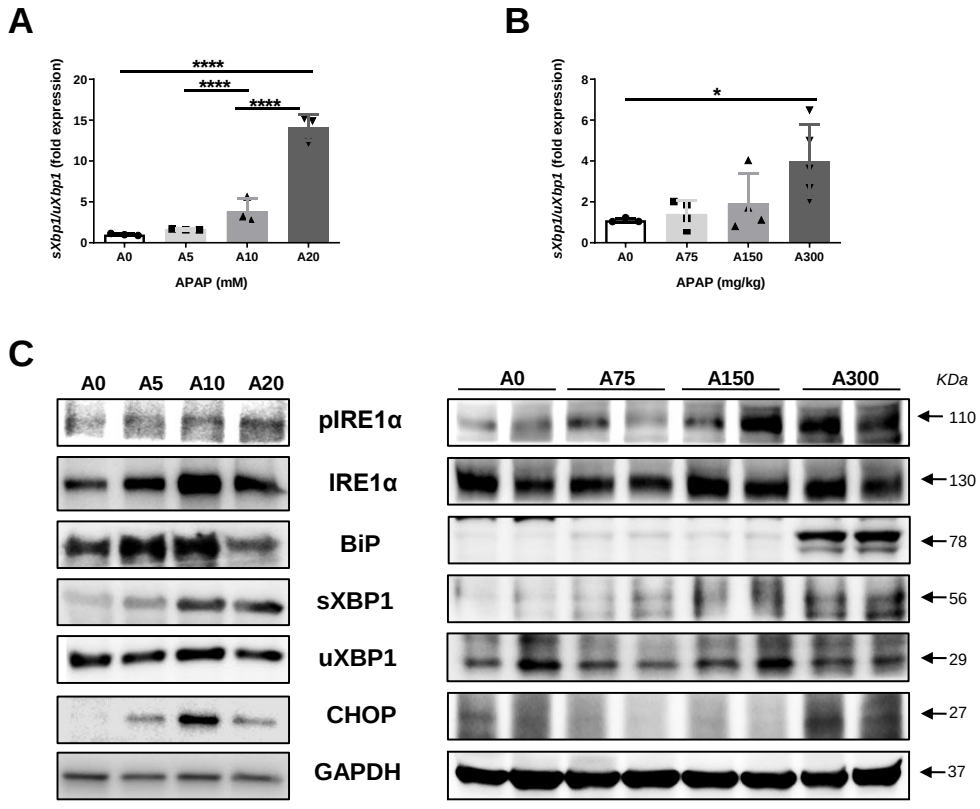

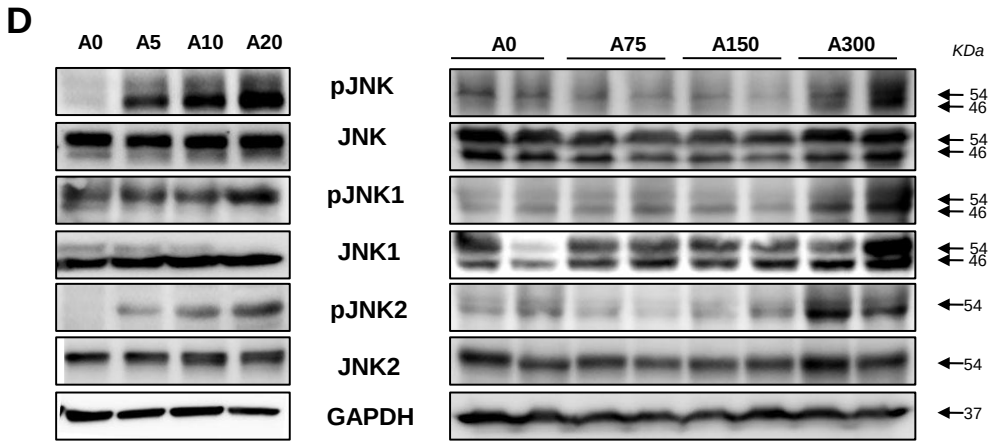

Figure 12. APAP overdose triggers ER stress and cell death 24 h after APAP challenge in HepaRG cells (0-20 mM) and WT mice (0-300 mg/kg). (A) mRNA level of *sXbp1/uXbp1* in HepaRG cells was determined by RT-qPCR. **(B)** mRNA level of *sXbp1/uXbp1* in WT mice was determined by RT-qPCR. **(C)** Protein levels of pIRE1α, IRE1α, BiP, sXBP1, uXBP1, CHOP in HepaRG cells and WT mice were determined. **(D)** Protein levels of pJNK, JNK, pJNK1, JNK1, pJNK2, JNK2 in HepaRG cells and WT mice were determined. GAPDH was used as a loading control. Data are expressed as mean ± SEM (*p<0.05, ****p<0.0001).

6.8 Generation of knockout mice

Signaling through IRE1α is the most conserved one among the three arms of UPR, which is worthy of our more attention. Besides, *Xbp1* gene is required for optimal cytokine expression in macrophages and controls the inflammatory response (137). Therefore, in our study, we not only used WT mice, but also established *Xbp1* specific hepatic-knockout mice with C57BL/6 background to investigate *Xbp1* specific function in APAP-induced liver damage. We crossed $Xbp1^{f/f}$ mice with Alb-cre mice expressing Cre recombinase to achieve hepatocyte specific deletion of XBP1. The correct genotype and the effective excision of the genes of *Xbp1* was confirmed on DNA level by PCR analysis of tails from newborn mice tails. WT-*Xbp1* allele was detected in agarose gel electrophoresis as a 183-bp DNA fragment or a 141-bp DNA fragment for floxed-*Xbp1* allele. Mutant allele for *Albcre* was observed as a 390-bp band in gel electrophoresis and an artifact band of 150-bp was frequently present from the mutant allele, while wild type allele was a 351-bp band (**Fig. 13A**). We also extracted proteins from frozen mouse liver and did western blot with XBP1 antibody. The protein expression of XBP1 in the liver of $Xbp1^{\Delta hepa}$ mice was evidently downregulated compared to $Xbp1^{f/f}$ mice (**Fig.**

13B). Low residual protein expression of XBP1 in liver of *Xbp1*$^{\Delta hepa}$ mice might be due to the expression in non-parenchymal cells.

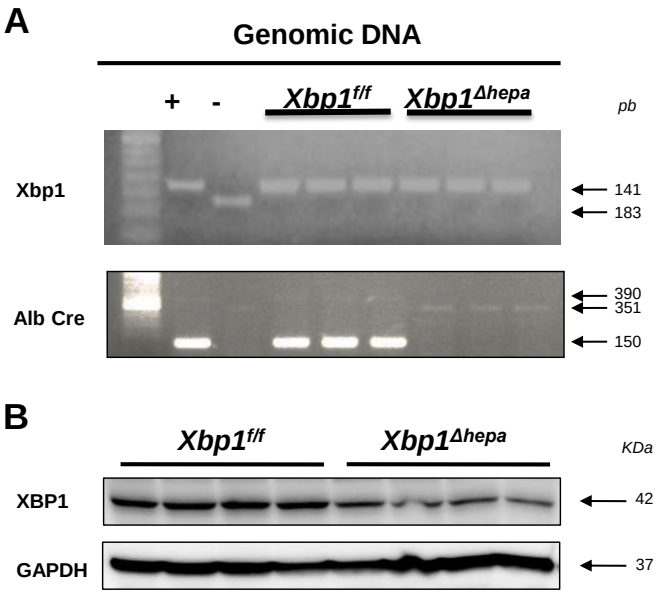

Figure 13. Proof of *Xbp1* deletion in *Xbp1*$^{\Delta hepa}$ mice. (A) Agarose gel showing the respective PCR results from mice tails DNA derived from *Xbp1*$^{\Delta hepa}$ and *Xbp1*$^{f/f}$ mice. **(B)** Protein levels of XBP1 in the liver were determined. GAPDH was used as a loading control.

6.9 Ablation of *Xbp1* in hepatocytes reduces APAP-induced hepatic damage

Since the UPR was activated after 24 h of exposure to 10 mM APAP in human HepaRG cells and a sublethal dose ≥300 mg/kg APAP in WT mice, and the splicing of *Xbp1* indicated that the IRE1-XBP1 branch of the UPR response might be involved in DILI, we generated mice with specific deletion of *Xbp1* in hepatocytes (*Xbp1*$^{\Delta hepa}$). Littermate *Xbp1*$^{f/f}$ mice were used as controls. First, we focused on the phenotypes of *Xbp1*$^{\Delta hepa}$ mice. *Xbp1*$^{\Delta hepa}$ mice were viable, grew smoothly and looked completely normal. Then we checked the protein expression of the IRE1α-XBP1 arm. Importantly, untreated *Xbp1*$^{\Delta hepa}$ livers displayed hyperactivation of IRE1α (**Fig. 14A**), which is consistent with the results of Hur (134). The ablation of *Xbp1* led to feedback activation of its upstream enzyme IRE1α in the liver.

8-12 weeks old *Xbp1*$^{\Delta hepa}$ mice and its littlemates *Xbp1*$^{f/f}$ mice were fasted overnight and challenged with a sublethal dose of APAP. Mortality in *Xbp1*$^{\Delta hepa}$ group was dramatically reduced after a single dose of 500 mg/kg (**Fig. 14B**). Only 60% mice in *Xbp1*$^{f/f}$ survived 48 h after APAP overdose while the survival rate in *Xbp1*$^{\Delta hepa}$ group

was up to 90%. Whilst the levels of serum transaminases markedly increased in *Xbp1*$^{f/f}$ animal, *Xbp1*$^{\Delta hepa}$ displayed only a modest induction of serum ALT, AST and LDH levels, 24 h after APAP treatment (**Fig. 14C-E**). Macroscopic and histological analysis of the liver revealed markedly reduced liver injury in *Xbp1*$^{\Delta hepa}$ mice compared with *Xbp1*$^{f/f}$ animals that exhibited severe centrilobular necrosis and hemorrhage (**Fig. 14F**) and significantly higher TUNEL-positive cells (**Figs. 14G-H**), demonstrating that *Xbp1* deficiency protected mice from APAP-induced hepatotoxicity. Caspase 3 plays a central role in the execution phase of cell apoptosis, which is activated to cleaved caspase-3 in the apoptotic cell both by extrinsic and intrinsic pathways. *Xbp1* knockout mice displayed lower protein expression level of CC3 in the liver compared to *Xbp1*$^{f/f}$ group 24 h after APAP exposure (**Fig. 14I**).

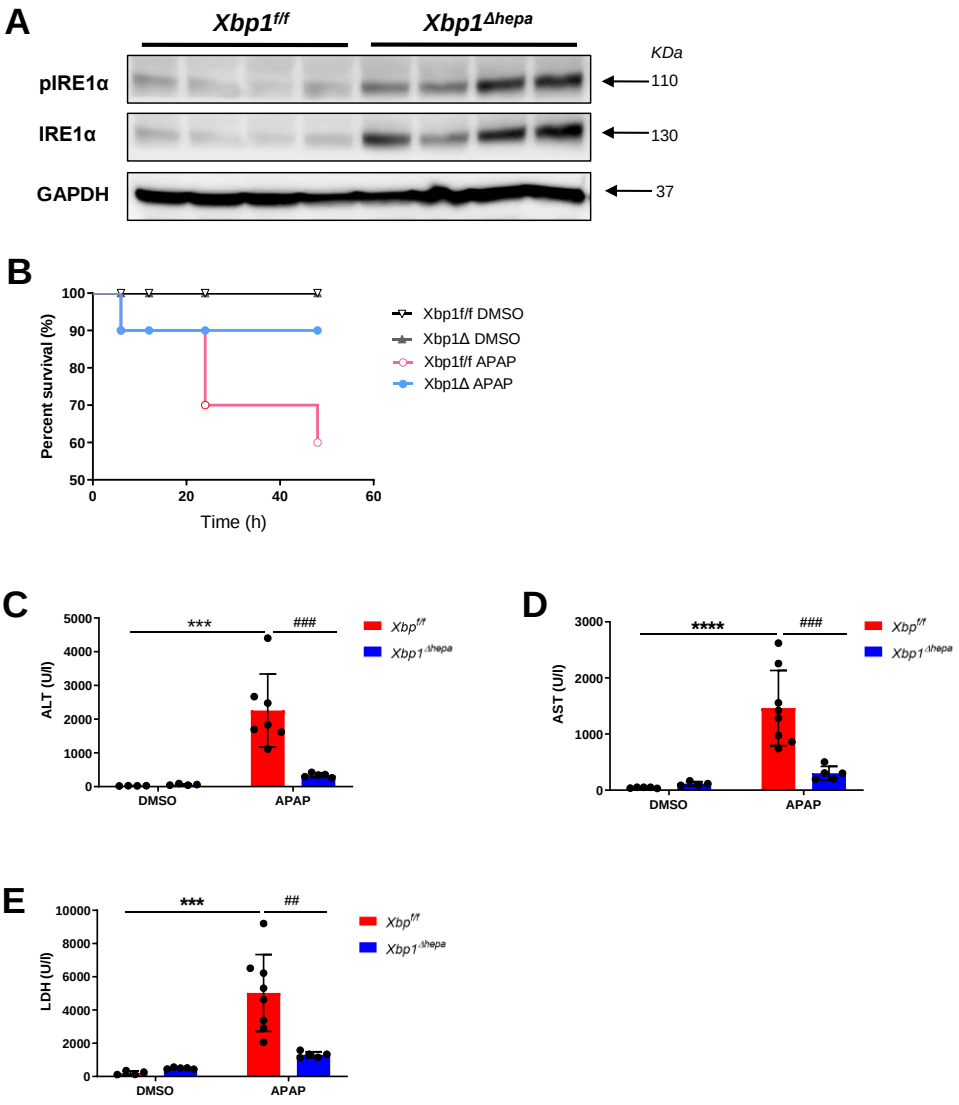

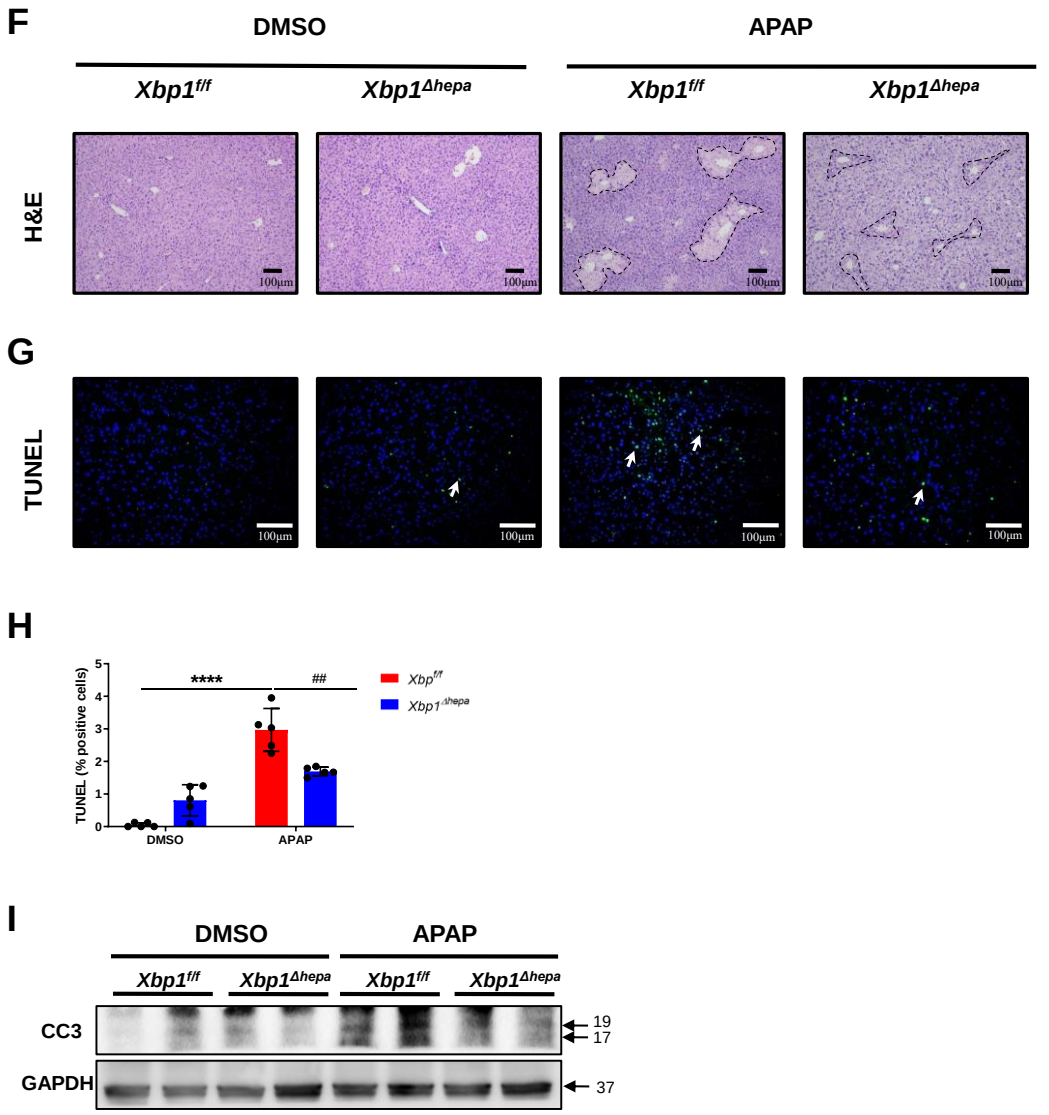

Figure 14. Ablation of *Xbp1* in hepatocytes reduces APAP-induced hepatic damage 24 h after APAP challenge. (A) Protein levels of pIRE1α and IRE1α in the liver were determined. **(B)** Survival of *Xbp1*$^{\Delta hepa}$ and *Xbp1*$^{f/f}$ mice (n=10) after APAP administration. P < 0.05 (Mantel–Cox test). **(C)** Serum ALT level represented as U/L. **(D)** Serum AST level represented as U/L. **(E)** Serum LDH level represented as U/L. **(F)** Representative H&E staining performed on paraffin liver sections. **(G)** Representative TUNEL staining performed on frozen liver sections. **(H)** Quantification of TUNEL positive cells per view field was shown. **(I)** Protein levels of CC3 in the liver were determined. GAPDH was used as a loading control. Data are expressed as mean ± SEM (***p<0.001, ****p<0.0001, $^{\#\#}$p<0.01, $^{\#\#\#}$p<0.001). Arrows denote positive cells.

6.10 Ablation of *Xbp1* in hepatocytes reduces oxidative stress at 24 h after APAP challenge

APAP-induced acute liver injury is initiated by N-acetyl-p-benzoquinone imine (NAPQI), generated by several CYP450 isoenzymes, mainly CYP2E1 and CYP3A4

(168). To investigate the mechanism by which XBP1 regulates APAP metabolism, we checked the expression of CYP450 enzymes. CYP2E1 protein levels visibly decreased after APAP overdose in *Xbp1*$^{f/f}$ mice, but they were clearly at low expression in basal conditions and after APAP challenge in *Xbp1*$^{\Delta hepa}$ mice (**Fig. 15A-B**). The CYP2E1 IHC staining also showed decreased number of CYP2E1 positive cells in livers after APAP toxicity in *Xbp1*$^{f/f}$ mice and low number of CYP2E1 positive cells in *Xbp1*$^{\Delta hepa}$ group.

CYP2E1 metabolism leads to the generation of ROS including lipid peroxidation - measured by 4-HNE IHC (**Fig. 15C**), a well-established consequence of severe ER stress. The positive cells of 4-HNE staining were significantly reduced in *Xbp1*$^{\Delta hepa}$ compared with *Xbp1*$^{f/f}$ mice, 24 h after APAP overdose. Heme oxygenese-1 (HO-1) is a stress-inducible enzyme that provides antioxidant protection and exerts marked anti-inflammatory actions (169). HO-1 is activated by various oxidative stress stimuli, and several studies demonstrated the up-regulation of hepatic HO-1 expression consequent to APAP toxicity (170, 171). In current study, APAP significantly increased the mRNA expression of *HO-1* in *Xbp1*$^{f/f}$ mice, and ablation of *Xbp1* in hepatocytes significantly reduced *HO-1* level (**Fig. 15D**)

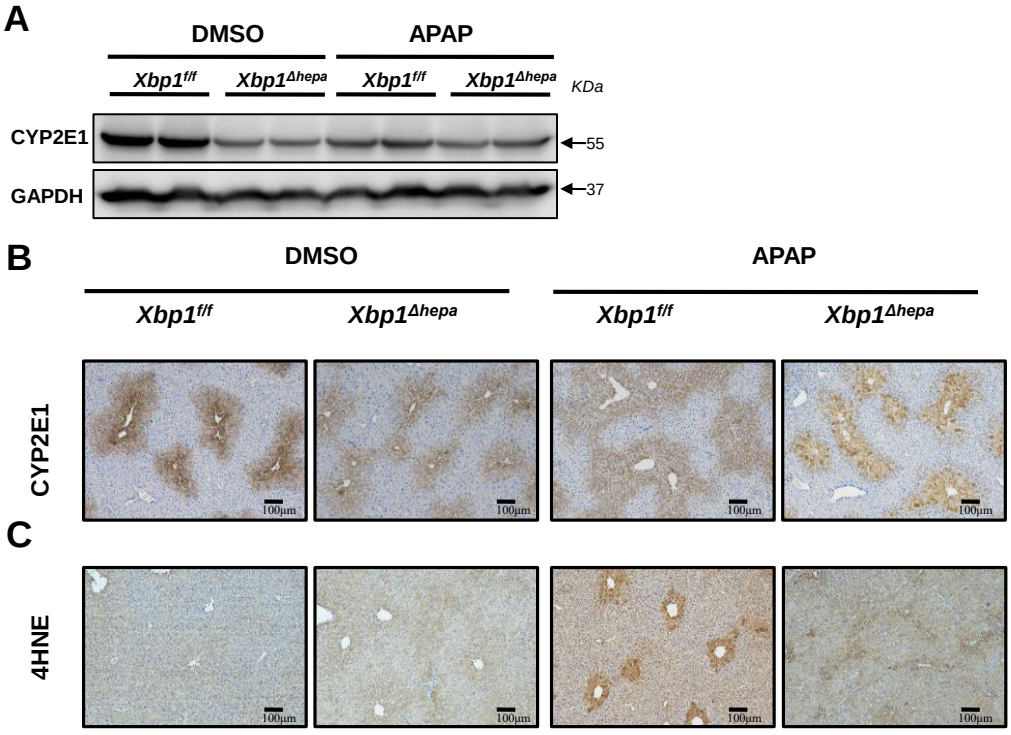

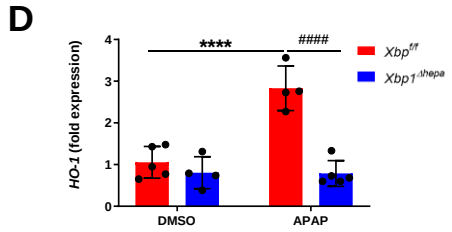

Figure 15. Ablation of *Xbp1* in hepatocytes reduces oxidative stress at 24h after APAP challenge. (A) Protein levels of CYP2E1 were determined by Western Blot. GAPDH was used as a loading control. **(B)** Representative CYP2E1 staining on paraffin liver sections. **(C)** Representative 4HNE staining performed on paraffin liver sections. **(D)** mRNA level of heme oxygenese-1 (*HO-1*) was determined by RT-qPCR. Data are expressed as mean ± SEM (****p<0.0001, ####p<0.0001).

6.11 Ablation of *Xbp1* in hepatocytes maintains TJs at 24 h after APAP challenge

Increased ROS, as a result of APAP hepatotoxity, disrupt hepatic TJs (172). Dysfunction of cell-cell tight junction adhesions is a major feature in APAP-induced DILI. To assess whether TJ-destabilization occurs, we analyzed ZO-1 expression in livers of $Xbp1^{f/f}$ and $Xbp1^{\Delta hepa}$ mice treated with APAP. Both $Xbp1^{f/f}$ and $Xbp1^{\Delta hepa}$ mice treated with DMSO (vehicle) maintained normal cell polarity and adhesion as shown by ZO-1 IF (**Fig. 16A**). ZO-1 expression characterized by IF exhibited mostly continuous, membranous staining that outlined hepatocyte cords in all areas. However, APAP caused dramatic decreased in the expression of ZO-1 in $Xbp1^{f/f}$ mice, but to a lesser extent in $Xbp1^{\Delta hepa}$ mice. Quantification of ZO-1 positive area validated these results (**Fig. 16B**). ZO-1 protein expression showed similar trend of staining results. ZO-1 protein expression was significantly decreased in livers due to APAP toxicity, but the level in $Xbp1^{\Delta hepa}$ mice was higher than that in $Xbp1^{f/f}$ mice, indicating ablation of *Xbp1* in hepatocytes maintained cellular polarity and the blood-biliary barrier (**Fig. 16C**).

Altogether, this set of data indicates deletion of *Xbp1* in liver parenchymal cell (LPC) protects against acute liver injury, hepatocellular necrosis, the generation of ROS and disruption of cell polarity and adhesion.

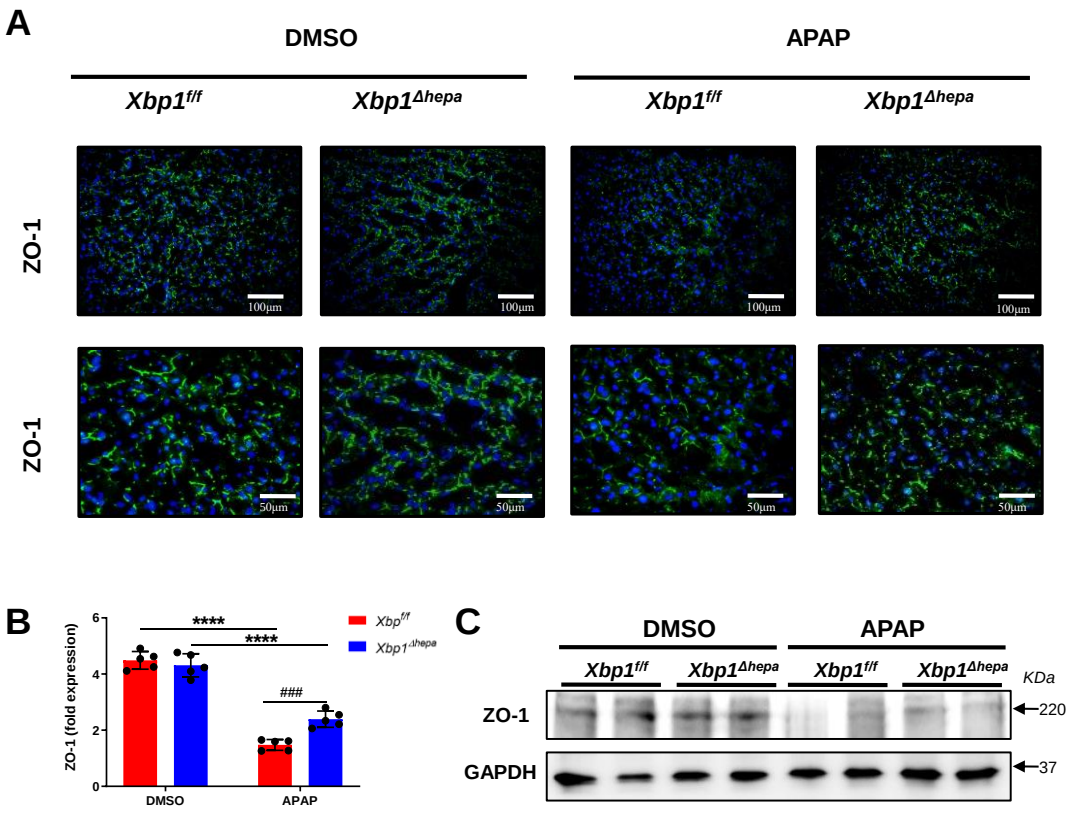

Figure 16. Ablation of *Xbp1* in hepatocytes maintains tight junction at 24h after APAP challenge. (A) Representative ZO-1 staining performed on frozen liver sections. **(B)** Quantification of ZO-1 positive cells per view field was shown. **(C)** Protein levels of ZO-1 were determined by Western Blot. GAPDH was used as a loading control. Data are expressed as mean ± SEM (****p<0.0001, ###p<0.001).

6.12 *Xbp1*$^{\Delta hepa}$ livers show decreased UPR and JNK1/2 activation in response to APAP

As shown by us (**Fig. 14A**) and others (134), loss of *Xbp1* in hepatocytes causes hyperactivation of IREα. Therefore, we next sought to investigate the UPR after APAP in *Xbp1*$^{\Delta hepa}$ mice. APAP toxicity can promote the occurrence of ER stress and the activation of UPR. So we analyzed protein expression of UPR markers 24 h after APAP injection. Whilst APAP did not increase IREα phosphorylation much in *Xbp1*$^{f/f}$ mice, protein levels were overexpressed in mice with hepatocyte-specific deletion of *Xbp1* (*Xbp1*$^{\Delta hepa}$) (**Fig. 17A**). In turn, APAP increased CHOP and BiP/GRP78 protein levels in *Xbp1*$^{f/f}$ compared with *Xbp1*$^{\Delta hepa}$ livers (**Fig. 17A**). Expectedly, the levels of uXBP1 were not altered by APAP overdose (**Fig. 17A**). These data may infer that *Xbp1*

knockout mice recover better that flox mice after ER stress.

JNK is activated by APAP and plays a crucial role in the hepatotoxicity (86, 173-175). To determine the effect of *Xbp1* knockout on JNK activation, we examined the JNK signaling pathway in liver tissues by immunoblotting 24 h after APAP treatment. In WT mice, JNK phosphorylation was strongly induced at 6 h after APAP treatment, and then declined at the 24 h time point. Similar to WT mice, low but detectable protein expression of pJNK was found in $Xbp1^{f/f}$ mice after APAP treatment, whereas lack of JNK induction was characteristic of $Xbp1^{\Delta hepa}$ livers at this time point (**Fig. 17B**). JNK1 and JNK2 activation was similar to JNK and was very mild in both $Xbp1^{f/f}$ and $Xbp1^{\Delta hepa}$ 24 h after APAP treatment (**Fig. 17B**), which might contribute to the protection of *Xbp1*-deficient mice from APAP-induced toxicity. Given that CYP2E1 generates ROS by metabolizing a variety of substrates (176), it is conceivable that the reduction of CYP2E1 in *Xbp1*-deficient liver might ameliorate JNK activation.

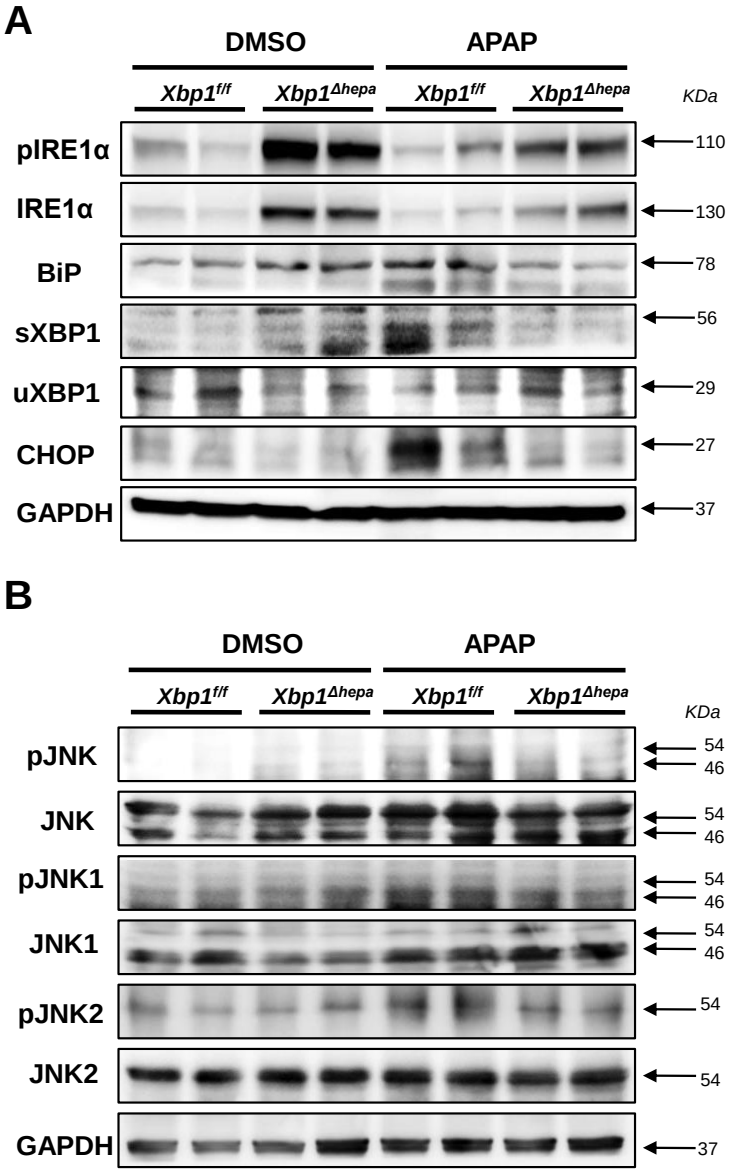

Figure 17. Ablation of *Xbp1* in hepatocytes increases the expression of pIRE1α, reduces the expression of BIP and CHOP and affects JNK activation. (A) Protein levels of pIRE1α, IRE1α, BiP, sXBP1, uXBP1, CHOP were determined. **(B)** Protein levels of pJNK, JNK, pJNK1, JNK1, pJNK2, JNK2 were determined. GAPDH was used as a loading control.

6.13 Immune infiltration, inflammation and inflammasome activation are ameliorated in APAP-treated *Xbp1*$^{\Delta hepa}$ animals

The presence of an inflammatory infiltrate is obvious both histologically and biochemically in APAP livers, also contribute to APAP hepatotoxicity (138). Therefore, we next examined the impact of inflammation in the mechanisms contributing hepatocyte death in APAP-mediated hepatotoxicity. Leukocytes, monocyte and macrophage infiltrates (**Fig. 18A-C**) were significantly increased 24 h after APAP

treatment in *Xbp1*$^{f/f}$ mice according to CD11b, CD45 and F4/80 IF staining. However, the number of CD45-positive cells was significantly reduced in *Xbp1*$^{\Delta hepa}$ mice compared to *Xbp1*$^{f/f}$ mice. No differences were found in CD11b, F4/80-positive cells (**Fig. 18D-F**) between two mice after exposure to APAP toxicity. Concomitantly, mRNA transcripts for *Tnfα* indicated significantly decreased inflammation in *Xbp1*$^{\Delta hepa}$ compared with *Xbp1*$^{f/f}$ livers, 24 h after APAP treatment (**Fig. 18G**).

The NLRP3 inflammasome is critical for host defenses against injuries and has been linked to the pathogenesis of several inflammatory disorders. Inflammasomes are intracellular signaling platforms that activate caspase 1, which then cleaves pro-interleukin-1β (pro-IL-1β) into active IL-1β (177). To investigate the mechanisms of inflammasome which play a role in *Xbp1*$^{\Delta hepa}$ mice, we analyzed the expression of markers of inflammasome. Noticeably, the mRNA expressions of *IL-1β* and *Nrlp3* were significantly lower in *Xbp1*$^{\Delta hepa}$ compared with *Xbp1*$^{f/f}$ livers, 24 h after APAP treatment (**Fig. 18H-I**). Furthermore, overexpression of NLRP3 and IL-1β protein was observed in APAP-treated *Xbp1*$^{f/f}$ compared to *Xbp1*$^{\Delta hepa}$ livers in western blot (**Fig. 18J**), indicating that immune infiltration, inflammation and inflammasome activation are ameliorated in *Xbp1*$^{\Delta hepa}$ animals.

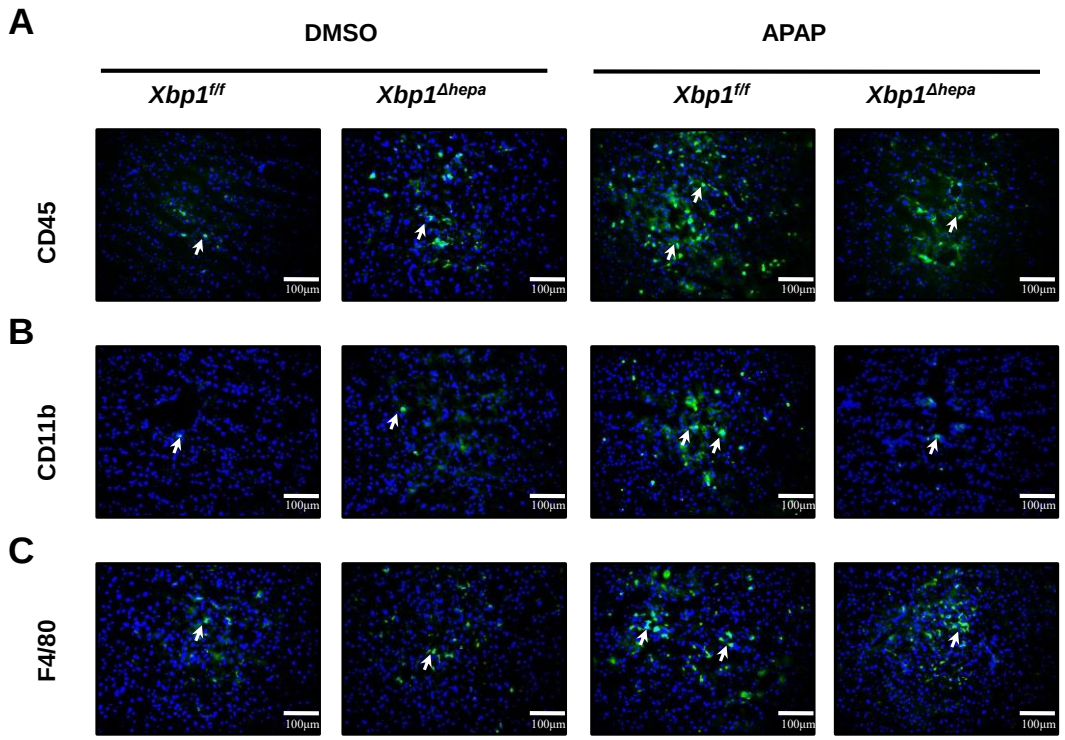

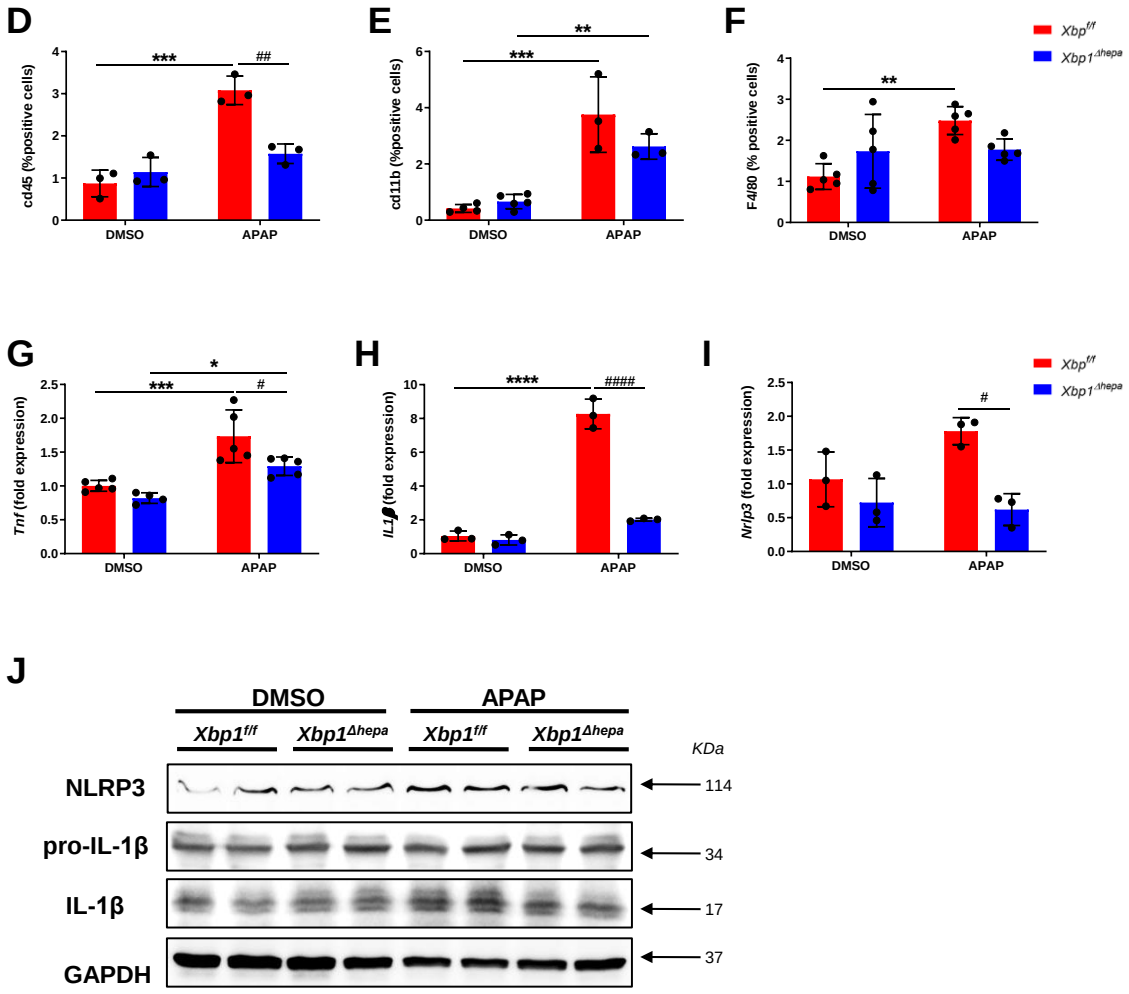

Figure 18. Ablation of *Xbp1* in hepatocytes alleviates inflammatory response and prevents hepatic activation of the NLRP3 inflammasome. (A) Representative CD45 staining performed on frozen liver sections. **(B)** Representative CD11b staining performed on frozen liver sections. **(C)** Representative F4/80 staining performed on frozen liver sections. **(D)** Quantification of CD45 positive cells per view field was shown. **(E)** Quantification of CD11b positive cells per view field was shown. **(F)** Quantification of F4/80 positive cells per view field was shown. **(G)** mRNA level of *Tnfα* was determined by RT-qPCR. **(H)** mRNA level of *IL-1β* was determined by RT-qPCR. **(I)** mRNA level of *Nlrp3* was determined by RT-qPCR. **(J)** Protein levels of NLRP3, pro-IL-1β, mature IL-1β were determined. GAPDH was used as a loading control. Data are expressed as mean ± SEM (**p<0.01, ***p<0.001, ****p<0.0001, $^{\#}$p<0.05, $^{\#\#}$p<0.01, $^{\#\#\#\#}$p<0.0001). Arrows denote positive cells.

6.14 Ablation of *Xbp1* reduces the lipid accumulation in the liver

Current data reinforce the role of XBP1 in hepatic lipid synthesis via both UPR and non-UPR pathways. *sXbp1* can directly increase the expression of several lipogenic genes, such as diacylglycerol acetyltransferase and acetyl-CoA carboxylase 2 (178). Deletion of *Xbp1* activates IRE1α, and IRE1α hyperactivation downregulates lipid

metabolism genes controlled by regulated IRE1-dependent decay (RIDD), such as angiopoietin-like 3 (ANGPTL3) and carboxylesterase 1 (CES1) (179, 180). As we expected, from the ORO staining, *Xbp1*$^{\Delta hepa}$ mice did not develop hepatic steatosis as did *Xbp1*$^{f/f}$ mice due to APAP, less lipid accumulation in the view fields. Morphometric analysis was used to quantify this difference to determine the fractional area occupied by vacuoles in each liver slice. After quantification, there were statistically differences between two groups after APAP injection (**Fig. 19A-B**). Hepatic triglyceride accumulation is a well-established consequence of severe ER stress (181). We find that, 24 h after exposure to APAP, *Xbp1*$^{f/f}$ mice showed a dramatic increase in hepatic triglyceride content while *Xbp1*$^{\Delta hepa}$ mice were protected (**Fig. 19 C**).

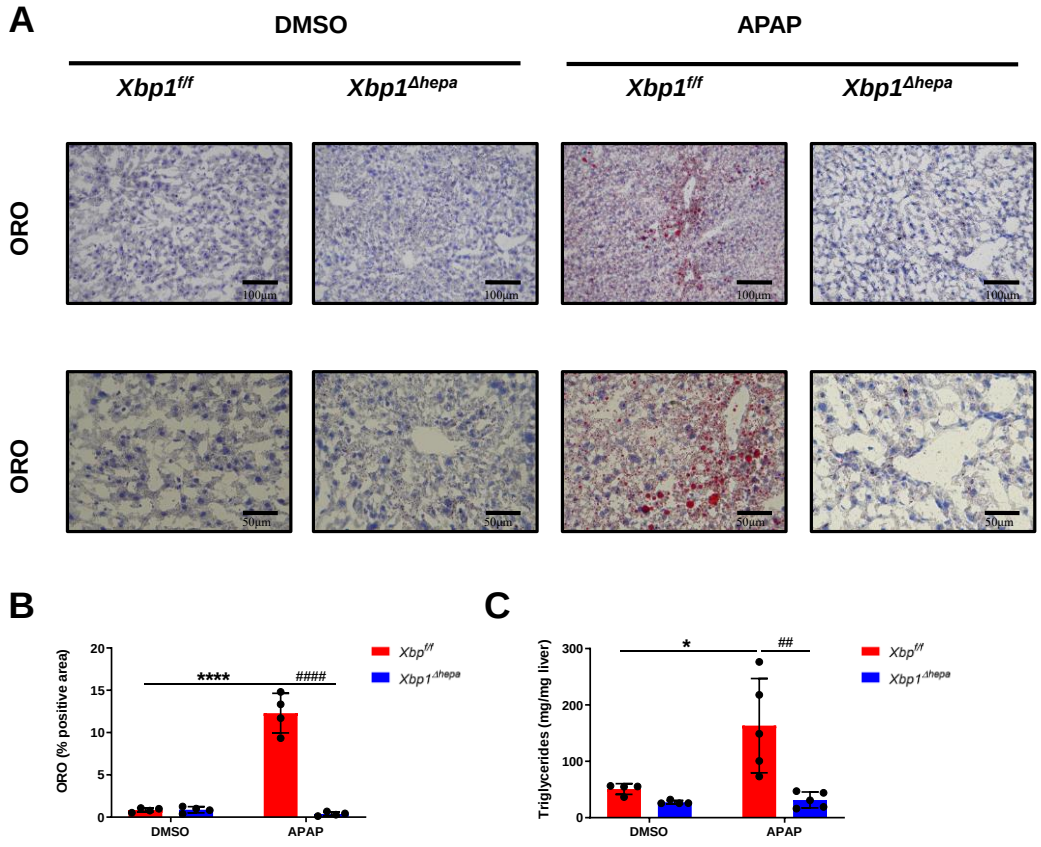

Figure 19. Ablation of *Xbp1* reduces the lipid accumulation in the liver. (A) Representative ORO staining performed on frozen liver sections. **(B)** Quantification of ORO positive cells per view field is shown. **(C)** Liver triglycerides content was tested by enzymatic colorimetric tests. Data are expressed as mean ± SEM (*p<0.05, ****p<0.0001, $^{\#\#}$p<0.01, $^{\#\#\#\#}$p<0.0001).

6.15 Loss of *Xbp1* in hepatocytes promotes autophagy after APAP treatment

Considerable evidence has shown that ER stress initiates autophagy, a cellular degradation process initiated in response to stress, which attempts to restore homeostasis through the catabolic lysis of unfolded/misfolded proteins (182). Chemicals that directly induced ER stress, such as tunicamycin and thapsigargin have been shown to induce autophagy (183). The IRE1α pathway deserves the most attention, since it has already published that the IRE1α pathway is involved in autophagy directly induced by stressing ER (184). To assess whether autophagy is activated in mice with hepatocyte-specific deletion of *Xbp1*, transmission electron microscopy (TEM) was performed. Severe necrosis and mitochondrial damages in hepatocytes of mice after APAP treatment was shown in TEM images, and the accumulation of abundant autophagosomes, the characteristics of autophagy-related ultrastructures, indicated the activation of autophagy in livers of $Xbp1^{\Delta hepa}$ mice following APAP treatment. Moreover, the number of autophagosomes was much bigger compared to $Xbp1^{f/f}$ animals. At the same time, the hepatic parenchyma of $Xbp1^{f/f}$ animals was predominantly necrotic (**Fig. 20A**).

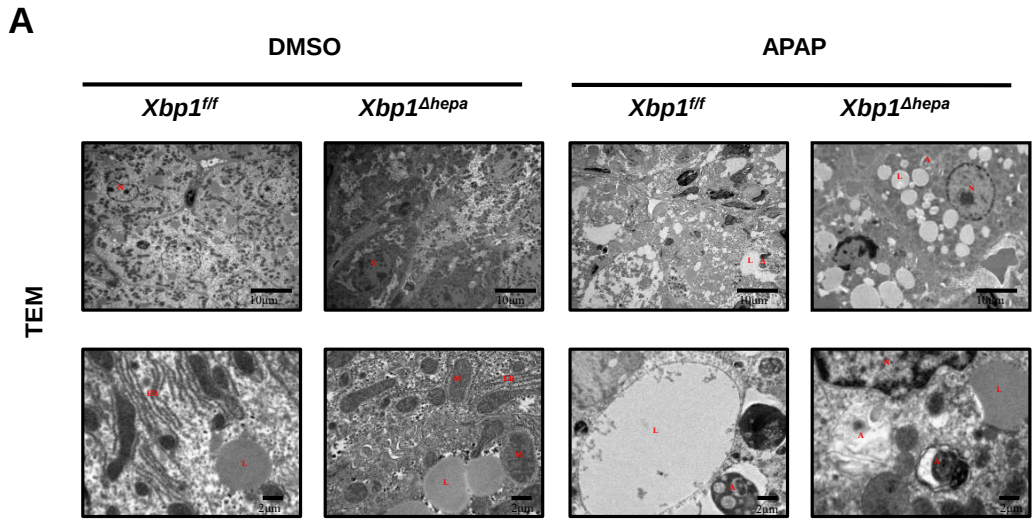

Figure 20. Ablation of *Xbp1* promotes autophagy. (A) TEM images of hepatocyte of control group and acetaminophen-treated group. APAP toxicity induced evident necrosis and severe mitochondrial damages in livers of $Xbp1^{f/f}$ animals while abundant autophagosomes were formed in $Xbp1^{\Delta hepa}$ mice. N = nucleus, M = mitochondria, A = autophagosome, L = lipid, ER = endoplasmic reticulum.

6.16 APAP treatment triggers autophagy in *Xbp1*$^{\Delta hepa}$ mice *via* AMPK activation and AKT inhibition

ER stress activation is frequently accompanied by Ca^{2+} release into the cytosol which leads to the activation of several Ca^{2+}-regulated signaling pathways (185). One of the mechanisms connecting Ca^{2+} release from the ER and autophagy is the stimulation of AMPK, and inhibition of the AKT pathway. Next, we tried to discover the mechanism of autophagy in *Xbp1*$^{\Delta hepa}$ mice. The mRNA expression of autophagy markers *Atg5* was upregulated and *p62* downregulated according to qPCR results (**Fig. 21A-B**). To determine the possible role of *Xbp1* in the regulation of autophagy and autophagic flux, we also measured the conversion of microtubule-associated protein light chain 3 (LC3) from the form I to II, as well as P62 expression in *Xbp1*$^{\Delta hepa}$ and *Xbp1*$^{f/f}$ mice. LC3 and P62 are commonly used markers for detecting the level of autophagy. Compared to *Xbp1*$^{f/f}$ mice, the degradation of P62 and the conversion of LC3-I to LC3-II were promoted in *Xbp1*$^{\Delta hepa}$ mice. Since autophagy may be one of the downstream positive feedback mechanisms of AMPK, protein level of pAMPK was also checked by immunoblotting, and significantly increased in livers of *Xbp1*$^{\Delta hepa}$ mice following APAP treatment, consequently inhibiting pAKT (**Fig. 21C).** Activated AMPK will initiate a protective feedback mechanism to maintain ATP production and promote cell survival. The data suggest that ablation of *Xbp1* may effectively elevate the autophagy level, thus protecting against APAP hepatotoxicity.

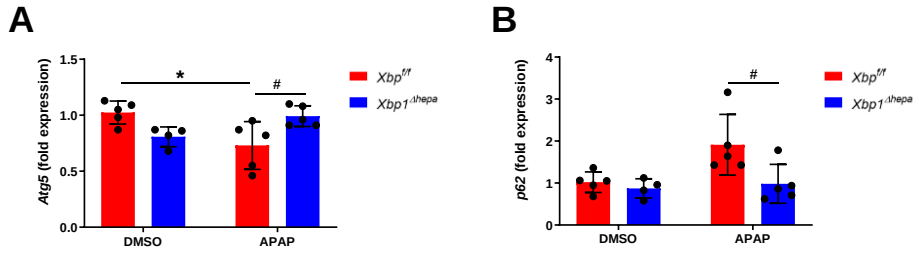

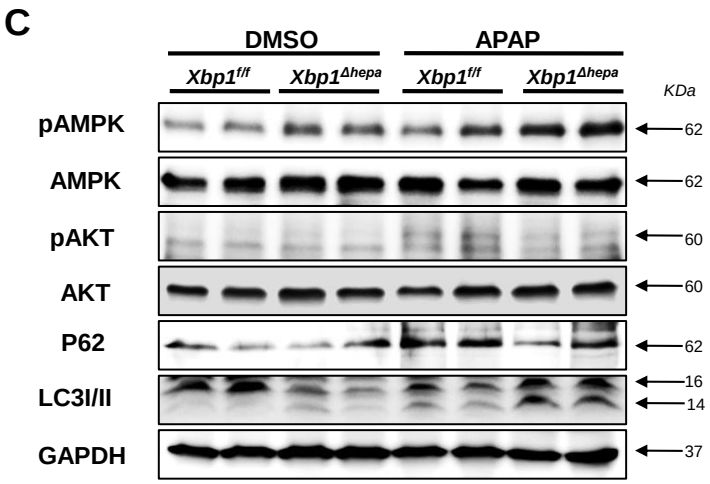

Figure 21. Ablation of *Xbp1* promotes autophagy *via* the AMPK activation and AKT inhibition. **(A)** mRNA level of *Atg5* was determined by RT-qPCR. **(B)** mRNA level of *p62* was determined by RT-qPCR. **(C)** Protein levels of pAMPK, AMPK, pAKT, AKT, P62, LC3I/II were determined. GAPDH was used as a loading control. Data are expressed as mean ± SEM (*p<0.05, #p<0.05).

6.17 STF-083010 mitigates liver injury induced by a sublethal dose of APAP

To further study the role of IRE1α-XBP1 signaling in APAP-induced liver injury, we also used inhibitor to suppress this arm in vivo. STF-083010 is an inhibitor of the endonuclease activity of IRE1α without affecting its kinase activity. STF-083010 can block *Xbp1* mRNA splicing and XBP1 activity after ER stress both *in vivo* and *in vitro*. It has been reported that STF-083010 protected against thioacetamide (TAA)-induced liver injury (186) and carbon tetrachloride (CCl4)-induced liver fibrosis (187). In our case, we aimed to check the phenotype after blocking *Xbp1* in hepatocytes. This study analyzed the effect of STF-083010 on serum biological parameters. Obviously, STF-083010 extenuated the elevation of ALT, AST and LDH levels induced by a sublethal dose of APAP **(Fig. 22A-C).** The effects of STF-083010 on hepatic histopathological damage were presented by H&E staining **(Fig. 22D).** Extensive necrosis areas and infiltration of immune cells were observed in APAP-treated liver tissue sections while STF-083010 manifestly mitigated APAP-induced hepatic necrosis and inflammation. According to the quantification, the necrotic area in APAP+STF-083010 group was significantly decreased than that in only APAP group (**Fig. 22E**). It is possible that this protective effect comes from decreased infiltration of immuce cells and inflammatory

response. As an important part of APAP hepatotoxicity, we are going to further explore its specific mechanism in subsequent studies in the future.

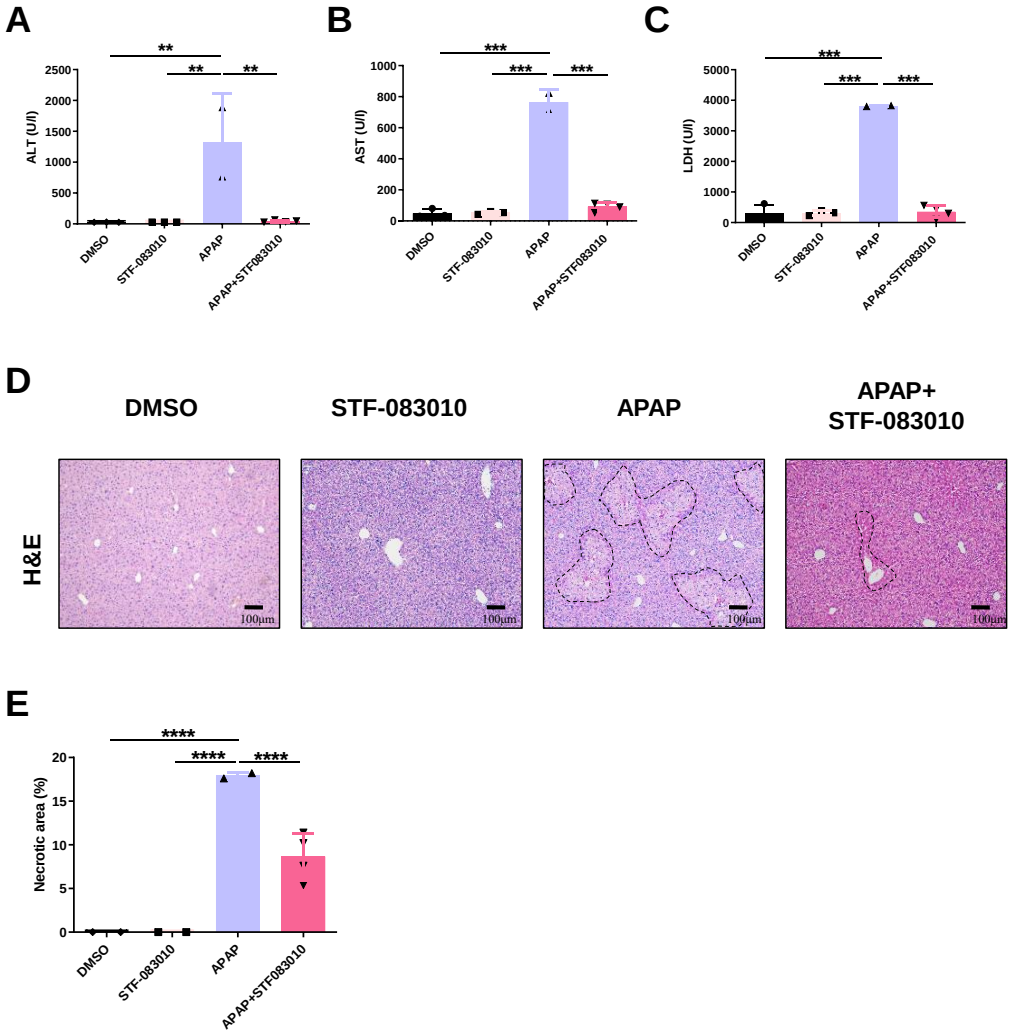

Figure 22. Effects of STF-083010 on liver injury and inflammation induced by a sublethal dose of APAP injection. (A) Serum ALT level represented as U/L. **(B)** Serum AST level represented as U/L. **(C)** Serum LDH level represented as U/L. **(D)** Representative H&E staining performed on paraffin liver sections. **(E)** Quantification of necrotic area per view field is shown. Data are expressed as mean ± SEM (**p<0.01, **p<0.001, ****p<0.0001).

7. Discussion

Acetaminophen overdose-induced liver injury threatens human health and restricts drug use. The hepatic injury model induced by APAP occupies an indestructible position in the study of liver disease. The identification of the molecular mechanisms could provide possible therapeutic strategy. Many important steps in APAP toxicity, including the production of NAPQI and depletion of GSH, have been known for decades. However, many controversies around APAP mechanisms still exist and need to be explored. In our study, we have demonstrated that *Xbp1* gene in the hepatocytes is crucial for protecting against APAP-induced hepatotoxicity. The knockout of *Xbp1* resulted in the upregulation of autophagy though activation of AMPK, then to decrease liver inflammation and oxidative stress.

It was reported that the threshold for a single dose of APAP to induce hepatotoxicity in humans was estimated to be approximately 250 mg/kg (188). After exposure to overdosing APAP, the metabolized NAPQI depleted hepatic GSH, leading to necrosis of hepatocytes and acute liver injury. HepaRGs provide a physiologically-relevant *in vitro* liver model, with intact drug metabolism, and functional polarity, delineated by junctional complexes. Concentrations of APAP higher than 10 mM in human HepaRGs triggered significant cytotoxicity, loss of TJs and lipid accumulation. Mechanisms of APAP hepatotoxicity are reported to be similar in both human and mice. Indeed, clinically-relevant mechanisms of APAP toxicity in human hepatic cells are consistent with murine studies of APAP hepatotoxicity (158). Mice are more commonly used than the other species, and mice with APAP model is considered to be the golden model for studying the mechanisms for APAP-induced hepatotoxicity and searching for effective therapies for liver injury. Our study was carried out with male mice, because their metabolism remains stable compared to the physiological variations of female mice (189). Prior to injection, animals were fasted, as fasting improves the uniformity of drug administration, reduces APAP glucuronidation and potentiates hepatotoxicity (190). 200 to 400 mg/kg APAP is reported to have liver toxicity in mice (191, 192). Therefore, in our study, we used different doses of APAP (from 75 mg/kg to 300 mg/kg) to assess the liver toxicity. And we found in mice challenged with 300 mg/kg, huge areas of

parenchymal necrosis and massive hepatocyte death were observed, accompanied by the increase of ALT, AST and LDH. Activity of aminotransferase is a traditional biomarker of liver injury (193). Thus, the dosage at 300 mg/kg were verified that could induce evident hepatic injury. APAP induces not only necrosis, but also apoptosis and necroptosis. In our thesis, we aimed to show that sublethal application of APAP induces significant hepatocyte death. However, we did not check the type of cell death, which we plan to do for the paper submission.

In hepatocytes, the ER is the major site for protein synthesis, folding and metabolism. It has been reported that APAP overdose can induce the activation of three arms of UPR. We prove that IRE1α-XBP1-CHOP signaling cascade is involved in APAP-induced liver damage. ER stress is induced late after APAP intoxication (500 mg/kg) in murine models, and becomes significant 12 h following APAP administration (122), while Hur did not observe the activation of IRE1α or other UPR branches in the liver of APAP-treated mice within 8 h after APAP injection (134). In our study, we observed increased mRNA and protein levels of sXBP1 both *in vitro* and *in vivo*, indicating the IRE1α-XBP1 arm of the UPR might be activated in APAP-mediated hepatotoxicity. Compared with other two modulators of UPR, PERK and ATF6, IRE1α appears to be activated when the unfolded proteins directly bind to it rather than by disassociation with BiP (194). Upon APAP-mediated ER stress, PERK, IRE1α and ATF6 induce signal transduction events, which increases the expression of ER molecular chaperones, inhibits proteins enter to the ER by preventing mRNA translation and stimulates the retrograde transport of misfolded proteins from the ER into the cytosol, thereby alleviating the accumulation of misfolded proteins in the ER. IRE1α oligomerization and phosphorylation initiates splicing of the mRNA encoding *Xbp1*, promoting restoration of homeostasis and cytoprotection (127). When the various UPR-induced mechanisms fail to relieve stress, intrinsic and extrinsic pathways for apoptosis are activated (130). A downstream transcription repressor of UPR, CHOP is activated (130). Once activated, CHOP translocates to the nucleus, where inhibits the expression of anti-apoptotic genes and activates pro-apoptotic genes (127). CHOP deficient mice are protected from APAP-induced damage (122).

From our data, CHOP and BiP are also activated at high dose of APAP in human HepaRGs and in animals 24 h after a sublethal exposure to APAP *in vivo*.

In APAP-induced hepatocyte death or ALF, the mitochondria are the primary targeted organelles. Oxidative stress and lipid peroxidation mediated by production of ROS have been implicated as an important cause of DILI (161). The intermediate metabolites NAPQI leads to mitochondrial dysfunction by altering mitochondrial membrane permeability, increasing ROS formation and diminishing the capacity of the electron transportation system. The release of mitochondrial ROS induces the activation of JNK within a short period, and a feedforward self-sustaining signaling pathway referred as the JNK amplification loop would maintain sustained JNK activation (91, 92), directly leading to liver damage and dysfunction (93). In fact, JNK is activated by APAP and plays a crucial role in the hepatotoxicity (86, 173-175). In the liver, two JNK genes, JNK1 and JNK2, are expressed (195). Silencing of the JNK pathway - using the classical inhibitor SP600125 - has protective effects against APAP-induced liver injury, by significantly reducing necrosis both *in vivo* and *in vitro* (88, 196). Nevertheless, no differences in APAP hepatotoxicity in JNK1 knockout mice were observed (173). Regarding JNK2, increased susceptibility towards APAP-induced liver injury was reported upon JNK2 deficiency (197), whilst the group of Kaplowitz showed that JNK2 disruption protected against APAP-induced liver injury (173). In our human hepatocytes and murine model phosphorylation of JNK1 and JNK2 after high dose of APAP increased accompany the accumulation of ROS and oxidative stress.

Meanwhile, lipid accumulation and immune infiltration and inflammation were also found in WT mice with 300 mg/kg APAP, agreeing with the prior reports (198). APAP administration inhibits fatty acid β-oxidation in mitochondria and disrupts lipid metabolism in the liver, ultimately leading to increased triglyceride level in the serum and liver. Hepatic triglycerides accumulate as a large lipid vacuole displacing the nucleus at the periphery of the hepatocyte. APAP-induced oxidative stress also provokes sterile inflammation by enhancing the production of pro-inflammatory cytokines, such as IL-1β and TNFα (199). The increase of ROS and free radicals

trigger several pro-apoptotic molecules including caspase 3, the principle executor enzyme of apoptosis (200, 201). The rupture of the outer membrane and release of intermembrane proteins leads to DNA fragmentation, triggering the release of cellular contents including the potent HMGB1, nuclear DNA fragments, mitochondrial DNA, ATP and many others. These DAMPs also cause the transcriptional activation of pro-inflammatory cytokines in macrophages through TLRs and inflammasome activation (138).

According to the above results, ER stress and IRE1α-XBP1 axis play a vital role in liver injury caused by a sublethal dose of APAP. Dysregulation of the hepatic IRE1α-XBP1 axis have been associated with advanced liver disease in patients with nonalcoholic fatty liver disease (NAFLD), but the role of XBP1 in the progression of many liver diseases remains controversial (202). Shantel Olivares and Anne S. Henkel thought that failure to activate hepatic XBP1 in response to ER stress may promote liver disease progression on the basis of their findings, and hepatic XBP1 may be a therapeutic target for the chronic liver disease (203). Moreover, the role of the IRE1α signaling in ER stress-induced apoptosis is complex and incompletely understood. Prolongation of IRE1α signaling has been proved to promote cell survival (204, 205). However, under certain diseases, activation of IRE1α is recognized to promote apoptosis (206, 207). Besides, activated IRE1α can also recruits TRAF2 and ASK1, leading to activation of JNK (208). BAK and BAX interact directly with IRE1α during ER stress, facilitating the activation of XBP1 and JNK (209).

Interestingly, our results show that in *Xbp1* hepatocyte-knockout mice, increased survival rate and reduced cell death were observed in response to a sublethal dose of APAP. Pharmacological inhibition of STF-083010 on IRE1α RNase activity also markedly reduced the levels of serum transaminases and mitigated liver injury induced by APAP in mice. STF-083010, a specific inhibitor of IRE1α RNase, inhibits both endogenous and chemically-induced *Xbp1* splicing without affecting IRE1α phosphorylation. It has been reported that STF-083010 exerted anti-oxidant and anti-inflammation capability in liver injury (187, 210). Moreover, STF-083010 facilitated hepatocyte autophagy in response to TAA stimulation (186). Our study proved that

IRE1α RNase inhibitor STF-083010 had a protective effect against APAP hepatotoxicity, but its specific mechanism remains to be further explored in subsequent studies.

Hepatic deletion of *Xbp1* leads to marked hyperactivation of IRE1α as previously reported (134, 211), made evident by robust splicing of the mutant XBP1 expression and induction of both IRE1α protein and its phosphorylation. Hence, IRE1α is activated in *Xbp1*-deficient liver, suggesting feedback regulation of IRE1α by its downstream target XBP1 in an ER stress independent manner. The hyperactivation of IRE1α is considered to be associated with protection against APAP-mediated liver injury. Hur and colleagues (134) reported that IRE1α hyperactivation in hepatocytes results in reduced JNK activation and protection from APAP through activation of regulated IRE1α-dependent decay (RIDD) and regulating the stability of CYP450 activity by RIDD (134). RIDD was shown to reduce ER localized mRNA in mouse cells (212). The RIDD process selectively targets and degrades mRNA encoding proteins, which include but are not limited to mRNA encoding CYP450 drug-metabolizing enzymes. From our data, reduction of *Cyp2e1* mRNA and protein levels were also observed in *Xbp1*-deficient mice with APAP-induced hepatotoxicity, and correspondingly intracellular free radicals and oxidative stress were also decreased in *Xbp1*-deficient mice.

Consistent with the known role of XBP1 in the transcriptional regulation of hepatic lipogenesis (211), $Xbp1^{\Delta hepa}$ mice showed reduced hepatic lipid and triglyceride accumulation. RIDD also play important roles in hepatic lipid metabolism. IRE1 hyperactivation as a feedback of *Xbp1* deficiency induced the degradation of mRNAs of a cohort of lipid metabolism genes, such as *Dgat2, Acacb, Pcsk9, Angptl3* and *Ces1*, which regulate triglyceride and cholesterol metabolism at multiple levels. Suppression of RIDD by IRE1 siRNA markedly restored plasma triglyceride and cholesterol levels in *Xbp1*-deficient mice, along with the induction of lipid metabolism genes (213). Moreover, associated with IRE1α hyperactivation, CHOP and BiP/GRP78, and JNK1/2 were dramatically reduced in *Xbp1*-deficient mice 24 h after APAP injection. JNK is activated by oxidative stress, and mediates a

crucial role in APAP-induced liver injury. However, JNK was not strongly activated in *Xbp1*-deficient mice, compared to $Xbp1^{f/f}$ mice, which might imply the possible mechanism of the observed protection from APAP liver toxicity. In addition, hepatocyte polarity and junctions-measured as ZO-1, and immune infiltration, inflammation and inflammasome activation were also ameliorated in $Xbp1^{\Delta hepa}$ animals after APAP injection.

In recent years, accumulating evidences indicate that autophagy is activated in response to APAP overdose in specific liver zone areas, and protects against APAP-induced liver injury (109, 214). Autophagy is a catabolic process that degrades and recycles damaged organelles and misfolded proteins through the lysosomal machinery (215, 216). Autophagy can eliminate damaged mitochondria and maintain mitochondrial homeostasis (217), which are the major source of intracellular ROS during APAP hepatotoxicity. Moreover, inhibition of autophagy exacerbated APAP-induced liver injury while induction of autophagy have a protective effect against APAP hepatotoxicity (109). Besides, mitophagy critically mediates regulating cell death process through the removal of damage mitochondria (218).

In our mice, TEM showed hepatocytes had normal ER ultrastructure in $Xbp1^{\Delta hepa}$ mice, but abundant autophagosomes formation and less mitochondrial damage under APAP toxicity. Additionally, *Xbp1* deficiency significantly promoted the phosphorylation of AMPK, augmented the effect of APAP overdose on the induction of *Atg5* and LC3-II levels and suppressed the levels of P62, indicating that APAP-induced autophagosome formation in the liver was promoted by ablation of *Xbp1* gene. Autophagy starts from the formation of a double-membrane structure, the autophagosome, which enwrap cytoplasm and organelle. Autophagosomes then fuse with lysosomes to form autolysosomes thus degrading the enveloped contents (219). More than 30 *Atg* genes have been defined to participate in autophagy processes (220).

The first step in vesicle nucleation is to activate Vps34 (Class III phosphatidylinositol 3-kinase), which associates with a complex formed by Beclin-1, UV radiation resistance and the kinase Vps15/p150 (221). Beclin-1 can also interact with the anti-apoptotic protein Bcl-2 at the ER (222). The next stage of extension

involves two ubiquitin-like binding steps. First, under the joint action of ATG7 (E1 like) and ATG10 (E2 like), the proteins ATG12 and ATG5 are covalently bound together. Second, the conjugation of ATG8 with phosphatidylethanolamine (PE) in the autophagic vesicle membrane occurs after proteolytic cleavage by the cysteine protease ATG4. It is believed that the subsequent recruitment of ATG8 and other autophagy-related proteins will trigger vesicle expansion in a consistent manner (223). Transient conjugation of ATG8 to the membrane lipid PE is essential for the expansion of phagophore, because its mutations can cause defects in autophagosome formation (224). After vesicle expansion is completed, the autophagosome is ready to fuse with the lysosome, and ATG8 can be released from the membrane for recycling or degradation in the autolysate. The PE-conjugated and ATG4 cleavage form of LC3, called LC3-II, is commonly used as an autophagy marker (225). The regulatory process of autophagy involves the inhibition of mammalian target of rapamycin (mTOR) Ser/Thr kinase, which prevents autophagy through the phosphorylation of ATG13, and dissociates the protein from the complex formed by ATG1 (a protein kinase) and ATG17. Therefore, when mTOR becomes inhibited by, for example, rapamycin, autophagy is induced (226). AMPK is an upstream regulator targeting on the activity of the Unc-51 like autophagy activating kinase 1 (ULK1) complex. When cells suffer from stress, AMPK is activated and phosphorylates ULK1 and promotes autophagy (227, 228).

The relationship between ER stress and autophagy is complex. Elucidation of the precise mechanism regulating autophagy is warranted to identify a therapeutic target for this prevalent and serious liver disease. Unfolded or misfolded proteins can be also reversed back to the cytoplasm and trigger ER-associated protein degradation (ERAD) which mainly consists of two mechanisms: ubiquitinproteasome-dependent ERAD and autophagy-lysosome dependent ERAD (229). Although it is recognized that ERAD is the main cellular mechanism for removing unfolded proteins during ER stress, many studies have shown that ER stress can effectively activate autophagy. For example, it has been reported that the release of Ca^{2+} from ER stimulates the CamKK/AMPK-dependent pathway and induces autophagy (230). Sakaki et al.

suggested that the release of Ca^{2+} from the ER induced the activation of protein kinase C (PKC) and autophagy through an mTOR-independent mechanism (231). The PERK/elF2α signaling pathway has been proved to induce ATG12 expression and mediate autophagy through ATF4-driven transcriptional regulation of ATG genes (232, 233). In addition, previous studies have indicated that IRE1α forms a complex with TRAF2 and ASK1, which causes activation downstream of stress kinases JNK (194). JNK mediates phosphorylation of Bcl-2 and causes the release of Beclin-1, thereby promoting autophagy (221).

Recently, accumulating evidence has revealed the bidirectional linkage between autophagy and ER stress (183, 234), and ER stress can modulate autophagy *via* the AMPK activation and AKT/mTOR inhibition (183, 234). AMPK can be activated under many conditions, such as hypoxia, DNA damage, glucose deprivation and free radical generation (235). Activated AMPK induces autophagy by direct phosphorylaiton of ULK1 at multiple sites, in turn initiating autophagosome formation (236). ULK1 is the most upstream signaling component of the core autophagy machinery (237). Our study showed the upregulation of pAMPK expression in *Xbp1*-deficient mice against APAP, which is parallel to IRE1α activation. These data give a possibility of regulatory cross talk between IRE1α-XBP1 arm and AMPK signaling pathways. Gordon P Meares et al have proved that AMPK phosphorylation in response to nitric oxide is attenuated in cells depleted of IRE1α by siRNA knockdown, confirming that IRE1α participates in AMPK activation (238). Besides, activated AMPK then phosphorylates Raptor and influences mTOR signaling. mTOR is a key kinase regulating the synthesis and metabolism of protein and lipid, which can phosphorylate ULK1 at its inhibitory site (S757) and inhibit autophagy (239). The AKT/mTOR pathway has been recognized as a significant regulator of autophagy (240). Inhibition of the AKT/mTOR pathway has been reported to promote autophagy and apoptosis to produce anticancer effect (241). Our study showed that the overexpression of pAKT reduced expression of LC3-II in $Xbp1^{f/f}$ mice, demonstrating that the downregulation of AKT signaling

pathway markedly contributed to autophagy and protection against APAP in *Xbp1*-deficient mice.

Additionally, now it is also supported that an autophagy-cargo receptor complex, including ubiquitin and P62, mediates the selective autophagic removal of protein aggregates and organells (242). The increase in necrosis due to APAP toxicity in *p62* knockdown hepatocytes indicates that *p62*-mediated selective autophagy plays a role in protecting against APAP-induced liver injury (243). In terms of mechanism, P62 directly binds to polyubiquitin or monoubiquitin through its C-terminal ubiquitin-associated domain (UBA). P62 also directly binds to LC3 through its LC3-interaction region (LIR), thereby acting as a cargo adaptor for ubiquitinated proteins and linking them with autophagy degradation (244). P62 can bind to APAP-adducts (APAP-AD) and promote the transition of APAP-AD to a detergent-insoluble "protein aggregate"-like structure, which can only be removed by autophagy. Therefore, P62 can be used as a selective receptor for APAP-AD for its selective autophagy removal. P62 also serves as a marker of autophagic flux through its involvement in recognizing cargo for autophagosomes. High cytoplasmic P62 expression accompanied with either a low or high LC3II expression indicates the impairment of autophagy under basal or activated autophagic activity (**Fig. 23**).

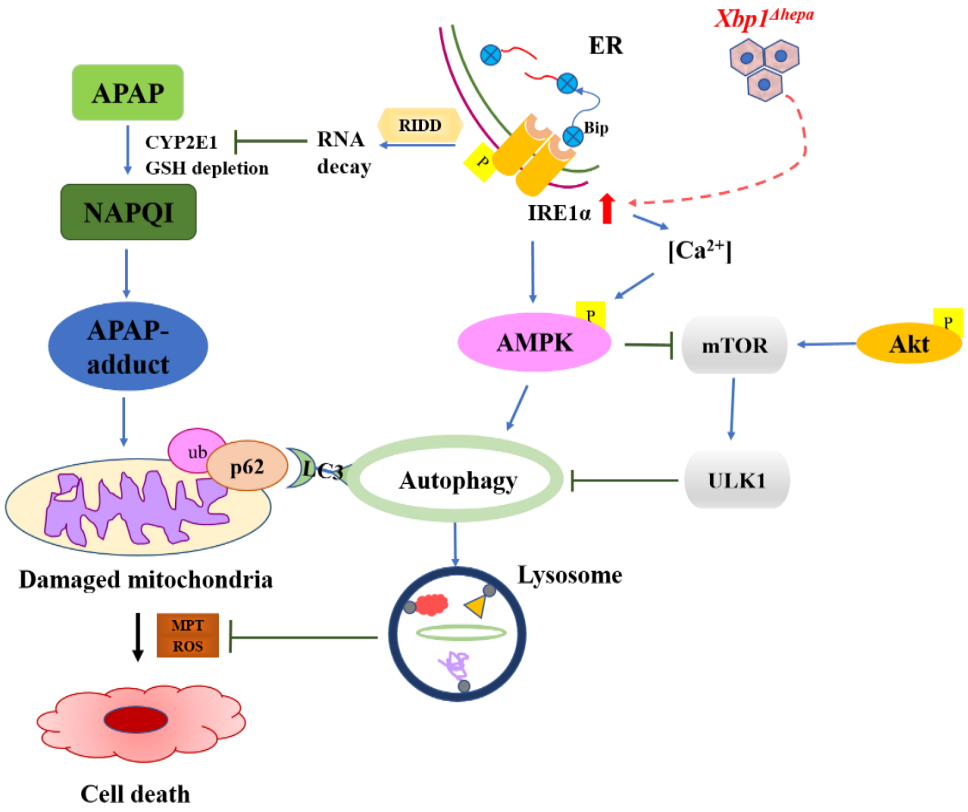

Figure 23. Schematic diagram of the protective effects observed in *Xbp1*$^{\Delta hepa}$ mice. APAP hepatotoxicity induces ER stress and mitochondrial dysfunction. The ablation of *Xbp1* in hepatocytes upregulates the expression of pIRE1α and promotes the activation of AMPK. Enhanced pAMPK expression is associated with an enhancement of autophagy (increased LC3-II formation and p62 degradation), which can degrade and recycle damaged organelles and misfolded proteins through the lysosomal machinery, thus protecting liver against APAP hepatotoxicity. Besides, activated IRE1α can limit translation of some mRNA through regulated IRE1α-regulated decay (RIDD).

Furthermore, autophagy and inflammation are the two major innate immune pathways in the body that are mutually regulated by each other, which can control the invasion of pathogens. In 2008, Saitoh et al. reported for the first time that autophagy can regulate the activation of inflammasomes (245). Use of the inhibitors of autophagy or silencing Beclin, *Atg7* or *Atg5* can lead to the activation of inflammasomes (246), further confirming the regulatory role of autophagy in the activation of inflammasomes. Although it is generally believed that autophagy can regulate the activation of inflammasomes, the mechanism is not yet confirmed. Studies have found that at least the accumulation of ROS, mitochondrial DNA and inflammasome degradation are involved. It is worth noting that a recent study found

that autophagy can selectively remove damaged mitochondria, inhibit the activation of inflammasomes, and delay the inflammatory response. In contrast, knockout of autophagy-related genes *Lc3* and *beclin1* can upregulate NLRP3 levels and increase inflammation (247). This also provides a possible explanation for the protective effects against APAP in $Xbp1^{\Delta hepa}$ animals.

In summary, the present thesis provides a novel scheme in APAP-induced liver injury. APAP overdose could induce oxidative stress, ER stress and infiltration of inflammatory factors both *in vivo* and *in vitro*, thereby leading to cell death and liver parenchyma necrosis. However, ablation of *Xbp1* in hepatocytes would protect against APAP hepatotoxicity, likely due to the activation of autophagy through the AMPK activation and AKT inhibition. Meanwhile, our team now are also checking the expression of *Xbp1* in human liver suffering APAP damage, and tries to provide a theoretical basis for the clinical treatment in the future.

8. Conclusions

1) APAP of 10 mM in HepaRG cells induces apparent hepatocyte death, loss of TJs and lipid accumulation.
2) A sublethal dose of APAP (≥300 mg/kg) suffices to induce liver damage, hepatocyte necrosis, loss of TJs, oxidative stress, immune infiltration and inflammation and lipid accumulation in WT mice.
3) Activation of the IRE1α-XBP1 arm and JNK1/2 is feature both in human and murine APAP-mediated hepatotoxicity, demonstrating the functionality of IRE1-XBP1 arm to the APAP-induced injury.
4) Loss of *Xbp1* in hepatocytes have a protective effect against APAP-induced liver injury, evidenced by decreased hepatocyte death and maintenance of TJs.
5) Ablation of *Xbp1* in hepatocytes decreases activation of UPR and JNK1/2 in response to a sublethal dose of APAP
6) Ablation of *Xbp1* in hepatocytes also reduces oxidative stress and lipid accumulation, ameliorates the infiltration of immune cells and inhibits activation of inflammasome.
7) The protective effect in $Xbp1^{\Delta hepa}$ mice is likely due to the activation of autophagy via AMPK activation and AKT inhibition, which provides the basis for therapies targeting the restoration of LPC function after acute liver injury.

9. References

1. Racanelli V, Rehermann B. The liver as an immunological organ. Hepatology 2006;43:S54-62.
2. The Liver: Biology and Pathobiology, Sixth Edition: John Wiley & Sons Ltd, 2020.
3. Lautt WW: In: Hepatic Circulation: Physiology and Pathophysiology. San Rafael (CA), 2009.
4. Ishibashi H, Nakamura M, Komori A, Migita K, Shimoda S. Liver architecture, cell function, and disease. Semin Immunopathol 2009;31:399-409.
5. Rappaport AM, Borowy ZJ, Lougheed WM, Lotto WN. Subdivision of hexagonal liver lobules into a structural and functional unit; role in hepatic physiology and pathology. Anat Rec 1954;119:11-33.
6. Cummings B. Human Anatomy & Physiology. 5th Edition ed: Addison Wesley Longman, Inc., 2001.
7. Blouin A, Bolender RP, Weibel ER. Distribution of organelles and membranes between hepatocytes and nonhepatocytes in the rat liver parenchyma. A stereological study. J Cell Biol 1977;72:441-455.
8. Weibel ER, Staubli W, Gnagi HR, Hess FA. Correlated morphometric and biochemical studies on the liver cell. I. Morphometric model, stereologic methods, and normal morphometric data for rat liver. J Cell Biol 1969;42:68-91.
9. Ali ES, Hua J, Wilson CH, Tallis GA, Zhou FH, Rychkov GY, Barritt GJ. The glucagon-like peptide-1 analogue exendin-4 reverses impaired intracellular Ca(2+) signalling in steatotic hepatocytes. Biochim Biophys Acta 2016;1863:2135-2146.
10. http://www.vivo.colostate.edu/hbooks/pathphys/digestion/liver/histo_hcytes.html.
11. McMahan RH, Porsche CE, Edwards MG, Rosen HR. Free Fatty Acids Differentially Downregulate Chemokines in Liver Sinusoidal Endothelial Cells: Insights into Non-Alcoholic Fatty Liver Disease. PLoS One 2016;11:e0159217.
12. Yokomori H. New insights into the dynamics of sinusoidal endothelial fenestrae in liver sinusoidal endothelial cells. Med Mol Morphol 2008;41:1-4.
13. Anderson CL. The liver sinusoidal endothelium reappears after being eclipsed by the Kupffer cell: a 20th century biological delusion corrected. J Leukoc Biol 2015;98:875-876.
14. Niki T, De Bleser PJ, Xu G, Van Den Berg K, Wisse E, Geerts A. Comparison of glial fibrillary acidic protein and desmin staining in normal and CCl4-induced fibrotic rat livers. Hepatology 1996;23:1538-1545.
15. Ballardini G, Groff P, Badiali de Giorgi L, Schuppan D, Bianchi FB. Ito cell heterogeneity: desmin-negative Ito cells in normal rat liver. Hepatology 1994;19:440-446.
16. Jenne CN, Kubes P. Immune surveillance by the liver. Nat Immunol 2013;14:996-1006.
17. Zhang H, Leung PSC, Gershwin ME, Ma X. How the biliary tree maintains immune tolerance? Biochim Biophys Acta Mol Basis Dis 2018;1864:1367-1373.
18. Doherty DG, O'Farrelly C. Innate and adaptive lymphoid cells in the human liver. Immunol Rev 2000;174:5-20.
19. Gomez Perdiguero E, Klapproth K, Schulz C, Busch K, Azzoni E, Crozet L, Garner H, et al. Tissue-resident macrophages originate from yolk-sac-derived erythro-myeloid progenitors. Nature 2015;518:547-551.
20. Almazroo OA, Miah MK, Venkataramanan R. Drug Metabolism in the Liver. Clin Liver Dis 2017;21:1-20.
21. Guengerich FP. Mechanisms of drug toxicity and relevance to pharmaceutical development. Drug Metab Pharmacokinet 2011;26:3-14.
22. Park BK, Laverty H, Srivastava A, Antoine DJ, Naisbitt D, Williams DP. Drug bioactivation and

protein adduct formation in the pathogenesis of drug-induced toxicity. Chem Biol Interact 2011;192:30-36.

23. Reichen J, Paumgartner G. Uptake of bile acids by perfused rat liver. Am J Physiol 1976;231:734-742.

24. Cressman AM, Petrovic V, Piquette-Miller M. Inflammation-mediated changes in drug transporter expression/activity: implications for therapeutic drug response. Expert Rev Clin Pharmacol 2012;5:69-89.

25. Kim RB. 3-Hydroxy-3-methylglutaryl-coenzyme A reductase inhibitors (statins) and genetic variability (single nucleotide polymorphisms) in a hepatic drug uptake transporter: what's it all about? Clin Pharmacol Ther 2004;75:381-385.

26. Hagenbuch B, Dawson P. The sodium bile salt cotransport family SLC10. Pflugers Arch 2004;447:566-570.

27. Borst P, Zelcer N, van de Wetering K. MRP2 and 3 in health and disease. Cancer Lett 2006;234:51-61.

28. Kobayashi Y, Ohshiro N, Sakai R, Ohbayashi M, Kohyama N, Yamamoto T. Transport mechanism and substrate specificity of human organic anion transporter 2 (hOat2 [SLC22A7]). J Pharm Pharmacol 2005;57:573-578.

29. Heise M, Lautem A, Knapstein J, Schattenberg JM, Hoppe-Lotichius M, Foltys D, Weiler N, et al. Downregulation of organic cation transporters OCT1 (SLC22A1) and OCT3 (SLC22A3) in human hepatocellular carcinoma and their prognostic significance. BMC Cancer 2012;12:109.

30. Zhou SF. Structure, function and regulation of P-glycoprotein and its clinical relevance in drug disposition. Xenobiotica 2008;38:802-832.

31. Saito H, An R, Hirano H, Ishikawa T. Emerging new technology: QSAR analysis and MO Calculation to characterize interactions of protein kinase inhibitors with the human ABC transporter, ABCG2 (BCRP). Drug Metab Pharmacokinet 2010;25:72-83.

32. Gerloff T, Stieger B, Hagenbuch B, Madon J, Landmann L, Roth J, Hofmann AF, et al. The sister of P-glycoprotein represents the canalicular bile salt export pump of mammalian liver. J Biol Chem 1998;273:10046-10050.

33. Tornio A, Vakkilainen J, Neuvonen M, Backman JT, Neuvonen PJ, Niemi M. SLCO1B1 polymorphism markedly affects the pharmacokinetics of lovastatin acid. Pharmacogenet Genomics 2015;25:382-387.

34. Shitara Y, Hirano M, Sato H, Sugiyama Y. Gemfibrozil and its glucuronide inhibit the organic anion transporting polypeptide 2 (OATP2/OATP1B1:SLC21A6)-mediated hepatic uptake and CYP2C8-mediated metabolism of cerivastatin: analysis of the mechanism of the clinically relevant drug-drug interaction between cerivastatin and gemfibrozil. J Pharmacol Exp Ther 2004;311:228-236.

35. Pond SM, Tozer TN. First-pass elimination. Basic concepts and clinical consequences. Clin Pharmacokinet 1984;9:1-25.

36. Ghobadi E, Moloudizargari M, Asghari MH, Abdollahi M. The mechanisms of cyclophosphamide-induced testicular toxicity and the protective agents. Expert Opin Drug Metab Toxicol 2017;13:525-536.

37. Hrycay EG, Bandiera SM. Monooxygenase, peroxidase and peroxygenase properties and reaction mechanisms of cytochrome P450 enzymes. Adv Exp Med Biol 2015;851:1-61.

38. FP G. Human cytochrome P450 enzymes. 3rd edition ed. New York: Kluwer Academic/Plenum, 2005.

39. Preissner SC, Hoffmann MF, Preissner R, Dunkel M, Gewiess A, Preissner S. Polymorphic cytochrome P450 enzymes (CYPs) and their role in personalized therapy. PLoS One 2013;8:e82562.
40. Manikandan P, Nagini S. Cytochrome P450 Structure, Function and Clinical Significance: A Review. Curr Drug Targets 2018;19:38-54.
41. Orellana Bown M, Guajardo Tobar V. Actividad del citocromo P450 y su alteración en diversas patologías. 2004.
42. Granfors MT, Backman JT, Neuvonen M, Ahonen J, Neuvonen PJ. Fluvoxamine drastically increases concentrations and effects of tizanidine: a potentially hazardous interaction. Clin Pharmacol Ther 2004;75:331-341.
43. Perucca E, Richens A. Drug interactions with phenytoin. Drugs 1981;21:120-137.
44. Palleria C, Di Paolo A, Giofre C, Caglioti C, Leuzzi G, Siniscalchi A, De Sarro G, et al. Pharmacokinetic drug-drug interaction and their implication in clinical management. J Res Med Sci 2013;18:601-610.
45. Feldman M FL, editor. Sleisenger and Fordtran's Gastrointestinal and Liver Disease. Philadelphia; 2016.
46. Miguel A, Azevedo LF, Araujo M, Pereira AC. Frequency of adverse drug reactions in hospitalized patients: a systematic review and meta-analysis. Pharmacoepidemiol Drug Saf 2012;21:1139-1154.
47. Ye H, Nelson LJ, Gomez Del Moral M, Martinez-Naves E, Cubero FJ. Dissecting the molecular pathophysiology of drug-induced liver injury. World J Gastroenterol 2018;24:1373-1385.
48. Kaplowitz N. Drug-induced liver injury. Clin Infect Dis 2004;38 Suppl 2:S44-48.
49. Verma S, Kaplowitz N. Diagnosis, management and prevention of drug-induced liver injury. Gut 2009;58:1555-1564.
50. Hernandez N, Bessone F, Sanchez A, di Pace M, Brahm J, Zapata R, R AC, et al. Profile of idiosyncratic drug induced liver injury in Latin America: an analysis of published reports. Ann Hepatol 2014;13:231-239.
51. Myers RP, Shaheen AA, Li B, Dean S, Quan H. Impact of liver disease, alcohol abuse, and unintentional ingestions on the outcomes of acetaminophen overdose. Clin Gastroenterol Hepatol 2008;6:918-925; quiz 837.
52. Zhao X, Cong X, Zheng L, Xu L, Yin L, Peng J. Dioscin, a natural steroid saponin, shows remarkable protective effect against acetaminophen-induced liver damage in vitro and in vivo. Toxicol Lett 2012;214:69-80.
53. Craig DG, Bates CM, Davidson JS, Martin KG, Hayes PC, Simpson KJ. Overdose pattern and outcome in paracetamol-induced acute severe hepatotoxicity. Br J Clin Pharmacol 2011;71:273-282.
54. Jaeschke H, McGill MR, Williams CD, Ramachandran A. Current issues with acetaminophen hepatotoxicity--a clinically relevant model to test the efficacy of natural products. Life Sci 2011;88:737-745.
55. Bunchorntavakul C, Reddy KR. Acetaminophen-related hepatotoxicity. Clin Liver Dis 2013;17:587-607, viii.
56. Blieden M, Paramore LC, Shah D, Ben-Joseph R. A perspective on the epidemiology of acetaminophen exposure and toxicity in the United States. Expert Rev Clin Pharmacol 2014;7:341-348.
57. Jaeschke H, McGill MR. Cytochrome P450-derived versus mitochondrial oxidant stress in acetaminophen hepatotoxicity. Toxicol Lett 2015;235:216-217.
58. Jaeschke H, Knight TR, Bajt ML. The role of oxidant stress and reactive nitrogen species in

acetaminophen hepatotoxicity. Toxicol Lett 2003;144:279-288.

59. Park BK, Dear JW, Antoine DJ. Paracetamol (acetaminophen) poisoning. BMJ Clin Evid 2015;2015.

60. McGill MR, Jaeschke H. Metabolism and disposition of acetaminophen: recent advances in relation to hepatotoxicity and diagnosis. Pharm Res 2013;30:2174-2187.

61. Yuan L, Kaplowitz N. Mechanisms of drug-induced liver injury. Clin Liver Dis 2013;17:507-518, vii.

62. Clark R, Fisher JE, Sketris IS, Johnston GM. Population prevalence of high dose paracetamol in dispensed paracetamol/opioid prescription combinations: an observational study. BMC Clin Pharmacol 2012;12:11.

63. Yoon E, Babar A, Choudhary M, Kutner M, Pyrsopoulos N. Acetaminophen-Induced Hepatotoxicity: a Comprehensive Update. J Clin Transl Hepatol 2016;4:131-142.

64. Davern TJ, 2nd, James LP, Hinson JA, Polson J, Larson AM, Fontana RJ, Lalani E, et al. Measurement of serum acetaminophen-protein adducts in patients with acute liver failure. Gastroenterology 2006;130:687-694.

65. Heard K, Green JL, Anderson V, Bucher-Bartelson B, Dart RC. Paracetamol (acetaminophen) protein adduct concentrations during therapeutic dosing. Br J Clin Pharmacol 2016;81:562-568.

66. McGill MR, Lebofsky M, Norris HR, Slawson MH, Bajt ML, Xie Y, Williams CD, et al. Plasma and liver acetaminophen-protein adduct levels in mice after acetaminophen treatment: dose-response, mechanisms, and clinical implications. Toxicol Appl Pharmacol 2013;269:240-249.

67. McGill MR, Yan HM, Ramachandran A, Murray GJ, Rollins DE, Jaeschke H. HepaRG cells: a human model to study mechanisms of acetaminophen hepatotoxicity. Hepatology 2011;53:974-982.

68. Jollow DJ, Mitchell JR, Potter WZ, Davis DC, Gillette JR, Brodie BB. Acetaminophen-induced hepatic necrosis. II. Role of covalent binding in vivo. J Pharmacol Exp Ther 1973;187:195-202.

69. Hu J, Ramshesh VK, McGill MR, Jaeschke H, Lemasters JJ. Low Dose Acetaminophen Induces Reversible Mitochondrial Dysfunction Associated with Transient c-Jun N-Terminal Kinase Activation in Mouse Liver. Toxicol Sci 2016;150:204-215.

70. Xie Y, McGill MR, Du K, Dorko K, Kumer SC, Schmitt TM, Ding WX, et al. Mitochondrial protein adducts formation and mitochondrial dysfunction during N-acetyl-m-aminophenol (AMAP)-induced hepatotoxicity in primary human hepatocytes. Toxicol Appl Pharmacol 2015;289:213-222.

71. Heard KJ. Acetylcysteine for acetaminophen poisoning. N Engl J Med 2008;359:285-292.

72. Kerr F, Dawson A, Whyte IM, Buckley N, Murray L, Graudins A, Chan B, et al. The Australasian Clinical Toxicology Investigators Collaboration randomized trial of different loading infusion rates of N-acetylcysteine. Ann Emerg Med 2005;45:402-408.

73. Chun LJ, Tong MJ, Busuttil RW, Hiatt JR. Acetaminophen hepatotoxicity and acute liver failure. J Clin Gastroenterol 2009;43:342-349.

74. Jaeschke H, Williams CD, Ramachandran A, Bajt ML. Acetaminophen hepatotoxicity and repair: the role of sterile inflammation and innate immunity. Liver Int 2012;32:8-20.

75. McGill MR, Sharpe MR, Williams CD, Taha M, Curry SC, Jaeschke H. The mechanism underlying acetaminophen-induced hepatotoxicity in humans and mice involves mitochondrial damage and nuclear DNA fragmentation. J Clin Invest 2012;122:1574-1583.

76. Brand MD, Affourtit C, Esteves TC, Green K, Lambert AJ, Miwa S, Pakay JL, et al. Mitochondrial superoxide: production, biological effects, and activation of uncoupling proteins. Free Radic Biol Med 2004;37:755-767.

77. Casteilla L, Rigoulet M, Penicaud L. Mitochondrial ROS metabolism: modulation by uncoupling

proteins. IUBMB Life 2001;52:181-188.

78. Sies H, de Groot H. Role of reactive oxygen species in cell toxicity. Toxicol Lett 1992;64-65 Spec No:547-551.

79. Aust SD, Morehouse LA, Thomas CE. Role of metals in oxygen radical reactions. J Free Radic Biol Med 1985;1:3-25.

80. Cover C, Mansouri A, Knight TR, Bajt ML, Lemasters JJ, Pessayre D, Jaeschke H. Peroxynitrite-induced mitochondrial and endonuclease-mediated nuclear DNA damage in acetaminophen hepatotoxicity. J Pharmacol Exp Ther 2005;315:879-887.

81. Gardner CR, Heck DE, Yang CS, Thomas PE, Zhang XJ, DeGeorge GL, Laskin JD, et al. Role of nitric oxide in acetaminophen-induced hepatotoxicity in the rat. Hepatology 1998;27:748-754.

82. Radi R, Peluffo G, Alvarez MN, Naviliat M, Cayota A. Unraveling peroxynitrite formation in biological systems. Free Radic Biol Med 2001;30:463-488.

83. Koop DR. Oxidative and reductive metabolism by cytochrome P450 2E1. FASEB J 1992;6:724-730.

84. Yan M, Huo Y, Yin S, Hu H. Mechanisms of acetaminophen-induced liver injury and its implications for therapeutic interventions. Redox Biol 2018;17:274-283.

85. Seki E, Brenner DA, Karin M. A liver full of JNK: signaling in regulation of cell function and disease pathogenesis, and clinical approaches. Gastroenterology 2012;143:307-320.

86. Cubero FJ, Zoubek ME, Hu W, Peng J, Zhao G, Nevzorova YA, Al Masaoudi M, et al. Combined Activities of JNK1 and JNK2 in Hepatocytes Protect Against Toxic Liver Injury. Gastroenterology 2016;150:968-981.

87. Sharma M, Gadang V, Jaeschke A. Critical role for mixed-lineage kinase 3 in acetaminophen-induced hepatotoxicity. Mol Pharmacol 2012;82:1001-1007.

88. Shinohara M, Ybanez MD, Win S, Than TA, Jain S, Gaarde WA, Han D, et al. Silencing glycogen synthase kinase-3beta inhibits acetaminophen hepatotoxicity and attenuates JNK activation and loss of glutamate cysteine ligase and myeloid cell leukemia sequence 1. J Biol Chem 2010;285:8244-8255.

89. Kallunki T, Deng T, Hibi M, Karin M. c-Jun can recruit JNK to phosphorylate dimerization partners via specific docking interactions. Cell 1996;87:929-939.

90. Whitmarsh AJ, Davis RJ. Role of mitogen-activated protein kinase kinase 4 in cancer. Oncogene 2007;26:3172-3184.

91. Win S, Than TA, Min RW, Aghajan M, Kaplowitz N. c-Jun N-terminal kinase mediates mouse liver injury through a novel Sab (SH3BP5)-dependent pathway leading to inactivation of intramitochondrial Src. Hepatology 2016;63:1987-2003.

92. Zhang J, Min RWM, Le K, Zhou S, Aghajan M, Than TA, Win S, et al. The role of MAP2 kinases and p38 kinase in acute murine liver injury models. Cell Death Dis 2017;8:e2903.

93. Hanawa N, Shinohara M, Saberi B, Gaarde WA, Han D, Kaplowitz N. Role of JNK translocation to mitochondria leading to inhibition of mitochondria bioenergetics in acetaminophen-induced liver injury. J Biol Chem 2008;283:13565-13577.

94. Win S, Than TA, Han D, Petrovic LM, Kaplowitz N. c-Jun N-terminal kinase (JNK)-dependent acute liver injury from acetaminophen or tumor necrosis factor (TNF) requires mitochondrial Sab protein expression in mice. J Biol Chem 2011;286:35071-35078.

95. Saito C, Lemasters JJ, Jaeschke H. c-Jun N-terminal kinase modulates oxidant stress and peroxynitrite formation independent of inducible nitric oxide synthase in acetaminophen hepatotoxicity. Toxicol Appl Pharmacol 2010;246:8-17.

96. Walker RM, Racz WJ, McElligott TF. Acetaminophen-induced hepatotoxicity in mice. Lab Invest 1980;42:181-189.
97. Bulera SJ, Cohen SD, Khairallah EA. Acetaminophen-arylated proteins are detected in hepatic subcellular fractions and numerous extra-hepatic tissues in CD-1 and C57B1/6J mice. Toxicology 1996;109:85-99.
98. Tirmenstein MA, Nelson SD. Subcellular binding and effects on calcium homeostasis produced by acetaminophen and a nonhepatotoxic regioisomer, 3'-hydroxyacetanilide, in mouse liver. J Biol Chem 1989;264:9814-9819.
99. Burcham PC, Harman AW. Acetaminophen toxicity results in site-specific mitochondrial damage in isolated mouse hepatocytes. J Biol Chem 1991;266:5049-5054.
100. Donnelly PJ, Walker RM, Racz WJ. Inhibition of mitochondrial respiration in vivo is an early event in acetaminophen-induced hepatotoxicity. Arch Toxicol 1994;68:110-118.
101. Vendemiale G, Grattagliano I, Altomare E, Turturro N, Guerrieri F. Effect of acetaminophen administration on hepatic glutathione compartmentation and mitochondrial energy metabolism in the rat. Biochem Pharmacol 1996;52:1147-1154.
102. Andersson BS, Rundgren M, Nelson SD, Harder S. N-acetyl-p-benzoquinone imine-induced changes in the energy metabolism in hepatocytes. Chem Biol Interact 1990;75:201-211.
103. Weis M, Kass GE, Orrenius S, Moldeus P. N-acetyl-p-benzoquinone imine induces Ca2+ release from mitochondria by stimulating pyridine nucleotide hydrolysis. J Biol Chem 1992;267:804-809.
104. Gomez-Lechon MJ, Tolosa L, Donato MT. Metabolic activation and drug-induced liver injury: in vitro approaches for the safety risk assessment of new drugs. J Appl Toxicol 2016;36:752-768.
105. Hinson JA, Pike SL, Pumford NR, Mayeux PR. Nitrotyrosine-protein adducts in hepatic centrilobular areas following toxic doses of acetaminophen in mice. Chem Res Toxicol 1998;11:604-607.
106. Karch J, Kwong JQ, Burr AR, Sargent MA, Elrod JW, Peixoto PM, Martinez-Caballero S, et al. Bax and Bak function as the outer membrane component of the mitochondrial permeability pore in regulating necrotic cell death in mice. Elife 2013;2:e00772.
107. Honda HM, Korge P, Weiss JN. Mitochondria and ischemia/reperfusion injury. Ann N Y Acad Sci 2005;1047:248-258.
108. Ramachandran A, Lebofsky M, Baines CP, Lemasters JJ, Jaeschke H. Cyclophilin D deficiency protects against acetaminophen-induced oxidant stress and liver injury. Free Radic Res 2011;45:156-164.
109. Ni HM, Bockus A, Boggess N, Jaeschke H, Ding WX. Activation of autophagy protects against acetaminophen-induced hepatotoxicity. Hepatology 2012;55:222-232.
110. Kon K, Ikejima K, Okumura K, Aoyama T, Arai K, Takei Y, Lemasters JJ, et al. Role of apoptosis in acetaminophen hepatotoxicity. J Gastroenterol Hepatol 2007;22 Suppl 1:S49-52.
111. Reid AB, Kurten RC, McCullough SS, Brock RW, Hinson JA. Mechanisms of acetaminophen-induced hepatotoxicity: role of oxidative stress and mitochondrial permeability transition in freshly isolated mouse hepatocytes. J Pharmacol Exp Ther 2005;312:509-516.
112. Boobis AR, Tee LB, Hampden CE, Davies DS. Freshly isolated hepatocytes as a model for studying the toxicity of paracetamol. Food Chem Toxicol 1986;24:731-736.
113. Tee LB, Boobis AR, Huggett AC, Davies DS. Reversal of acetaminophen toxicity in isolated hamster hepatocytes by dithiothreitol. Toxicol Appl Pharmacol 1986;83:294-314.
114. Dejean LM, Martinez-Caballero S, Manon S, Kinnally KW. Regulation of the mitochondrial

apoptosis-induced channel, MAC, by BCL-2 family proteins. Biochim Biophys Acta 2006;1762:191-201.
115. Kinnally KW, Antonsson B. A tale of two mitochondrial channels, MAC and PTP, in apoptosis. Apoptosis 2007;12:857-868.
116. Ramachandran A, Jaeschke H. Acetaminophen Toxicity: Novel Insights Into Mechanisms and Future Perspectives. Gene Expr 2018;18:19-30.
117. Antonsson B, Montessuit S, Lauper S, Eskes R, Martinou JC. Bax oligomerization is required for channel-forming activity in liposomes and to trigger cytochrome c release from mitochondria. Biochem J 2000;345 Pt 2:271-278.
118. Dejean LM, Martinez-Caballero S, Guo L, Hughes C, Teijido O, Ducret T, Ichas F, et al. Oligomeric Bax is a component of the putative cytochrome c release channel MAC, mitochondrial apoptosis-induced channel. Mol Biol Cell 2005;16:2424-2432.
119. Dejean LM, Martinez-Caballero S, Kinnally KW. Is MAC the knife that cuts cytochrome c from mitochondria during apoptosis? Cell Death Differ 2006;13:1387-1395.
120. Boelsterli UA, Lim PL. Mitochondrial abnormalities--a link to idiosyncratic drug hepatotoxicity? Toxicol Appl Pharmacol 2007;220:92-107.
121. Kon K, Kim JS, Jaeschke H, Lemasters JJ. Mitochondrial permeability transition in acetaminophen-induced necrosis and apoptosis of cultured mouse hepatocytes. Hepatology 2004;40:1170-1179.
122. Uzi D, Barda L, Scaiewicz V, Mills M, Mueller T, Gonzalez-Rodriguez A, Valverde AM, et al. CHOP is a critical regulator of acetaminophen-induced hepatotoxicity. J Hepatol 2013;59:495-503.
123. Letelier ME, Lopez-Valladares M, Peredo-Silva L, Rojas-Sepulveda D, Aracena P. Microsomal oxidative damage promoted by acetaminophen metabolism. Toxicol In Vitro 2011;25:1310-1313.
124. Shin NY, Liu Q, Stamer SL, Liebler DC. Protein targets of reactive electrophiles in human liver microsomes. Chem Res Toxicol 2007;20:859-867.
125. King YA, Chiu YJ, Chen HP, Kuo DH, Lu CC, Yang JS. Endoplasmic reticulum stress contributes to arsenic trioxide-induced intrinsic apoptosis in human umbilical and bone marrow mesenchymal stem cells. Environ Toxicol 2016;31:314-328.
126. Xu C, Bailly-Maitre B, Reed JC. Endoplasmic reticulum stress: cell life and death decisions. J Clin Invest 2005;115:2656-2664.
127. McCullough KD, Martindale JL, Klotz LO, Aw TY, Holbrook NJ. Gadd153 sensitizes cells to endoplasmic reticulum stress by down-regulating Bcl2 and perturbing the cellular redox state. Mol Cell Biol 2001;21:1249-1259.
128. Lei K, Davis RJ. JNK phosphorylation of Bim-related members of the Bcl2 family induces Bax-dependent apoptosis. Proc Natl Acad Sci U S A 2003;100:2432-2437.
129. Deng X, Xiao L, Lang W, Gao F, Ruvolo P, May WS, Jr. Novel role for JNK as a stress-activated Bcl2 kinase. J Biol Chem 2001;276:23681-23688.
130. Kim I, Xu W, Reed JC. Cell death and endoplasmic reticulum stress: disease relevance and therapeutic opportunities. Nat Rev Drug Discov 2008;7:1013-1030.
131. Puthalakath H, O'Reilly LA, Gunn P, Lee L, Kelly PN, Huntington ND, Hughes PD, et al. ER stress triggers apoptosis by activating BH3-only protein Bim. Cell 2007;129:1337-1349.
132. Yamaguchi H, Wang HG. CHOP is involved in endoplasmic reticulum stress-induced apoptosis by enhancing DR5 expression in human carcinoma cells. J Biol Chem 2004;279:45495-45502.
133. Zinszner H, Kuroda M, Wang X, Batchvarova N, Lightfoot RT, Remotti H, Stevens JL, et al. CHOP is implicated in programmed cell death in response to impaired function of the endoplasmic

reticulum. Genes Dev 1998;12:982-995.

134. Hur KY, So JS, Ruda V, Frank-Kamenetsky M, Fitzgerald K, Koteliansky V, Iwawaki T, et al. IRE1alpha activation protects mice against acetaminophen-induced hepatotoxicity. J Exp Med 2012;209:307-318.

135. Liu X, Green RM. Endoplasmic reticulum stress and liver diseases. Liver Res 2019;3:55-64.

136. Antoine DJ, Jenkins RE, Dear JW, Williams DP, McGill MR, Sharpe MR, Craig DG, et al. Molecular forms of HMGB1 and keratin-18 as mechanistic biomarkers for mode of cell death and prognosis during clinical acetaminophen hepatotoxicity. J Hepatol 2012;56:1070-1079.

137. Martin-Murphy BV, Holt MP, Ju C. The role of damage associated molecular pattern molecules in acetaminophen-induced liver injury in mice. Toxicol Lett 2010;192:387-394.

138. Woolbright BL, Jaeschke H. Role of the inflammasome in acetaminophen-induced liver injury and acute liver failure. J Hepatol 2017;66:836-848.

139. Kubes P, Mehal WZ. Sterile inflammation in the liver. Gastroenterology 2012;143:1158-1172.

140. Liu ZX, Han D, Gunawan B, Kaplowitz N. Neutrophil depletion protects against murine acetaminophen hepatotoxicity. Hepatology 2006;43:1220-1230.

141. Jaeschke H, Liu J. Neutrophil depletion protects against murine acetaminophen hepatotoxicity: another perspective. Hepatology 2007;45:1588-1589; author reply 1589.

142. Cover C, Liu J, Farhood A, Malle E, Waalkes MP, Bajt ML, Jaeschke H. Pathophysiological role of the acute inflammatory response during acetaminophen hepatotoxicity. Toxicol Appl Pharmacol 2006;216:98-107.

143. James LP, McCullough SS, Knight TR, Jaeschke H, Hinson JA. Acetaminophen toxicity in mice lacking NADPH oxidase activity: role of peroxynitrite formation and mitochondrial oxidant stress. Free Radic Res 2003;37:1289-1297.

144. Williams CD, Bajt ML, Sharpe MR, McGill MR, Farhood A, Jaeschke H. Neutrophil activation during acetaminophen hepatotoxicity and repair in mice and humans. Toxicol Appl Pharmacol 2014;275:122-133.

145. Imaeda AB, Watanabe A, Sohail MA, Mahmood S, Mohamadnejad M, Sutterwala FS, Flavell RA, et al. Acetaminophen-induced hepatotoxicity in mice is dependent on Tlr9 and the Nalp3 inflammasome. J Clin Invest 2009;119:305-314.

146. Williams CD, Farhood A, Jaeschke H. Role of caspase-1 and interleukin-1beta in acetaminophen-induced hepatic inflammation and liver injury. Toxicol Appl Pharmacol 2010;247:169-178.

147. Zhang C, Feng J, Du J, Zhuo Z, Yang S, Zhang W, Wang W, et al. Macrophage-derived IL-1alpha promotes sterile inflammation in a mouse model of acetaminophen hepatotoxicity. Cell Mol Immunol 2018;15:973-982.

148. Kataoka H, Kono H, Patel Z, Kimura Y, Rock KL. Evaluation of the contribution of multiple DAMPs and DAMP receptors in cell death-induced sterile inflammatory responses. PLoS One 2014;9:e104741.

149. Lawson JA, Farhood A, Hopper RD, Bajt ML, Jaeschke H. The hepatic inflammatory response after acetaminophen overdose: role of neutrophils. Toxicol Sci 2000;54:509-516.

150. Dambach DM, Watson LM, Gray KR, Durham SK, Laskin DL. Role of CCR2 in macrophage migration into the liver during acetaminophen-induced hepatotoxicity in the mouse. Hepatology 2002;35:1093-1103.

151. Holt MP, Cheng L, Ju C. Identification and characterization of infiltrating macrophages in acetaminophen-induced liver injury. J Leukoc Biol 2008;84:1410-1421.

152. Bourdi M, Masubuchi Y, Reilly TP, Amouzadeh HR, Martin JL, George JW, Shah AG, et al.

Protection against acetaminophen-induced liver injury and lethality by interleukin 10: role of inducible nitric oxide synthase. Hepatology 2002;35:289-298.

153. Adolph TE, Tomczak MF, Niederreiter L, Ko HJ, Bock J, Martinez-Naves E, Glickman JN, et al. Paneth cells as a site of origin for intestinal inflammation. Nature 2013;503:272-276.

154. Shen C, Ma W, Ding L, Li S, Dou X, Song Z. The TLR4-IRE1alpha pathway activation contributes to palmitate-elicited lipotoxicity in hepatocytes. J Cell Mol Med 2018;22:3572-3581.

155. Pfaffl MW. A new mathematical model for relative quantification in real-time RT-PCR. Nucleic Acids Res 2001;29:e45.

156. An L, Wang X, Cederbaum AI. Cytokines in alcoholic liver disease. Arch Toxicol 2012;86:1337-1348.

157. Kurien BT, Scofield RH. Western blotting. Methods 2006;38:283-293.

158. Gamal W, Treskes P, Samuel K, Sullivan GJ, Siller R, Srsen V, Morgan K, et al. Low-dose acetaminophen induces early disruption of cell-cell tight junctions in human hepatic cells and mouse liver. Sci Rep 2017;7:37541.

159. Yokoyama Y, Sasaki Y, Terasaki N, Kawataki T, Takekawa K, Iwase Y, Shimizu T, et al. Comparison of Drug Metabolism and Its Related Hepatotoxic Effects in HepaRG, Cryopreserved Human Hepatocytes, and HepG2 Cell Cultures. Biol Pharm Bull 2018;41:722-732.

160. Cubero FJ, Mohamed MR, Woitok MM, Zhao G, Hatting M, Nevzorova YA, Chen C, et al. Loss of c-Jun N-terminal Kinase 1 and 2 Function in Liver Epithelial Cells Triggers Biliary Hyperproliferation Resembling Cholangiocarcinoma. Hepatol Commun 2020;4:834-851.

161. Bhattacharyya S, Pence L, Beger R, Chaudhuri S, McCullough S, Yan K, Simpson P, et al. Acylcarnitine profiles in acetaminophen toxicity in the mouse: comparison to toxicity, metabolism and hepatocyte regeneration. Metabolites 2013;3:606-622.

162. Itoh M, Nagafuchi A, Moroi S, Tsukita S. Involvement of ZO-1 in cadherin-based cell adhesion through its direct binding to alpha catenin and actin filaments. J Cell Biol 1997;138:181-192.

163. Du K, Ramachandran A, Jaeschke H. Oxidative stress during acetaminophen hepatotoxicity: Sources, pathophysiological role and therapeutic potential. Redox Biol 2016;10:148-156.

164. Oak JH, Cai H. Attenuation of angiotensin II signaling recouples eNOS and inhibits nonendothelial NOX activity in diabetic mice. Diabetes 2007;56:118-126.

165. Zhao Q, Zhang J, Wang H. PGC-1alpha overexpression suppresses blood pressure elevation in DOCA-salt hypertensive mice. Biosci Rep 2015;35.

166. Miller JD, Chu Y, Brooks RM, Richenbacher WE, Pena-Silva R, Heistad DD. Dysregulation of antioxidant mechanisms contributes to increased oxidative stress in calcific aortic valvular stenosis in humans. J Am Coll Cardiol 2008;52:843-850.

167. Begriche K, Massart J, Robin MA, Borgne-Sanchez A, Fromenty B. Drug-induced toxicity on mitochondria and lipid metabolism: mechanistic diversity and deleterious consequences for the liver. J Hepatol 2011;54:773-794.

168. Lu Y, Zhang C, Chen YH, Wang H, Zhang ZH, Chen X, Xu DX. Immature mice are more susceptible than adult mice to acetaminophen-induced acute liver injury. Sci Rep 2017;7:42736.

169. Paine A, Eiz-Vesper B, Blasczyk R, Immenschuh S. Signaling to heme oxygenase-1 and its anti-inflammatory therapeutic potential. Biochem Pharmacol 2010;80:1895-1903.

170. Li L, Tang J, Sun Y, Wu J, Yu P, Wang G. Upregulation of HO-1 Attenuates LPS-Stimulated Proinflammatory Responses Through Downregulation of p38 Signaling Pathways in Rat Ovary. Inflammation 2015;38:1085-1092.

171. Chiu H, Brittingham JA, Laskin DL. Differential induction of heme oxygenase-1 in macrophages and hepatocytes during acetaminophen-induced hepatotoxicity in the rat: effects of hemin and biliverdin. Toxicol Appl Pharmacol 2002;181:106-115.
172. Rao R. Oxidative stress-induced disruption of epithelial and endothelial tight junctions. Front Biosci 2008;13:7210-7226.
173. Gunawan BK, Liu ZX, Han D, Hanawa N, Gaarde WA, Kaplowitz N. c-Jun N-terminal kinase plays a major role in murine acetaminophen hepatotoxicity. Gastroenterology 2006;131:165-178.
174. Nakagawa H, Maeda S, Hikiba Y, Ohmae T, Shibata W, Yanai A, Sakamoto K, et al. Deletion of apoptosis signal-regulating kinase 1 attenuates acetaminophen-induced liver injury by inhibiting c-Jun N-terminal kinase activation. Gastroenterology 2008;135:1311-1321.
175. Henderson NC, Pollock KJ, Frew J, Mackinnon AC, Flavell RA, Davis RJ, Sethi T, et al. Critical role of c-jun (NH2) terminal kinase in paracetamol- induced acute liver failure. Gut 2007;56:982-990.
176. Cederbaum AI, Lu Y, Wu D. Role of oxidative stress in alcohol-induced liver injury. Arch Toxicol 2009;83:519-548.
177. Kelley N, Jeltema D, Duan Y, He Y. The NLRP3 Inflammasome: An Overview of Mechanisms of Activation and Regulation. Int J Mol Sci 2019;20.
178. Piperi C, Adamopoulos C, Papavassiliou AG. XBP1: A Pivotal Transcriptional Regulator of Glucose and Lipid Metabolism. Trends Endocrinol Metab 2016;27:119-122.
179. Wu R, Zhang QH, Lu YJ, Ren K, Yi GH. Involvement of the IRE1alpha-XBP1 pathway and XBP1s-dependent transcriptional reprogramming in metabolic diseases. DNA Cell Biol 2015;34:6-18.
180. Park SW, Ozcan U. Potential for therapeutic manipulation of the UPR in disease. Semin Immunopathol 2013;35:351-373.
181. Henkel A, Green RM. The unfolded protein response in fatty liver disease. Semin Liver Dis 2013;33:321-329.
182. Song S, Tan J, Miao Y, Zhang Q. Crosstalk of ER stress-mediated autophagy and ER-phagy: Involvement of UPR and the core autophagy machinery. J Cell Physiol 2018;233:3867-3874.
183. Yorimitsu T, Nair U, Yang Z, Klionsky DJ. Endoplasmic reticulum stress triggers autophagy. J Biol Chem 2006;281:30299-30304.
184. Ogata M, Hino S, Saito A, Morikawa K, Kondo S, Kanemoto S, Murakami T, et al. Autophagy is activated for cell survival after endoplasmic reticulum stress. Mol Cell Biol 2006;26:9220-9231.
185. Verfaillie T, Salazar M, Velasco G, Agostinis P. Linking ER Stress to Autophagy: Potential Implications for Cancer Therapy. Int J Cell Biol 2010;2010:930509.
186. Zhan F, Zhao G, Li X, Yang S, Yang W, Zhou S, Zhang F. Inositol-requiring enzyme 1 alpha endoribonuclease specific inhibitor STF-083010 protects the liver from thioacetamide-induced oxidative stress, inflammation and injury by triggering hepatocyte autophagy. Int Immunopharmacol 2019;73:261-269.
187. Chen QQ, Zhang C, Qin MQ, Li J, Wang H, Xu DX, Wang JQ. Inositol-Requiring Enzyme 1 Alpha Endoribonuclease Specific Inhibitor STF-083010 Alleviates Carbon Tetrachloride Induced Liver Injury and Liver Fibrosis in Mice. Front Pharmacol 2018;9:1344.
188. Prescott LF. Paracetamol overdosage. Pharmacological considerations and clinical management. Drugs 1983;25:290-314.
189. Shi CX, Lin YX, Liu FP, Chang YC, Li R, Li CW, Li Y, et al. Hepatoprotective effects of ethanol extracts from Folium Syringae against acetaminophen-induced hepatotoxicity in vitro and in vivo. J Chin Med Assoc 2017;80:623-629.

190. Price VF, Jollow DJ. Effect of glucose and gluconeogenic substrates on fasting-induced suppression of acetaminophen glucuronidation in the rat. Biochem Pharmacol 1989;38:289-297.
191. Barman PK, Mukherjee R, Prusty BK, Suklabaidya S, Senapati S, Ravindran B. Chitohexaose protects against acetaminophen-induced hepatotoxicity in mice. Cell Death Dis 2016;7:e2224.
192. Murray TV, Dong X, Sawyer GJ, Caldwell A, Halket J, Sherwood R, Quaglia A, et al. NADPH oxidase 4 regulates homocysteine metabolism and protects against acetaminophen-induced liver damage in mice. Free Radic Biol Med 2015;89:918-930.
193. Liu F, Lin Y, Li Z, Ma X, Han Q, Liu Y, Zhou Q, et al. Glutathione S-transferase A1 (GSTA1) release, an early indicator of acute hepatic injury in mice. Food Chem Toxicol 2014;71:225-230.
194. Gardner BM, Walter P. Unfolded proteins are Ire1-activating ligands that directly induce the unfolded protein response. Science 2011;333:1891-1894.
195. Johnson GL, Nakamura K. The c-jun kinase/stress-activated pathway: regulation, function and role in human disease. Biochim Biophys Acta 2007;1773:1341-1348.
196. Matsumaru K, Ji C, Kaplowitz N. Mechanisms for sensitization to TNF-induced apoptosis by acute glutathione depletion in murine hepatocytes. Hepatology 2003;37:1425-1434.
197. Cederbaum AI, Yang L, Wang X, Wu D. CYP2E1 Sensitizes the Liver to LPS- and TNF alpha-Induced Toxicity via Elevated Oxidative and Nitrosative Stress and Activation of ASK-1 and JNK Mitogen-Activated Kinases. Int J Hepatol 2012;2012:582790.
198. Iorga A, Dara L, Kaplowitz N. Drug-Induced Liver Injury: Cascade of Events Leading to Cell Death, Apoptosis or Necrosis. Int J Mol Sci 2017;18.
199. Lee HC, Liao CC, Day YJ, Liou JT, Li AH, Liu FC. IL-17 deficiency attenuates acetaminophen-induced hepatotoxicity in mice. Toxicol Lett 2018;292:20-30.
200. Kim H, Lee JH, Park JW. IDH2 deficiency exacerbates acetaminophen hepatotoxicity in mice via mitochondrial dysfunction-induced apoptosis. Biochim Biophys Acta Mol Basis Dis 2019;1865:2333-2341.
201. Wang Z, Hu JN, Yan MH, Xing JJ, Liu WC, Li W. Caspase-Mediated Anti-Apoptotic Effect of Ginsenoside Rg5, a Main Rare Ginsenoside, on Acetaminophen-Induced Hepatotoxicity in Mice. J Agric Food Chem 2017;65:9226-9236.
202. Puri P, Mirshahi F, Cheung O, Natarajan R, Maher JW, Kellum JM, Sanyal AJ. Activation and dysregulation of the unfolded protein response in nonalcoholic fatty liver disease. Gastroenterology 2008;134:568-576.
203. Olivares S, Henkel AS. Hepatic Xbp1 Gene Deletion Promotes Endoplasmic Reticulum Stress-induced Liver Injury and Apoptosis. J Biol Chem 2015;290:30142-30151.
204. Lin JH, Li H, Yasumura D, Cohen HR, Zhang C, Panning B, Shokat KM, et al. IRE1 signaling affects cell fate during the unfolded protein response. Science 2007;318:944-949.
205. Lin JH, Li H, Zhang Y, Ron D, Walter P. Divergent effects of PERK and IRE1 signaling on cell viability. PLoS One 2009;4:e4170.
206. Tabas I, Ron D. Integrating the mechanisms of apoptosis induced by endoplasmic reticulum stress. Nat Cell Biol 2011;13:184-190.
207. Szegezdi E, Logue SE, Gorman AM, Samali A. Mediators of endoplasmic reticulum stress-induced apoptosis. EMBO Rep 2006;7:880-885.
208. Hu P, Han Z, Couvillon AD, Kaufman RJ, Exton JH. Autocrine tumor necrosis factor alpha links endoplasmic reticulum stress to the membrane death receptor pathway through IRE1alpha-mediated NF-kappaB activation and down-regulation of TRAF2 expression. Mol Cell Biol

2006;26:3071-3084.
209. Hetz C, Bernasconi P, Fisher J, Lee AH, Bassik MC, Antonsson B, Brandt GS, et al. Proapoptotic BAX and BAK modulate the unfolded protein response by a direct interaction with IRE1alpha. Science 2006;312:572-576.
210. Lebeaupin C, Vallee D, Rousseau D, Patouraux S, Bonnafous S, Adam G, Luciano F, et al. Bax inhibitor-1 protects from nonalcoholic steatohepatitis by limiting inositol-requiring enzyme 1 alpha signaling in mice. Hepatology 2018;68:515-532.
211. Lee AH, Scapa EF, Cohen DE, Glimcher LH. Regulation of hepatic lipogenesis by the transcription factor XBP1. Science 2008;320:1492-1496.
212. Bailey D, O'Hare P. Transmembrane bZIP transcription factors in ER stress signaling and the unfolded protein response. Antioxid Redox Signal 2007;9:2305-2321.
213. So JS, Hur KY, Tarrio M, Ruda V, Frank-Kamenetsky M, Fitzgerald K, Koteliansky V, et al. Silencing of lipid metabolism genes through IRE1alpha-mediated mRNA decay lowers plasma lipids in mice. Cell Metab 2012;16:487-499.
214. Baulies A, Ribas V, Nunez S, Torres S, Alarcon-Vila C, Martinez L, Suda J, et al. Lysosomal Cholesterol Accumulation Sensitizes To Acetaminophen Hepatotoxicity by Impairing Mitophagy. Sci Rep 2015;5:18017.
215. Hale AN, Ledbetter DJ, Gawriluk TR, Rucker EB, 3rd. Autophagy: regulation and role in development. Autophagy 2013;9:951-972.
216. Wirawan E, Vanden Berghe T, Lippens S, Agostinis P, Vandenabeele P. Autophagy: for better or for worse. Cell Res 2012;22:43-61.
217. Kim I, Rodriguez-Enriquez S, Lemasters JJ. Selective degradation of mitochondria by mitophagy. Arch Biochem Biophys 2007;462:245-253.
218. Youle RJ, Narendra DP. Mechanisms of mitophagy. Nat Rev Mol Cell Biol 2011;12:9-14.
219. Parzych KR, Klionsky DJ. An overview of autophagy: morphology, mechanism, and regulation. Antioxid Redox Signal 2014;20:460-473.
220. Ding WX, Manley S, Ni HM. The emerging role of autophagy in alcoholic liver disease. Exp Biol Med (Maywood) 2011;236:546-556.
221. Pattingre S, Tassa A, Qu X, Garuti R, Liang XH, Mizushima N, Packer M, et al. Bcl-2 antiapoptotic proteins inhibit Beclin 1-dependent autophagy. Cell 2005;122:927-939.
222. Tanida I, Sou YS, Ezaki J, Minematsu-Ikeguchi N, Ueno T, Kominami E. HsAtg4B/HsApg4B/autophagin-1 cleaves the carboxyl termini of three human Atg8 homologues and delipidates microtubule-associated protein light chain 3- and GABAA receptor-associated protein-phospholipid conjugates. J Biol Chem 2004;279:36268-36276.
223. Mizushima N, Yamamoto A, Hatano M, Kobayashi Y, Kabeya Y, Suzuki K, Tokuhisa T, et al. Dissection of autophagosome formation using Apg5-deficient mouse embryonic stem cells. J Cell Biol 2001;152:657-668.
224. Xie Z, Klionsky DJ. Autophagosome formation: core machinery and adaptations. Nat Cell Biol 2007;9:1102-1109.
225. Satoo K, Noda NN, Kumeta H, Fujioka Y, Mizushima N, Ohsumi Y, Inagaki F. The structure of Atg4B-LC3 complex reveals the mechanism of LC3 processing and delipidation during autophagy. EMBO J 2009;28:1341-1350.
226. Sano R, Reed JC. ER stress-induced cell death mechanisms. Biochim Biophys Acta 2013;1833:3460-3470.

227. Kim J, Guan KL. Regulation of the autophagy initiating kinase ULK1 by nutrients: roles of mTORC1 and AMPK. Cell Cycle 2011;10:1337-1338.

228. Lin Z, Wu F, Lin S, Pan X, Jin L, Lu T, Shi L, et al. Adiponectin protects against acetaminophen-induced mitochondrial dysfunction and acute liver injury by promoting autophagy in mice. J Hepatol 2014;61:825-831.

229. Fujita E, Kouroku Y, Isoai A, Kumagai H, Misutani A, Matsuda C, Hayashi YK, et al. Two endoplasmic reticulum-associated degradation (ERAD) systems for the novel variant of the mutant dysferlin: ubiquitin/proteasome ERAD(I) and autophagy/lysosome ERAD(II). Hum Mol Genet 2007;16:618-629.

230. Hoyer-Hansen M, Bastholm L, Szyniarowski P, Campanella M, Szabadkai G, Farkas T, Bianchi K, et al. Control of macroautophagy by calcium, calmodulin-dependent kinase kinase-beta, and Bcl-2. Mol Cell 2007;25:193-205.

231. Sakaki K, Kaufman RJ. Regulation of ER stress-induced macroautophagy by protein kinase C. Autophagy 2008;4:841-843.

232. Kouroku Y, Fujita E, Tanida I, Ueno T, Isoai A, Kumagai H, Ogawa S, et al. ER stress (PERK/eIF2alpha phosphorylation) mediates the polyglutamine-induced LC3 conversion, an essential step for autophagy formation. Cell Death Differ 2007;14:230-239.

233. Harding HP, Zhang Y, Bertolotti A, Zeng H, Ron D. Perk is essential for translational regulation and cell survival during the unfolded protein response. Mol Cell 2000;5:897-904.

234. Huang Y, Wang Y, Feng Y, Wang P, He X, Ren H, Wang F. Role of Endoplasmic Reticulum Stress-Autophagy Axis in Severe Burn-Induced Intestinal Tight Junction Barrier Dysfunction in Mice. Front Physiol 2019;10:606.

235. Almeida A, Moncada S, Bolanos JP. Nitric oxide switches on glycolysis through the AMP protein kinase and 6-phosphofructo-2-kinase pathway. Nat Cell Biol 2004;6:45-51.

236. Alers S, Loffler AS, Wesselborg S, Stork B. Role of AMPK-mTOR-Ulk1/2 in the regulation of autophagy: cross talk, shortcuts, and feedbacks. Mol Cell Biol 2012;32:2-11.

237. Shang L, Wang X. AMPK and mTOR coordinate the regulation of Ulk1 and mammalian autophagy initiation. Autophagy 2011;7:924-926.

238. Meares GP, Hughes KJ, Naatz A, Papa FR, Urano F, Hansen PA, Benveniste EN, et al. IRE1-dependent activation of AMPK in response to nitric oxide. Mol Cell Biol 2011;31:4286-4297.

239. Kim J, Kundu M, Viollet B, Guan KL. AMPK and mTOR regulate autophagy through direct phosphorylation of Ulk1. Nat Cell Biol 2011;13:132-141.

240. Duan P, Hu C, Quan C, Yu T, Zhou W, Yuan M, Shi Y, et al. 4-Nonylphenol induces apoptosis, autophagy and necrosis in Sertoli cells: Involvement of ROS-mediated AMPK/AKT-mTOR and JNK pathways. Toxicology 2016;341-343:28-40.

241. Hu JL, Hu XL, Guo AY, Wang CJ, Wen YY, Cang SD. Endoplasmic reticulum stress promotes autophagy and apoptosis and reverses chemoresistance in human ovarian cancer cells. Oncotarget 2017;8:49380-49394.

242. Manley S, Williams JA, Ding WX. Role of p62/SQSTM1 in liver physiology and pathogenesis. Exp Biol Med (Maywood) 2013;238:525-538.

243. Ni HM, McGill MR, Chao X, Du K, Williams JA, Xie Y, Jaeschke H, et al. Removal of acetaminophen protein adducts by autophagy protects against acetaminophen-induced liver injury in mice. J Hepatol 2016;65:354-362.

244. Bjorkoy G, Lamark T, Brech A, Outzen H, Perander M, Overvatn A, Stenmark H, et al.

p62/SQSTM1 forms protein aggregates degraded by autophagy and has a protective effect on huntingtin-induced cell death. J Cell Biol 2005;171:603-614.

245. Saitoh T, Fujita N, Jang MH, Uematsu S, Yang BG, Satoh T, Omori H, et al. Loss of the autophagy protein Atg16L1 enhances endotoxin-induced IL-1beta production. Nature 2008;456:264-268.

246. Zhao Y, Yang J, Shi J, Gong YN, Lu Q, Xu H, Liu L, et al. The NLRC4 inflammasome receptors for bacterial flagellin and type III secretion apparatus. Nature 2011;477:596-600.

247. Lupfer C, Thomas PG, Anand PK, Vogel P, Milasta S, Martinez J, Huang G, et al. Receptor interacting protein kinase 2-mediated mitophagy regulates inflammasome activation during virus infection. Nat Immunol 2013;14:480-488.

10. Appendix

10.1 Publication

10.1.1 Poster presentation at the International Liver Congress 2019 in Vienna Austria:

Hui Ye, Kang Zheng, Yulia A. Nevzorova, Beatriz Martín-Adrados, Leonard J. Nelson, Manuel Gómez del Moral, Javier Vaquero, Rafael Bañares, Eduardo Martínez-Naves and Francisco Javier Cubero. A sublethal dose of acetaminophen suffices to induce the unfolded protein response in hepatocytes through an IRE1alpha-JNK1-XBP1s-dependent mechanism.

Kang Zheng, Hui Ye, Yulia A. Nevzorova, Beatriz Martín-Adrados, Iris Asensio, Manuel Gómez del Moral, Javier Vaquero, Rafael Bañares, Eduardo Martínez-Naves and Francisco Javier Cubero. Loss of X-Box Protein-1 in intestinal epithelial cells promotes the development of alcoholic liver disease in the liver.

10.1.2 Poster presentation at the International Liver Congress 2020 in London UK:

Hui Ye, Kang Zheng, Yulia A. Nevzorov, Beatriz Martín-Adrados, Leonard J. Nelson, Manuel Gómez del Moral, Iris Asensio, Javier Vaquero, Rafael Bañares, Eduardo Martínez-Naves and Francisco Javier Cubero. Deletion of *Xbp1* in liver parenchymal cells ameliorates acetaminophen (APAP)-induced hepatotoxicity via activation of IRE1alpha-JNK1-Atg5-dependent autophagy.

10.1.3 Poster presentation at the AASLD Digital Liver Meeting 2020:

Hui Ye, Kang Zheng, Chaobo Chen, Beatriz Martin-Adrados, Leonard J Nelson, Manuel Gómez Del Moral, Iris Asensio, Javier Vaquero, Rafael Bañares, Yulia Nevzorova, Eduardo Martinez-Naves and Francisco Javier Cubero. Endoplasmic reticulum (ER)-derived autophagy is a late event in acetaminophen (APAP)-mediated hepatotoxicity.

10.1.4 Original Publication

Ye H, Nelson LJ, Gómez Del Moral M, Martínez-Naves E, Cubero FJ. Dissecting the molecular pathophysiology of drug-induced liver injury. *World J Gastroenterol*. 2018;24(13):1373-1385. doi:10.3748/wjg.v24.i13.1373.

Chaobo Chen, Hui Ye, Hanghang Wu, Agustín Tortajada, Sandra Rodríguez-Perales, Raúl Torres-Ruiz, Alberto Villanueva, Isabel Peligros, Johannes Haybaeck, Leonard J Nelson, Roger J. Davis, Yulia A Nevzorova, Matias A Avila, Francisco Javier Cubero. Splicing of XBP1-mediated expression of BiP triggers cyst formationin early stages of cholangiocarcinogenesis. *Cancers*. Accepted.

TESIS DOCTORAL

MADRID, 2020